Master Thesis in Geosciences

An Assessment of Mapping Outfield Grazing Vegetation Quality in the Norwegian Mountains using Satellite Imagery

Kari-Anita Ruth Pulver

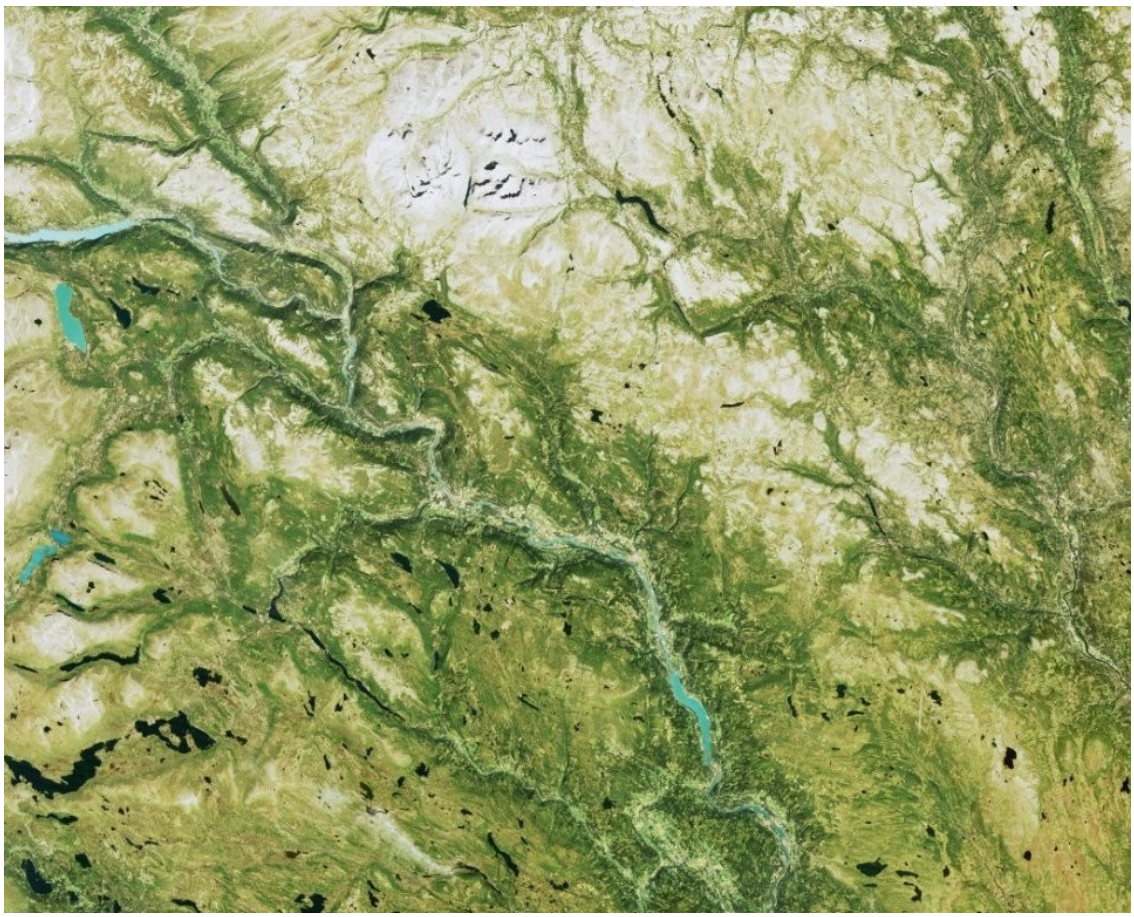

UNIVERSITY OF OSLO

FACULTY OF MATHEMATICS AND NATURAL SCIENCES

An Assessment of Mapping Outfield Grazing Vegetation Quality in the Norwegian Mountains using Satellite Imagery

Kari-Anita Ruth Pulver

Master Thesis in Geosciences

Discipline: Geomatics

Department of Geosciences

Faculty of Mathematics and Natural Sciences

UNIVERSITY OF OSLO

November 2006

Supervisor(s): Dagrun Vikhamar-Schuler, Norwegian Meteorological Institute and Bernd Etzelmuller, Professor at the University of Oslo.

This work is published digitally through DUO – Digitale Utgivelser ved UiO

www.duo.uio.no

It is also cataloged in BIBSYS (www.bibsys.no/english)

Front page image: copied from www.norgeibilder.no, © Geovekst. Series of 1:15000 orthophotos. Those over Venabygd taken 13.06.2004. UTM 32 (Euref89).

Acknowledgements

I would like to thank the Norwegian Computing Centre for the opportunity to work on this project and for the support and help from many of their staff members in the remote sensing department especially Rune Solberg, Jostein Amlien and Lars Aurdal.

My gratitude to Dagrun Vikhamar from the Norwegian Meteorological Institute for being my supervisor, for always coming with new ideas and being full of positiveness.

Thank you to Bernd Etzmuller and Andreas Kääb at the Department of Geosciences, University of Oslo, for their help in proof reading my report.

And finally to Håvard Frøiland, my partner, for his never failing support and encouragement in everything I do.

Thank you.

Abstract

Accurate vegetation mapping is a crucial tool in the decision making process for the proper management of outfield areas. This thesis assesses the use of Landsat TM and ETM+ data for mapping the grazing quality types identified by the Norwegian Institute for Land Inventory (NIJOS). The study site is located in the Venabygd Mountain area in central Norway. Using satellite imagery instead of traditional field mapping can reduce the time and cost of producing and updating grazing quality vegetation maps. Analyses showed that it is not possible to map the predefined grazing classes, but that it is possible to obtain unique spectral information for the vegetation types of Spruce, Birch and Alpine grasses. These can then be linked to an indication for grazing quality. Positive results were obtained from the topographic correction of the data and the use of a multi-temporal dataset.

Contents

Chapter 1

Introduction

The objective of this thesis is to assess the ability of satellite data in mapping vegetation. It is an important field of study due to the highly time consuming and costly methods used to currently map vegetation.

1.1 Rationale for Vegetation Mapping in Norway

The attention around the use of Norwegian outfield areas has increased in the last few years. Environmental management institutions are putting measures into place to ensure the safety of biodiversity by increasing the number of management plans and expanding national park areas. At the same time changes in land-use politics have lead to stronger investments and interest in the economic benefits of using outfield resources. Cleaner commercial interests in these areas is creating new ideas and inspiration especially from people with different backgrounds and attitudes to those of traditional outfield users (Bryn and Rekdal, 2002).

As resources become more valuable, and developments and changes take place, the need for more timely and accurate information about the type, quantity and extent of resources multiplies. A thorough scientific knowledge base on the ecology of an area is essential for correct planning. Correct planning enables resources to be used to their potential, but also that their use is sustainable and that measures are taken to avoid any damaging environmental consequences. Allocating and managing the Earth's resources requires knowing the distribution of these resources across space i.e. maps, and effective decisions require maps of known accuracy (Congalton and Green, 1999; Giannetti et al., 2001). Such objective knowledge provides the backbone for correct decision making when industry is to

be created, or environmental management measures are to be set in place.

In Norway, vegetation maps are today the map type that gives the best all round information on the environmental and ecological conditions in an area. They give a picture of the mosaic of vegetation types that natural plant coverage consists of. This overview of the spread of vegetation provides us with in this way information about the variation of ecological relationships such as climate, the nutrient content of water and soil, snow coverage, and the cultural affects in an area. Vegetation maps provide information that increases the knowledge and understanding of which natural resources there are and what should be conserved. They provide a common information system for many different users and create a central platform from which decisions can be made (Bryn and Rekdal, 2002).

Grazing quality vegetation maps are a key part of the information content of a vegetation map. Grazing quality information is not only useful for a grazer in determining where to graze his sheep, but also a very useful management tool. It can give vital information for estimations of grazing intensity, the numbers of grazing animals that an area can handle sustainably and provide the basis for change detection studies. Areas of less good grazing quality which can then be redefined for alternative land uses might be outlined as well.

Cingolani et al. (2004) summarised some of the positive and negative affects of domestic grazing on biodiversity, primary productivity, and forage / grazing quality that have been reported in the literature. Emphasised again is the importance of careful management-planning and continuous monitoring of outfield areas, for which having accurate base-line maps is an indispensable resource (Giannetti et al., 2001).

1.2 The Need for Improved Effectiveness

Successful management of extensive areas at the plant community level requires an efficient, cost-effective means of classification and mapping (Clark et al., 2001). Much of the effort behind traditional methods for landscape scale vegetation mapping lies however in expensive and time intensive field surveys.

The Norwegian Institute for Land Inventory (NIJOS) is the government agency responsible for vegetation mapping in Norway. Their methods for mapping vegetation to date include a combination of extensive field work as well as analysis of aerial photography. These methods demand good background botanic and ecology knowledge. With the kind of detail expected in an overview map a fieldworker

can only cover approximately $3\ km^2$ per day in forested areas and $5\ km^2$ in open mountainous terrain. The vegetation map created for the Venabygd mountain area (the study site) cost 4000 NOK per km^2 below the tree line and 3000 NOK per km^2 in the mountainous terrain above the treeline. Thus, it sis a time consuming and costly process (Bryn and Rekdal, 2002). Figure 1.1 shows a map over Norway with those outfield areas that have been mapped by NIJOS. There is far from full coverage over Norway and this is because of the expensive and time consuming nature of vegetation mapping.

Remote sensing is the collection and interpretation of information about an object from a remote vantage point. Because there is a high correlation between the variation in remotely sensed data and the variation across the earth's surface, such data provides an excellent basis for making maps of land use and land cover. The "bird's eye view" offered by a remotely sensing airplane or satellite is a view that can be readily understood. From the advent of the first aerial photograph in 1858 taken from a balloon to the launch of the latest satellite imaging system, remotely sensed data has become an increasingly important and efficient way of collecting map information. It also offers the ability to capture information about land cover that people can not sense such as reflectance data in the infrared parts of the electromagnetic (EM) spectrum (Congalton and Green, 1999; Kalliola and Syrjanen, 1991).

The launch of Landsat 1 by the US in 1972 resulted in a burst of exuberant research (Congalton and Green, 1999). Since then there has been almost exponential growth in the number of vegetation maps based on satellite data (Millington and Alexander, 2000). Technologies such as satellite-borne multispectral scanners and geographical information systems GIS are revolutionising vegetation mapping and modeling (Walsh and Davis, 1994).

Using satellite remotely sensed data is a more time and cost effective method for mapping vegetation. Earth observation satellites take images over the earth with a variety of sensors. Satellites such as the Landsat satellite (used in this project) uses an optical instrument which measures reflected solar radiation in the blue, green, red, near infrared (NIR), thermal infrared, and Mid Infrared (MIR) EM radiation bands. Aerial photographs have traditionally been taken with cameras that only detect visible and sometimes NIR light. Having extra bands such as the MIR can provide additional information that is very useful for vegetation classification.

Optical earth resource satellites lie at altitudes around $800\ km$ (e.g. Landsat ≈ 700 km) which enables them to cover much larger areas faster than aerial photography. Satellites take images over the same areas repeatedly. Landsat 7, for example, has a repeat cycle of 16 days and because Norway is quite far north, parts of

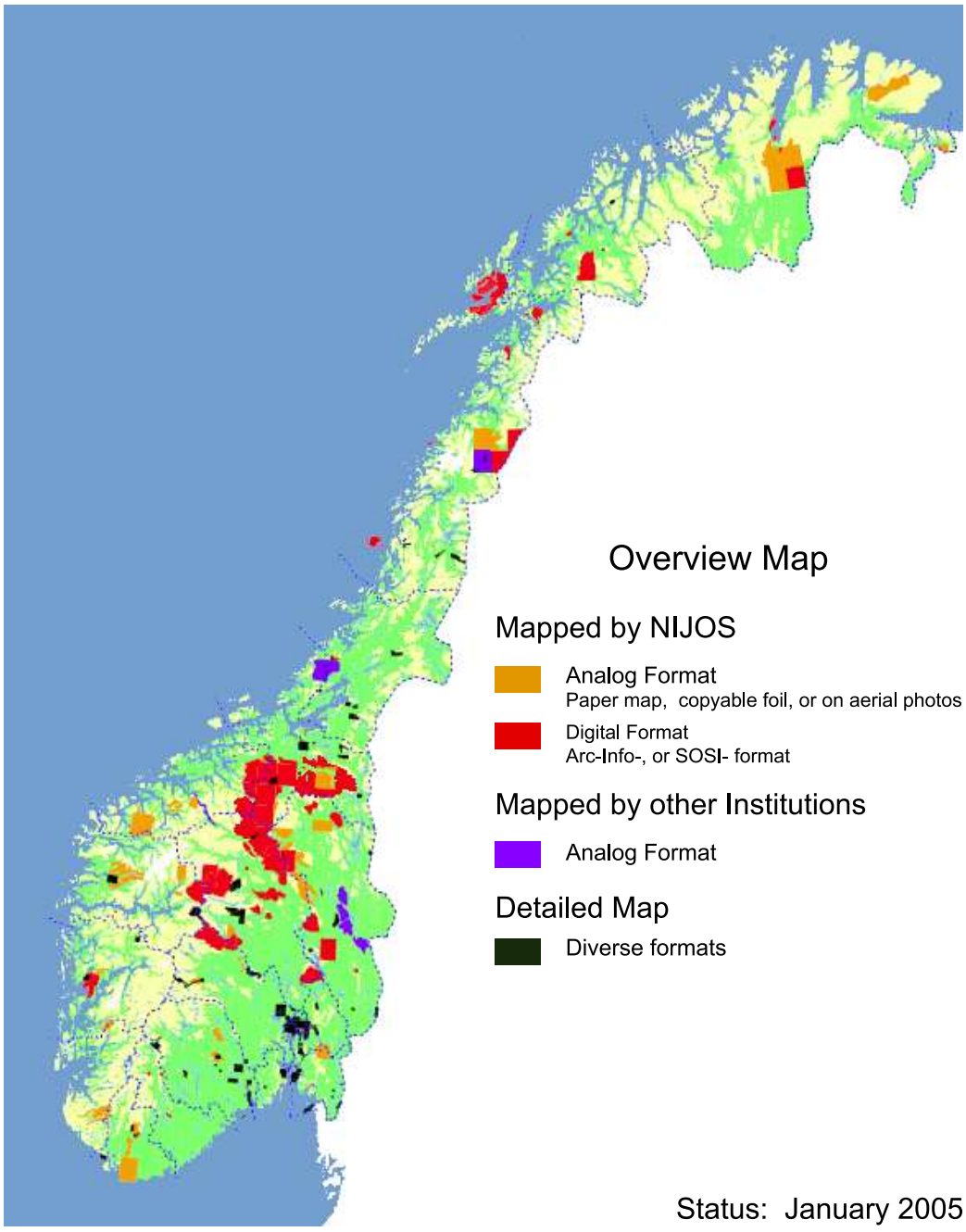

Figure 1.1: A map over Norway illustrating those outfield areas over Norway that have been mapped by NIJOS. It takes a great deal of time to map large areas based on field work and aerial photography analysis. Thus, satellite images have a great potential to map large areas in a time effective way. Map copied and modified from NIJOS website. Scale is 1:21 Km. Copied with permission from NIJOS. Co-ordinate system UTM33 WGS84.

the country will be covered by the satellite even more frequently (NASA, 2006). Having a satellite orbiting constantly has many advantages. Satellites such as Landsat take images that have been pre-ordered as well as taking image series without order. This means that in terms of mapping one has both the opportunity to buy archive images as well as order upcoming takes. This increases the chances of obtaining good quality cloud free data over the area of interest, as well as allowing for change detection studies.

Millington and Alexander (2000) discussed the major developments in vegetation mapping in the three last decades of the twentieth century with the most influential of these being:

- The increasing demands for vegetation information to assess and help in; the management of environmental problems, environmental policy-making and natural resource planning.
- The need for vegetation and land cover information for predictive modeling of future climate change and its wide range of impacts.
- The increasing availability of satellite remotely sensed data and its use as a prime data source for vegetation and land cover mapping.
- The development of techniques in spatial analysis and geographic information system (GIS) which have significant influences on map production and interpretation.

1.3 Thesis Aims

In focusing on finding more cost effective and timely ways of mapping vegetation this thesis aimed to assess the ability of satellite data in mapping vegetation. It focuses on the use of Landsat satellite data and applies these data to the more specific target of mapping grazing quality in an area in the Norwegian mountains called Venabygd.

This project took a starting point in the vegetation map with the grazing quality categories produced by NIJOS for the Venabygd mountain area. This data was used as ground truth. The objective was to investigate the possibility of discriminating between the predefined grazing classes, identifying how much information could be obtained from the Landsat images and how well a grazing quality map could be produced from these. The aim of this thesis was to use the brightness values in the Landsat images to find a pattern that connected these with the already

defined grazing quality classes of NIJOS. At the moment NIJOS's only way of systematically mapping outfield grazing quality is by assigning already mapped vegetation categories with a grazing quality class (Bryn and Rekdal, 2002).

Making and updating grazing maps in Norway is a costly and timely process. Potentially, automatic or semi-automatic processing of satellite remote sensing data could greatly reduce costs and make it possible to keep maps better updated. However, many published works indicate that there is no straightforward solution to this (Cingolani et al., 2004; Hoersch et al., 2002; Ahmad et al., 1992).

1.4 Thesis Structure

Chapter 1: introduces the topic of vegetation and grazing maps as well as why these maps are an important part of the decision making process and knowledge base for outfield areas. It presents how these maps have been traditionally made, and the need for improved effectiveness through the use of satellite remote sensing is also discussed. The project aims are laid down.

Chapter 2: outlines how this thesis fits into the framework of the Geoland project. The Venabygd area is described with location, climate, vegetation, and geology. The second part of this chapter then deals with the theory of remote sensing, including background on; the EM spectrum, satellite sensors, image processing and interpretation, as well as a literature review of satellite vegetation mapping.

Chapter 3: gives details of all the datasets used in this project. Which satellite sensors and images were used and the specifications of ancillary data such as digital elevation models (DEMs) and map data. It also describes the methods used by NIJOS to produce their maps and discusses data accuracy.

Chapter 4: describes all the methods used in the analysis of vegetation classes and satellite imagery.

Chapter 5: illustrates the obtained results through images, graphs, and tables. A brief discussion of each analysis is presented as well. Flow diagrams illustrate the process followed.

Chapter 6: gives an overall discussion of the results obtained and relates these to results obtained in similar studies.

Chapter 7: draws a conclusion to the presented work.

Chapter 2

Background and Theory

2.1 The Geoland Project

This thesis is based on a project that the the Norwegian computing centre (NR) (Norsk Regnesentral) undertook over a 3 year period from 2004-2006. The project was part of a much larger project called Geoland. Geoland is a project carried out in the context of the organisation Global Monitoring for Environment and Security (GMES), which is a joint initiative between the European Commission (EC) and the European Space Agency (ESA). The aim of the Geoland project is to build up a European capacity for Global Monitoring for Environment and Security (Geoland, 2005).

To achieve this aim the Geoland consortium is focused on developing and demonstrating a range of reliable and affordable European geo-information services which support the implementation of European and national directives and policies. Within eight sub-projects, (see figure 2.1) the 56 geoland partners develop products and services, utilizing available Earth Observation resources in combination with in-situ measurements, and integrating them with existing models into pre-operational, geo-information services with improved temporal and spatial resolutions.

This thesis is focused on regional monitoring and is defined within the Nature Protection Observatory (ONP) observatory. The regional services of the Geoland project focuses on the implementation of newly established European Directives e.g. the Habitats and Bird Directive, the Ramsar (wetland) Convention, and the Convention on Biological Diversity. Within the ONP there are 5 ecosystem themes defined for monitoring: (Geoland, 2005).

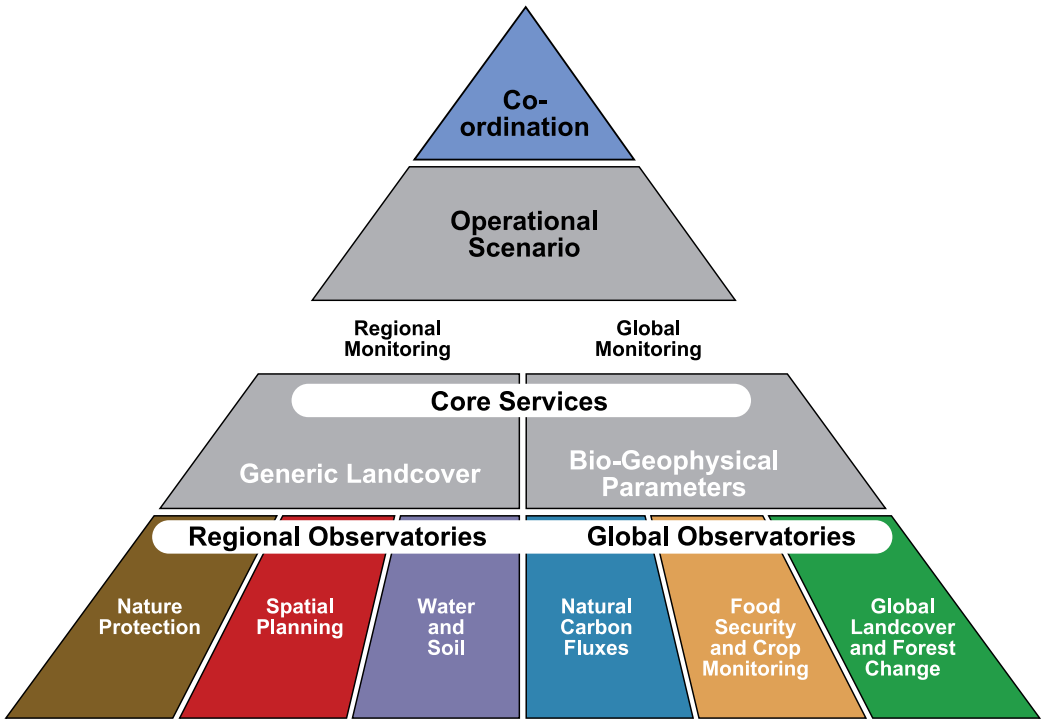

Figure 2.1: The organisational structure of the Geoland project. This thesis fits into the generic land cover core services and is part of the nature protection regional observatory. Within the nature protection observatory this project fits into the alpine monitoring theme with a focus on the grazing quality of vegetation. Copied and modified from Geoland (2005).

- Nature Protection Observatory
  - Alpine monitoring,
  - Forest protection monitoring,
  - Generic habitats and biotopes,
  - Ecotone characterisation mapping, and
  - Mountain environments - focused on;
    - Long-term vegetation changes
    - Grazing quality of vegetation
    - Snow distribution patterns
    - Snow wetness

Scandinavia was chosen as the test site for the Mountain Environments Service. Four focuses were defined for this service (shown in the list above) of which NR

was given the job of working on them. This thesis focused on the grazing quality of vegetation and was based on work done in cooperation with NR for the Geoland project.

2.2 Site Description

Location
The study area for this thesis is located in the Venabygd mountain area in central Norway. Figure 2.2 shows 2 areas (Venabygd and Sør-Fron) that have been mapped for vegetation and grazing quality by Norwegian Institute for Land Inventory (NIJOS). The Venabygd study area is defined by the NIJOS vegetation map which covers 160km^2. The area lies in Ringebu Community in Oppland county.

Figure 2.3 shows a more detailed map of the study area. The Sør-Fron community borders the western section while the northern border is defined by the state highway (RV) nr.27. The Eastern border of the area follows the valley and river south to Jønnhalt. The southern border of the area goes from Jønnhalt along the road to Venabygd. The highest point is Nødre Bølhøgda in the north at 1356m a.s.l. The town Venabygd, located at the southern end of the study area, is located at $61°34'60N$ and $10°3'0E$, at an elevation of 579m (Bryn and Rekdal, 2002).

The Venabygd site area is used to analyse the possibility of mapping grazing quality with Landsat imagery. The neighbouring site of Sør-Fron (seen in figure 2.2) was intended as a potential test sight for any classification procedures developed from the Venabygd site. The areas have very similar vegetation types and are on opposite sides of the valley to each other.

Vegetation
Besides natural environmental factors such as topography, climate and geology, the history impacts in terms of agricultural land use, animal husbandry and also natural disturbances (avalanches, rockfall, mudslides) play a major role in the spatial distribution of vegetation types (Hoersch et al., 2002). The vegetation distribution changes significantly in the Venabygd area from down the valley to up above the tree line in the mountains. This change in height leads to changes in climate of which temperature is the most influential factor for vegetation distribution. Figure 2.4 shows a list of the vegetation types in different height zones in the area. The tree line lies at approximately $1050ma.s.l$ and is dominated by mountain birch a tree species that because of rehabilitation is establishing itself in large areas around Venabu and Flaksjøen. Around $950ma.s.l$ the dominance of coniferous trees becomes more noticeable where as lower down the spruce trees

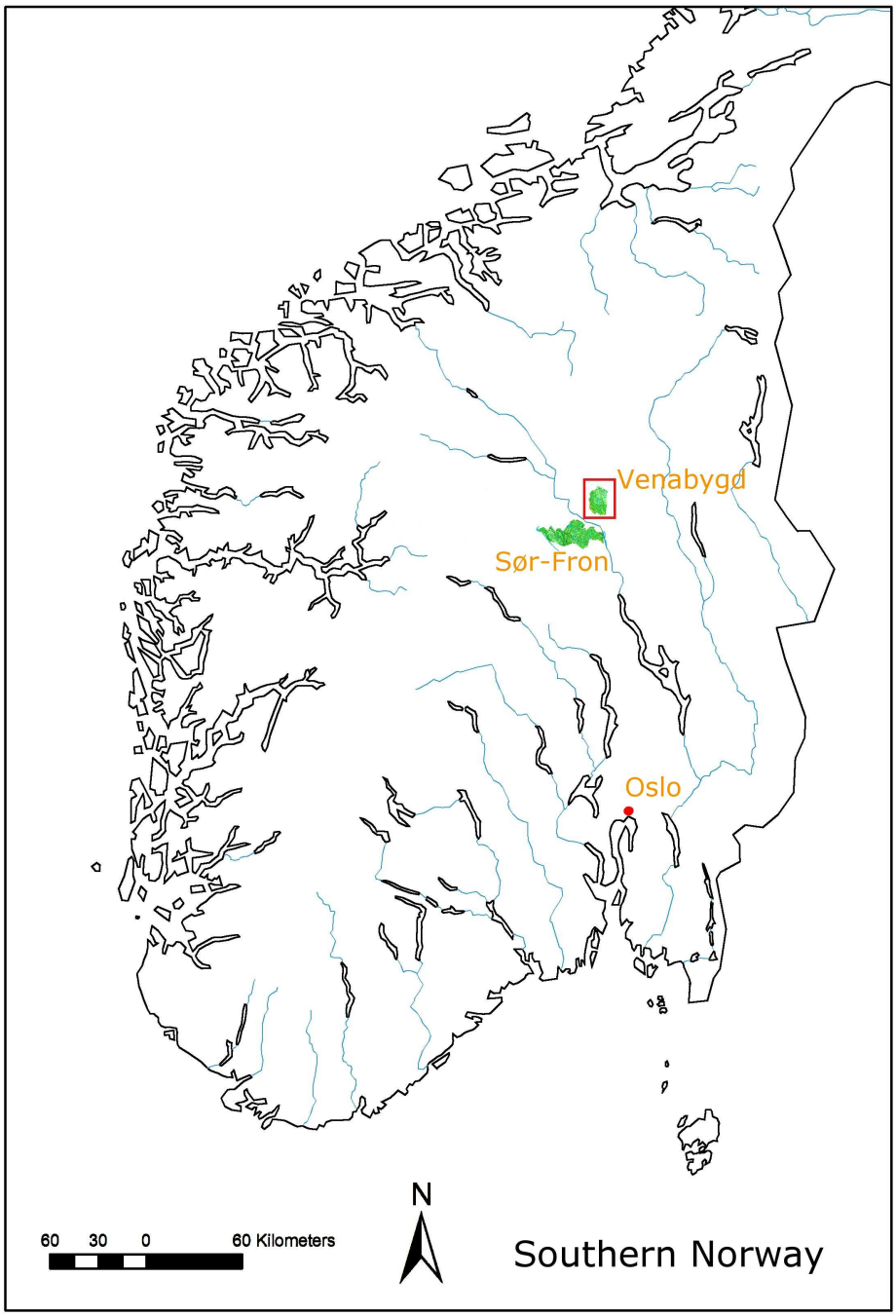

Figure 2.2: An outline map of southern Norway. The study area Venabygd is selected in red. Venabygd is the town located at the bottom of the study area (shown in fig 2.3). It has the location $61°34'60N$ and $10°3'0E$. On the other side of the valley is Sør-Fron an area which has also been mapped for vegetation and grazing quality by NIJOS. Co-ordinate system unknown.

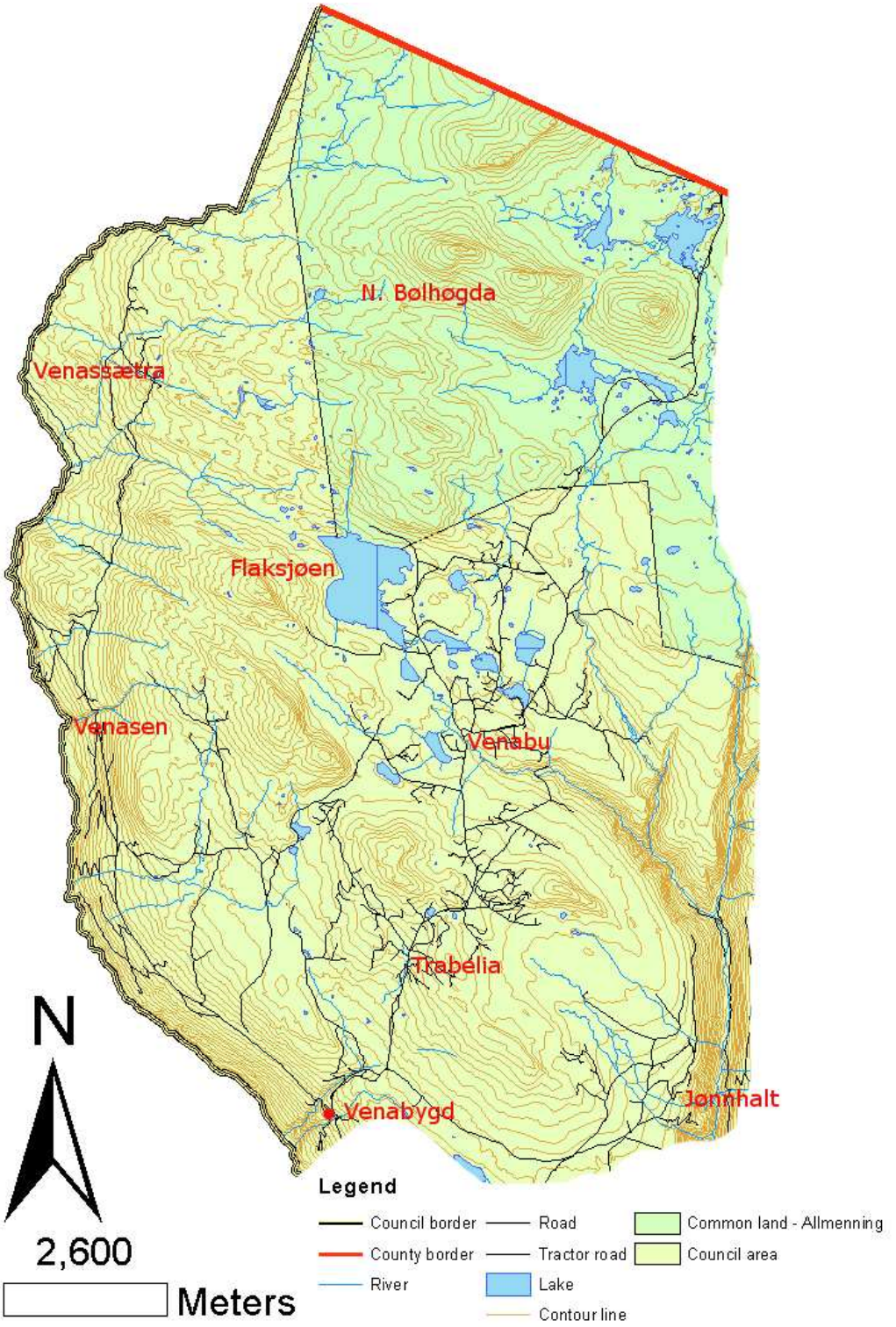

Figure 2.3: Overview map of the Venabygd study area. The study area covers $160km^2$. The council area is part of the Ringebu Community and Oppland county. The Sør-Fron community borders the western section of the area while the northern border is defined by the state highway (RV) nr.27. The Eastern border of the area follows the valley and river south to Jønnhalt. The southern border of the area goes from Jønnhalt along the road to Venabygd. Venabygd is located at $61°34'60N$ and $10°3'0E$, at an elevation of 579m. The highest point is Nødre Bølhøgda in the north at 1356m a.s.l The map shows the lakes, river network, road and tractor network, and some of the main place names. The contour lines are 20m. Co-ordinate system: UTM zone32, EUREF89 / WGS84.

dominate the forested areas (Bryn and Rekdal, 2002).

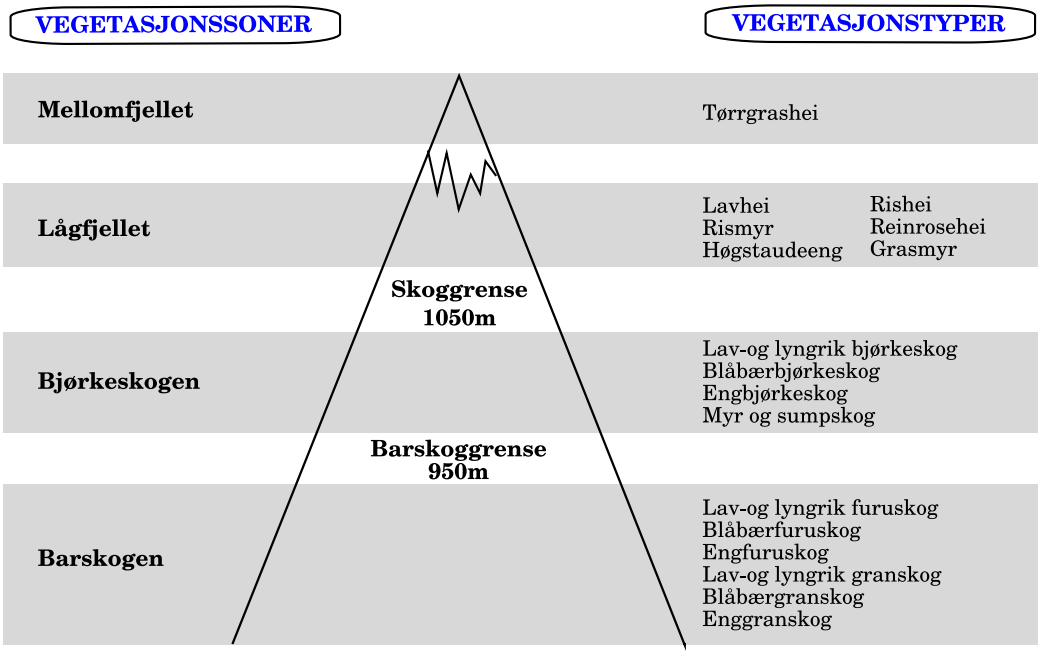

Figure 2.4: Vegetation zones in the Venabygd area divided according to elevation. Because elevation governs the climate and especially temperature it can be used as a main feature in dividing the vegetation into zones. Copied and modified from Bryn and Rekdal (2002).

Figure 2.5 shows an image of the Venabygd area and the coverage of the different grazing qualities in the area, defined by NIJOS. The Venabygd mountain area has $92km^2$ of productive sheep land and $107km^2$ of productive cattle grazing land. These productive areas are only productive from spring to autumn. Venabygd mountain has a large height variation but there is relatively little snowbed (*snøleie*) vegetation, this leads to a drop in grazing quality out over August. If grazing has been significant this can encourage renewed growth in the vegetation which can extend the grazing period further past August. The grazing impact is quite high in the areas north of Nødre Bølhøgda. In the summer farm and forest areas the grazing impact is middle, and on the valley sides it's low (Bryn and Rekdal, 2002).

Climate

Near the state highway at the top of the Venabygd mountain area the Norwegian meteorological institute has measured different climatic factors since 1980. The measurements show that the region has a typical inland climate with low winter temperatures and high summer temperatures in respect to the height above sea level. The mapped area has an elevation from 330 to $1365ma.s.l$. January has the lowest average temperature of $-9.7°C$ and July the highest with an average of

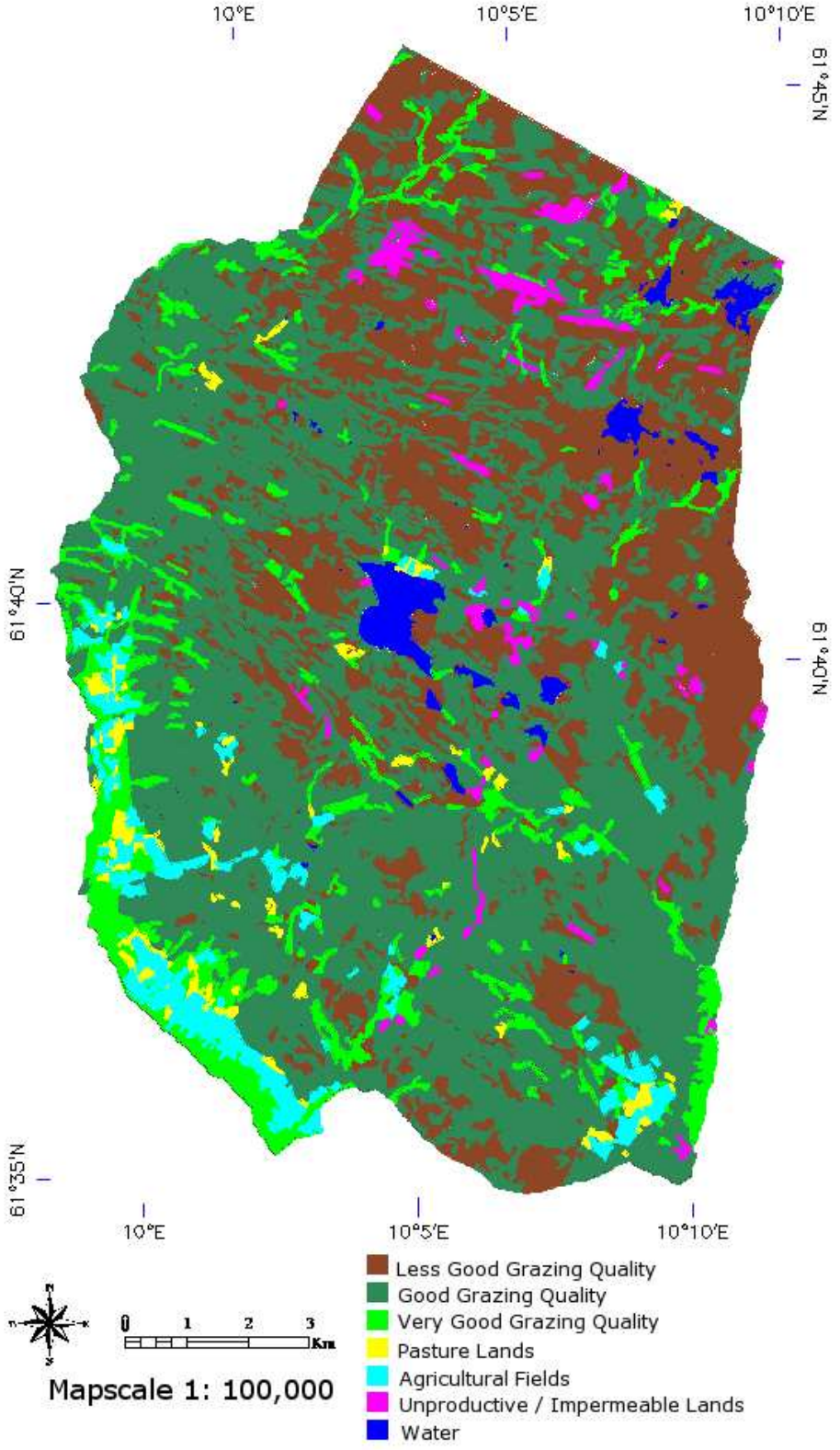

Figure 2.5: This map shows the grazing quality distribution over the study area, Venabygd. The grazing quality types are defined by NIJOS. Good quality grazing dominates the area, followed by Less Good and then smaller areas of Very Good. Coordinate system: UTM zone 33, WGS84.

$+10.4°C$. The average annual temperature is $-0.3°C$. The average annual precipitation is $660mm$. The rainfall pattern is similar to that of temperature meaning that the lowest rainfall occurs in the winter and the highest rainfall in the summer (Bryn and Rekdal, 2002).

Geology
Nutrient poor sandstone and quartzite dominate the geology, and the area has varying moraine sediment coverage as well as bare rock surfaces. Outlined in the geology map "Lillehammer" in scale $1 : 250,000$ the area is dominated by sliding slate made of feldspar sandstone and quartzite from the late Cambrian period (Siedlicka et al., 1987). This is a highly erodible rock type that gives little access to nutrients. However, growth of vegetation occurs in areas that have good access to water (Bryn and Rekdal, 2002).

2.3 Remote Sensing Theory

What is remote sensing?
Remote sensing is the science of obtaining and interpreting information about an object from a remote vantage point. This information could be measurements with sonar, acoustic waves, or measurements of force and magnetic field. The remote sensing referred to in this thesis is always referring to the detection of reflected or emitted electromagnetic (EM) energy. Our eyes acquire data on variations in electromagnetic energy within the tiny range of $0.4\mu m$ - $0.7\mu m$ known as visible light. Spaceborne remote sensing systems have a unique vantage point which allows a "birds eye view" of the planet and an almost constant acquisition of data with $24/7$ monitoring of the earths environments (Congalton and Green, 1999; Lillesand et al., 2004).

Remote sensing of the earth
Because there is a high correlation between variation in remotely sensed data and variation across the earth's surface, remotely sensed data provides an excellent basis for making maps of land use and land cover. With sensors that not only capture visible light but radiation in the near infrared (NIR) part of the electromagnetic spectrum, remote sensing is able to capture information about land cover that people themselves can not sense (Congalton and Green, 1999; Lillesand et al., 2004).

The processes involved in EM remote sensing of the earth's resources can be divided into two main categories; the acquisition of data, and the analysis of that data. The elements involved in data acquisition include; energy sources, propaga-

tion of energy through the atmosphere, energy interactions with the earth's surface and senors. Data analysis is the process of extracting information about the type, extent, location and condition of various land covers. This is done with the help of reference data (e.g. field ground truth) as well as the use of various computer algorithms and tools. The final product resulting from the data analysis is often a hard-copy or digital map which is used to convey information and aid in decision making processes (Lillesand et al., 2004).

2.3.1 Energy Sources and the Electromagnetic Spectrum

EM energy comes in many forms including visible light, radio waves, heat, ultraviolet light, and x-rays. All this energy is inherently similar and radiates in accordance with basic wave theory, see Lillesand et al. (2004). In remote sensing it is common to categorise EM waves in terms of their wavelength or frequency (Hashimoto et al., 1993). Figure 2.6 shows a diagram of the electromagnetic spectrum.

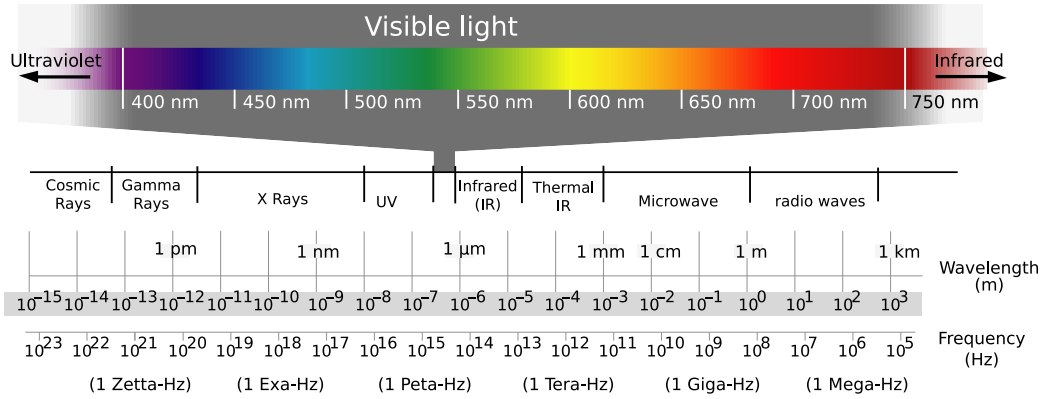

Figure 2.6: The electromagnetic spectrum. The labels indicate the main sections of the EM spectrum that are commonly used in remote sensing e.g. the visible and infrared regions. Copied and modified from wipipedia.org

2.3.2 Interactions with Surface Features

When radiation hits an object or particle parts of this energy penetrates the object and parts are reflected, absorbed, or emitted in unique ways. These unique characteristics of matter are called spectral characteristics. The reason why a leaf looks green to humans, for example, is that the chlorophyll in the leaves absorbs blue and red spectra and reflects the green spectrum which is what our eyes see.

A graph of the spectral reflectance of an object as a function of wavelength is called a spectral reflectance curve. Figure 2.7 shows some typical spectral signatures for vegetation, bare rock and soil. Soil has rather higher values for almost all spectral regions where as water for example has almost no reflectance in the infrared region. Measurements at a wavelength of $0.6\mu m$ could enable distinction between the objects of soil, water and vegetation. Why an object has a peculiar set of reflection, emission, and absorption characteristics is due to the relationship between molecular, atomic and electromagnetic radiation, see Hashimoto et al. (1993).

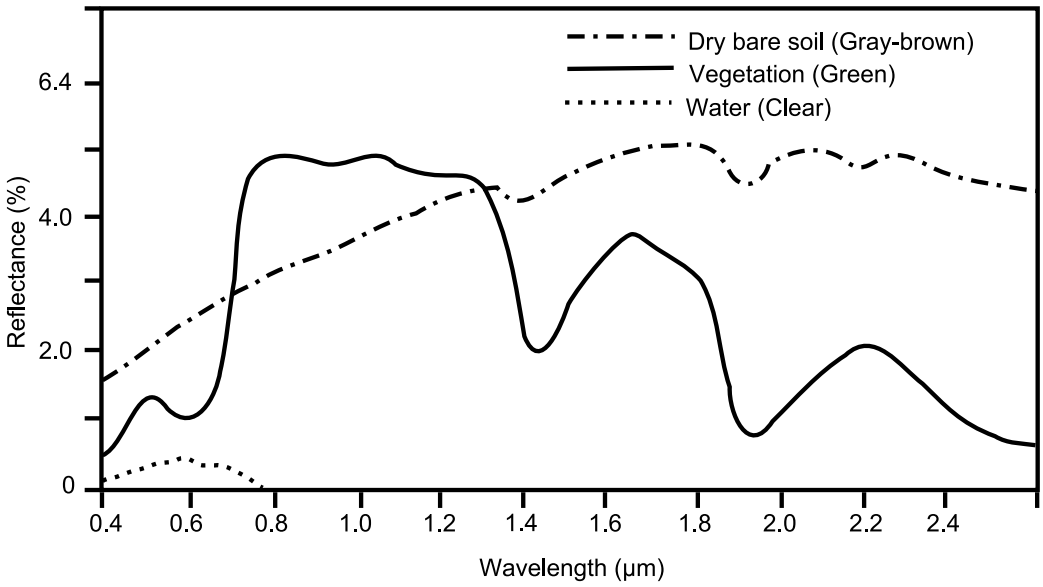

Figure 2.7: The typical spectral signatures for vegetation, bare rock, and soil. Soil has rather higher values for almost all spectral regions where as water for example has almost no reflectance in the infrared region. Vegetation has characteristics like strong absorption bands in the red, and MIR regions due to chlorophyll and plant water content respectively. These unique characteristics make it possible to separate from other land cover types such as soil and water. Copied from Lillesand et al. (2004) with permission from John Wiley & Sons Inc.

Applying the principle of conservation of energy, the reflected energy of an object is equal to the incident energy of an object (incoming energy) e.g. from the sun, minus that energy which was absorbed or transmitted. The geometric manner in which an object reflects this energy is also important in respect to the measurement of energy at the satellite. The way in which energy is reflected by an object depends on its surface roughness. Surface roughness is proportional to wavelength, the longer the wavelength the smoother an objects surface becomes. Specular surfaces are flat surfaces that reflect energy like a mirror, where the angle of reflection equals the angle of incidence. Diffuse (or Lambertian) reflectors are

rough surfaces which reflect the incident energy equally in all directions. Most earth surfaces are neither perfectly specular or diffuse but somewhere in between (Lillesand et al., 2004). Figure 2.8 illustrates a typical specular and diffuse reflector. Most often than not we are interested in objects with diffuse reflection characteristics because this enables a sensor to measure part of the reflectance. With a specular reflector e.g. a still lake, the sunlight will be reflected off in the opposite direction and very little, if anything will be recorded by the satellite sensor (i.e. that is why flat water bodies often appear black in optical satellite images).

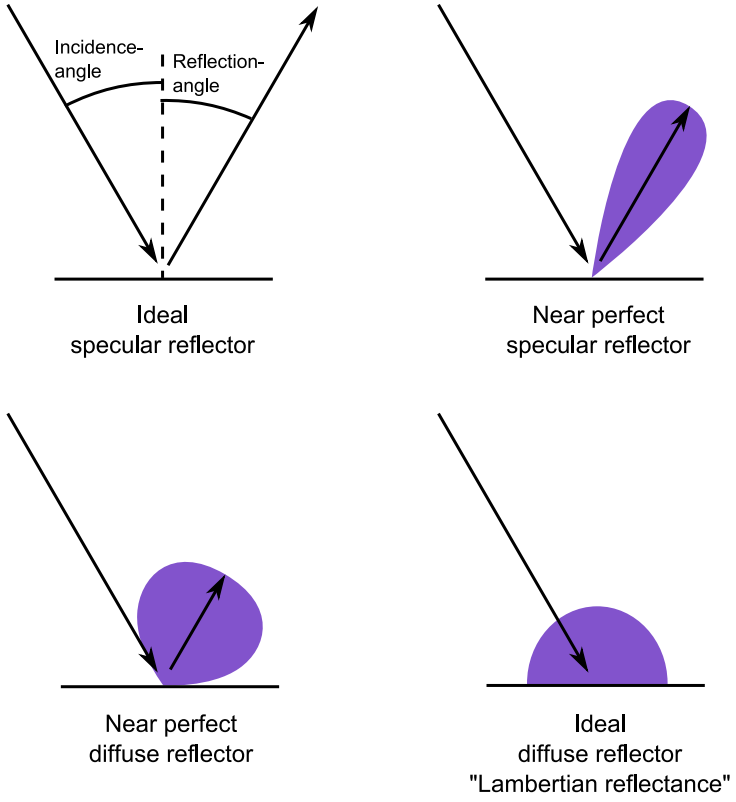

Figure 2.8: Diagrams illustrating the reflection characteristics of surfaces, ranging from specular to diffuse. The spectral reflection characteristics of an object define how the irradiance is reflected back to the satellite sensor. A specular reflector, for example, will lead to reflectance away from the sensor and hence results in a low at satellite radiance reading. Copied and modified from Lillesand et al. (2004) with permission from John Wiley & Sons Inc.

2.3.3 Atmospheric Interactions

Before radiation (e.g. solar) reacts with the earth's surface it has to pass through the atmosphere where any interactions occur between the radiation, particles and gases. Reflected sunlight, measured by a satellite sensor, travels through the full thickness of the atmosphere before it hits the surface and then again after being reflected. Thermal radiation, however, is emitted from objects so it only travels one way. The atmosphere can have a significant affect on the intensity and spectral composition of the radiation. These effects are primarily caused by two phenomena; scattering and absorption.

Atmospheric scattering
Atmospheric scattering is the unpredictable scattering of radiation by particles (e.g. smoke, dust, pollen). Rayleigh scatter occurs when radiation interacts with atmospheric molecules (e.g. N_2, CO_2, & O_2) and other tiny particles that have smaller diameters than the radiation wavelength. The smaller the wavelength the greater the tendency for this mechanism to occur because Rayleigh scattering is inversely proportional to the fourth power of the wavelength. Sunlight interacts with the atmosphere and because blue light has the shortest wavelength in the visible spectrum is is scattered the most, and hence we see the sky as blue. Without this scattering the sky would be black. At sunset and sunrise the sunlight has to travel a longer distance through the atmosphere than it does at midday so the scattering and absorption is more complete, meaning that we only see the less scattered, longer wavelengths of orange and red. Rayleigh scattering is the primary cause of "haze" in remote sensing imagery.

When the atmospheric particles are a similar diameter to the radiation wavelength Mie scattering occurs. Water vapour and dust are majour causes of Mie scattering. When the particle diameters are larger than the wavelength (e.g. water droplets) non-selective scattering occurs, scattering all wavelengths in the visible to NIR wavelengths about equally. Cloud and fog appear white for this reason (Lillesand et al., 2004).

Atmospheric absorption
Absorption on the other hand is the effective loss of energy to constituents in the atmosphere (e.g. water vapour, CO_2, and ozone (O^3)). These gases absorb radiation at particular wavelengths. Remote sensing acquisition is limited to those wavelengths that are not highly affected by absorption, known as atmospheric windows. Atmospheric transmission and the energy sources at certain wavelengths are shown in figure 2.9. The visible range for example, is not only an atmospheric window but the range of wavelengths that are emitted from the sun at it's energy peak (6000K $5700\circ$C). In contrast energy emitted from the earth

peaks at around (300K $28.9°$C) (see fig 2.9) (Lillesand et al., 2004).

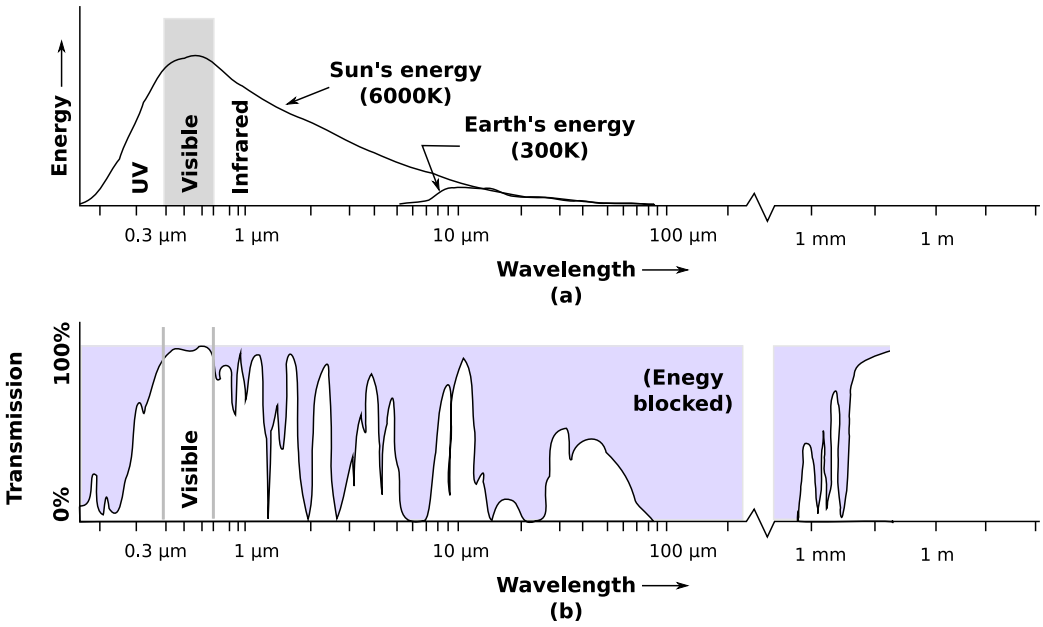

Figure 2.9: The spectral characteristics of (a) different energy sources, and (b) atmospheric transmittance. The wavelength scale is logarithmic. The visible spectral region, for example, is in an atmospheric window making it possible to sense from a satellite, as well as being the region of the EM spectrum that can be sensed with the human eye. Data from this region is recorded using multispectral scanners. Wavelengths in this region correspond to those with the highest energy coming from the sun. Copied and modified from Lillesand et al. (2004) with permission from John Wiley & Sons Inc.

2.3.4 Sensors

Sensors are used to record the variation in the way surface objects reflect EM energy and transform the data into digital form. The focus in this thesis is on the use of optical remote sensing which measures the reflected visible and infrared wavelengths whose energy source comes from the sun (energy peak at wavelength of $0.5\mu m$), see figure 2.9. Thermal infrared sensors record emitted energy from the object itself which radiates uniquely depending on it's temperature and emissivity. Every object on earth above $0K$ emits EM radiation, with the earths energy peak at a wavelength of about $10\mu m$ (fig 2.9). In the microwave region, there are two types of microwave sensors, passive sensors which measures object emittance, and active sensors which send out a pulse and record its backscatter.

The choice of sensor for analysis involves the consideration of; spectral resolu-

tion, radiometric resolution, the presence of atmospheric windows, and spatial resolution (Lillesand et al., 2004). The satellite the sensor sits on governs orbital factors such repeat time and geographic coverage. For more information on satellite platforms and sensors see Houston and Rycroft (1999).

2.3.5 Classification

The general process towards classifying a remote sensing image into information classes starts with assessing what kind of results you are looking for. This information is used to choose the right images and classification algorithms. The classification approach taken depends upon the nature of the data being analysed, the computational resources available, and the intended application of the classified data (Lillesand et al., 2004). A list, adapted from Jensen (1996), shown in appendix A, identifies the general steps needed to process a satellite image and extract land cover information.

2.3.6 Remote Sensing Accuracy

According to Congalton and Green (1999) the accuracy of maps made from remotely sensed data is assessed through two criteria; location accuracy and classification or thematic accuracy. Location accuracy is a measure of how accurately map items are located on the map relative to their true location on the ground. Thematic accuracy is a measure of how accurate the information label given to describe a class (e.g. landcover) or condition is.

Map errors can occur at many stages. Doing an accuracy assessment allows errors to be identified and maps improved, as well as allowing for objective comparison different techniques and algorithms. When information derived from remotely sensed data is to be used in a decision-making process, it is critical for a measure of quality to accompany the information. Error assessment can be qualitative or quantitative. Quantitative accuracy assessment involves the comparison of map data against reference information (i.e. some form of ground truth). This can then be illustrated in the form of a confusion matrix for example. For further information on error models for spatial data see Goodchild (1994). Figure 2.10 shows a schematic diagram of many of the possible sources of error at different stages of production.

Kalliola and Syrjanen (1991) note that many of the satellite based maps available are of limited value in terms of biological studies because of their accuracy, and

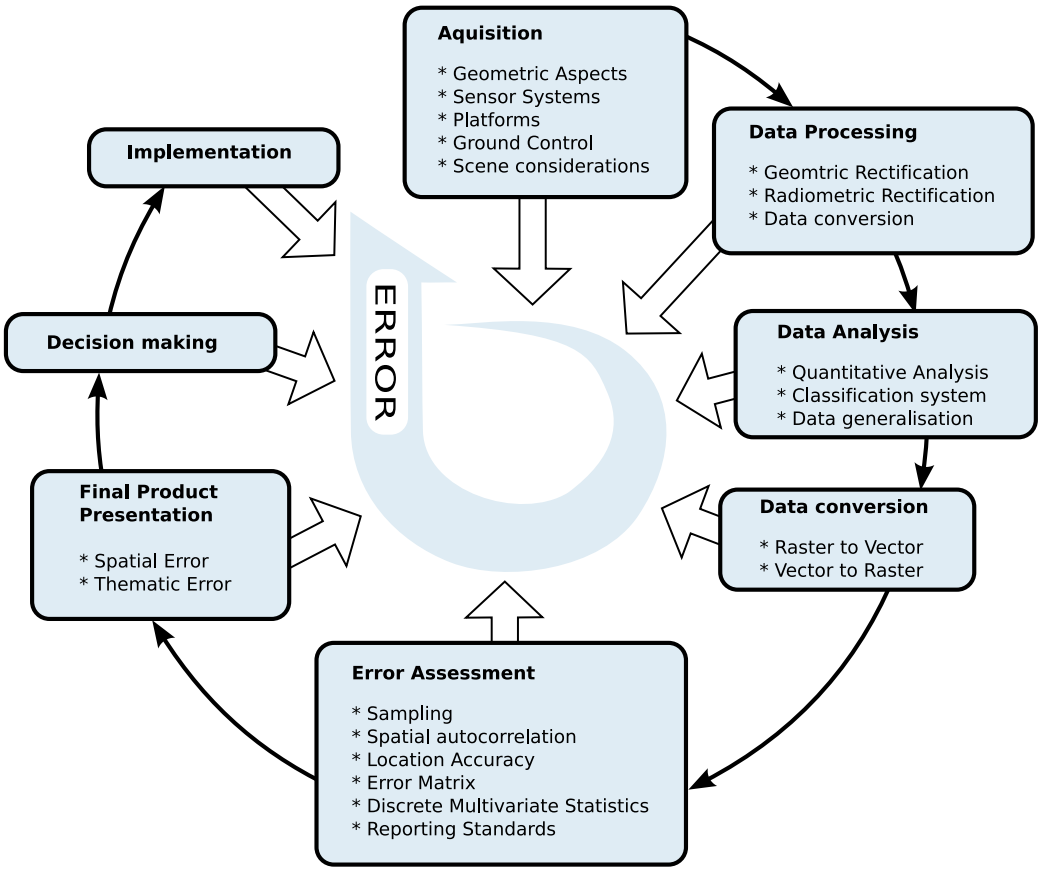

Figure 2.10: A flow diagram of the production of remotely sensed products. At each stage in the process it is possible to make errors. It is important to take in error factors from all parts of the production cycle not just the finished product. , Copied and modified from Lunetta et al. (1991). Copied with permission from ASPRS: The Imaging & Geospatial Information Society.

they emphasise an urgent need to develop a unified validation procedure to meet the needs of image users.

2.3.7 Remote Sensing of Vegetation

Vegetation has unique characteristics which make it very useful to study using remote sensing. Chlorophyll, for example, is a green pigment used for photosynthesis in plants (found mostly in the leaves). Chlorophyll absorbs radiation strongly at the wavelengths $0.45\mu m$ (blue) and $0.67\mu m$ (red). Figure 2.11 shows a general spectral reflectance curve for most vegetation types, the absorption areas can be seen as dips in the curve. The small reflectance peak in the green region

between 0.5 - $0.6\mu m$ gives rise to the visible green colour of vegetation.

Another unique characteristic is seen in the NIR region between 0.7 - $0.9\mu m$, where the reflectance is much higher than that in the visible bands. This is due to scattering in the cellular structure of the leaves as well as scattering in the vegetation canopy. Such a steep gradient between the low reflection in the red and high reflection in the NIR region, is only produced by vegetation (Hashimoto et al., 1993; CRISP, 2001; Fiella and Penuelas, 1994). Because plants reflect far more in the NIR compared to all other visible bands, this band is most often used to look at vegetation as apposed to the green band. See figure 2.7 for a comparison between the reflectance characteristics of vegetation, soil and water.

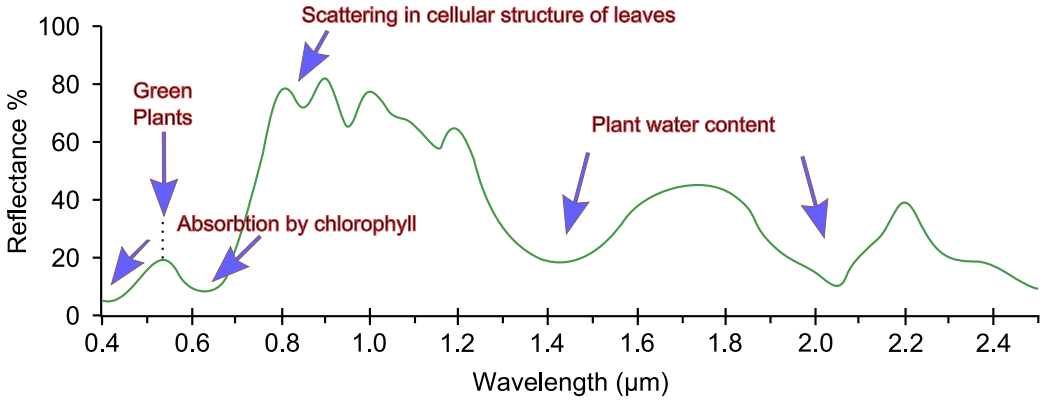

Figure 2.11: A general vegetation spectral signature. It is labeled with the main sections of the EM spectrum which have unique vegetation characteristics. Vegetation is characterised by high reflectance in the NIR region due to scattering in the cellular structure of the leaves. Chlorophyll in plant leaves is responsible for the high absorption in the blue and red regions. Vegetation reflects the most in the green region of the visible spectrum and is the reason we then see vegetation as green. The absorption bands in the SWIR region are affected by the plants water content. Copied and modified from CRISP (2001).

The reflectance of vegetation in the SWIR region (e.g. band 5 Landsat TM) is more varied depending on the types of plant and the plant's water content. Water has strong absorption bands around 1.45, 1.95 and $2.50\mu m$. Outside these absorption bands in the SWIR region, the reflectance from leaves generally increases when the liquid water content of the leaves decreases. This can be seen in figure 2.11 as dips in the curve.

The shape of a spectral reflectance curve can be used for identifying different vegetation types. Even though most vegetation exhibit the above mentioned characteristics of low reflectance in the red region and high in the NIR, these characteristics vary slightly between plants and can be used to identify plant species, leaf moisture content, and plant health. The SWIR region for example can be

used in detecting plant drought stress and delineating burnt areas and fire-affected vegetation (Fiella and Penuelas, 1994). Figure 2.12 shows the spectral reflectance curve for 2 tree types, a maple and a pine. Notice that their spectral signatures are slightly different and that with real data the signatures cover a narrow (or sometimes wide) range of spectral values.

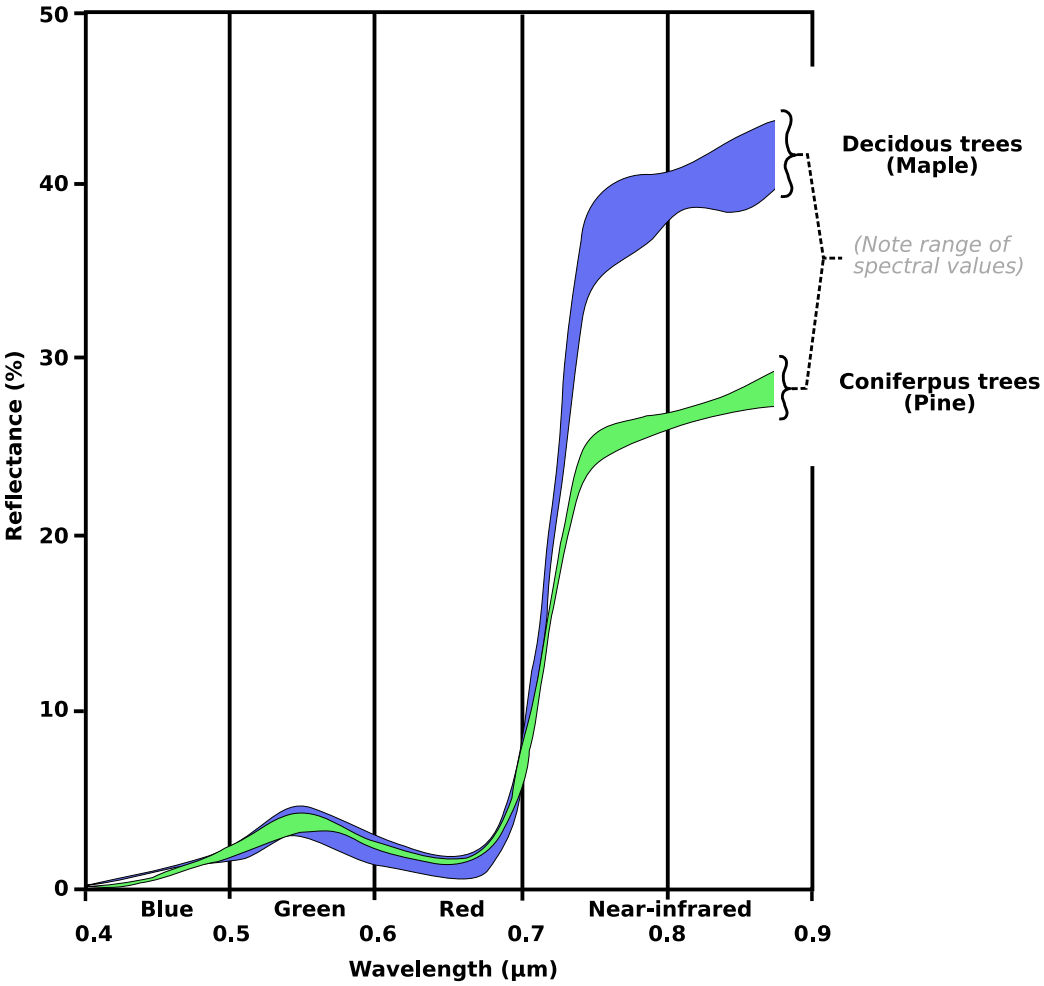

Figure 2.12: Examples of spectral signatures for deciduous maple trees and coniferous pine trees. Notice the small range of spectral reflectance values per curve rather than just a line of data as has been shown by the other spectral reflectance plots. In reality this is how a vegetation type would appear. Copied and modified from Lillesand et al. (2004) with permission from Wiley & sons Inc.

The red edge is a term used to describe the point of maximum slope in the vegetation reflectance spectra. It occurs between the wavelengths 0.68 to $0.75\mu m$, where the reflectance changes from very low in the red region to high in the NIR region. The wavelength and amplitude of this red edge point can be used to determine

chlorophyll content. It has been shown that as the chlorophyll content increases the red edge peak moves to longer wavelengths because the absorption band becomes broader. There is also a strong link between the area of the red edge peak and leaf area index (LAI) or total biomass (Fiella and Penuelas, 1994).

Various mathematical combinations of the red and NIR band have been found to be sensitive indicators of the presence and condition of green vegetation. These mathematical quantities are referred to as vegetation indices and one such index is the normalised difference vegetation index (NDVI). NDVI is a measure of "greenness", whose values range from -1 to $+1$. Vegetated areas will give high values because of their relatively high NIR reflectance and low visible reflectance. In contrast, for example, water, clouds and snow have higher visible reflectance than NIR reflectance, and hence result in negative values. Rock and bare soil areas have similar reflectances in the two bands and hence result in an NDVI value of around 0.

The reason NDVI is such an effective indicator of vegetation because no other land cover has the characteristic high reflectance in NIR and low in red as vegetation does. It has been related to several vegetation phenomena that range from LAI measurement, biomass estimation, percentage ground cover determination, tropical forest clearance, and vegetation seasonal dynamics at global and continental scales. In turn, these vegetation attributes are used in various models to study photosynthesis, carbon budgets, water balance, and related processes (Lillesand et al., 2004; Fiella and Penuelas, 1994). See figures 2.7 and 2.11 for an illustration of typical spectral reflection curves for vegetation and other landcover types.

2.4 Previous Work

Extra examples not included in other chapters from current literature on vegetation mapping using remote sensing imagery are discussed here under central topic headings surrounding this research area.

Advantages of using satellite remote sensing
Since the 1980s satellite monitoring has rapidly become one of the majour procedures for mapping vegetation and is especially useful for large and remotely accessible areas. Satellite monitoring has led to an increase in the number of vegetation maps, also linked to demand, and has made it possible to map vegetation at a continent scale with reasonable accuracy which was almost impossible before (Kalliola and Syrjanen, 1991; Millington and Alexander, 2000).

Issues in vegetation mapping
Millington and Jehangir (2000) discussed some issues faced when trying to map land cover in mountainous terrain:

- shadows caused by sun-topography interactions;
- anisotropic reflectance;
- seasonal snow and ice cover; and
- enhanced cloud cover due to orographic precipitation processes.

The latter two problems can be overcome, to some extent, by choosing satellite imagery with minimal snow, ice and cloud cover. Choosing snow-, ice- (seasonal) and cloud-free images is not always possible because data archives are limited and, even if they are available they may not be from the most optimal parts of the growing season for land cover mapping. Even if imagery free of these problems is acquired, the problem of shadowing remains. In the Venabygd site in this thesis the affect of shadowing is not great. Shadowing can become more of a problem when a multi-temporal approach is used because months with lower sun elevations are incorporated. Millington and Jehangir (2000) corrected for topographic effects using a solar radiation model for their study catchment of the day of image acquisition. Snow, ice and cloud were masked out before topographic correction.

The US National Parks Service (NPS) along with the United States Geological Survey (USGS) are managing a Vegetation Mapping Program (VMP). The mapping protocols developed for these projects principally employ manual interpretation of aerial photography in conjunction with ancillary field data and field observations. These techniques are time consuming and costly and de Colstoun et al. (2003) estimates that it may require up to 50 years to map all NPS park units. These mapping techniques are similar to those of NIJOS and brings to attention again the need for alternative mapping solutions. The goal that de Colstoun et al. (2003) had for their research was also to use satellite remotely sensed data to provide the NPS with a cost-effective, robust, and flexible vegetation mapping approach that would augment the VMP, and which could be potentially implemented at the national level. Landsat Enhanced Thematic Mapper (ETM)+ was chosen because it provided well-calibrated, synoptic, multitemporal imagery for every NPS park unit at a cost of less than 0.03UScents per hectare.

Millington and Alexander (2000) commented on two active research issues relating to vegetation mapping from satellite imagery: firstly, being able to match the type of information received about vegetation canopies by the sensors to the different types of vegetation classification; and secondly, representing the true nature

of vegetation classes or land cover types in a landscape, given the artificial grid imposed upon it due to the way sensors sample upwelling radiance. Most vegetation mapping from satellite imagery relies on simple approaches that reduce the complexity of vegetation canopies, e.g. vegetation indices.

A further issue discussed by Millington and Alexander (2000) relates to mapping the proportion of vegetation or land cover in pixels. Proportional mapping allows the artificial grid-like nature that pixels impose on vegetation maps to be broken down. Techniques for this include spectral mixture modeling, fuzzy classifiers, neural networks and object based classification.

There has been problem issues arising from the use of satellite images for vegetation classification especially when using less than high resolution data. Cingolani et al. (2004) outlined 3 of the major problems that are faced when mapping natural vegetation with mid-resolution satellite images (e.g. 25m Landsat images) through conventional classification techniques.

Firstly, determining the appropriate hierarchical level for mapping. The main goal of traditional vegetation mapping has been the identification of plant communities (repetitive combination of species), or structural types (repetitive combination of growth forms and other terrain attributes). However, when communities or structural types are arranged in the landscape as patches smaller than the pixel size (30x30m) then attempts to map them are hampered. Defining training sites of adequate size may be impossible to find. A more realistic approach for mapping this type of landscape is needed, such as the definition of informational units (land-cover classes based on terrain attributes) at a higher hierarchical level, i.e. as combinations (mosaics) of communities or structural types.

The second problem is also related to the definition of discrete informational units for mapping discernable by the satellite. When the basic components of the units to be defined (e.g. species, growth forms, community types) vary gradually, and to some extent independently, in response to multiple environmental units, mapping must be imposed arbitrarily by the researcher. However, the basic components of the terrain selected by the researcher as variables for performing the classification may not be detected by the satellite. This leads to the definition of informational units that are meaningful for the researcher but cannot be discriminated by the satellite sensor resulting in a time consuming trial and error process.

The third problem is related to the selection of the best representative training sites. Depending on their characteristics, the various spectral signatures ought to be merged, maintained separately or discarded as outliers leading again to a time-consuming trial and error process. To solve these problems ecologically meaningful units as mosaics or repetitive combinations of structural types based

on spectral information were defined.

Grazing vegetation studies
In outfield grazing ecosystems difficulties are likely to appear because of the influence of free ranging grazers combined with natural environmental gradients which often creates complex and heterogeneous vegetation patterns (Cingolani et al., 2004).

Kawamura et al. (2005) used a method of tracking sheep herds with GPS and then used a combination of MODerate Resolution Imaging Spectroradiometer (MODIS) imagery with NDVI to monitor the impact of grazing (combined in a geographic information system (GIS)). This provided useful information about the sustainable use of grasslands suitable for range managers. The relationship between grazing intensities and estimated plant biomass revealed a poor negative correlation, indicating that plant biomass reduced with increasing grazing intensities.

Satellite image information content
Kalliola and Syrjanen (1991) compared the information of different satellite images with ”traditional” vegetation data in three different areas. They looked at the conceptual and practical difficulties which arise in combining vegetation science with the capabilities of satellite remote sensing. Landsat data was used to asses this and it was found that it fails to distinguish many of the vegetation types recognised by the Finnish phytosociological school, though the majour physiognomic categories were for the most part discernible.

Hoersch et al. (2002) notes that satellite classification is capable of differentiating classes on the basis of second level sub-formations and third-level vegetation types. It can also be shown that vegetation types are distinguishable using low spatial resolution sensor data; however that only applies for vegetation covering large areas like montane oak forests. Vegetation that is characterised by a high degree of habitat fragmentation can not be distinguishable using sensor data and related techniques. Using high spatial resolution aerial photographs makes it possible to distinguish between different tree species. The two vegetation maps resulting from the work of Hoersch et al. (2002) with the classification of low and high spatial resolution remotely sensed data, discriminated 20 vegetation classes (included classes for water etc) with the 25m spatial resolution data, and 52 vegetation classes with the 5 m spatial resolution data using a majority filtering technique.

Armitage et al. (2000) looked at the spectral response of vegetation and species composition using airborne remote sensing. The results indicated that the pattern of integrating patches that form semi-natural upland vegetation in Britain should

be spectrally identifiable. The complexity of the relationship between spectral response and vegetation composition meant that detailed floristic descriptions of communities, like those collected from the National Vegetation Classification (NVC), were difficult to identify from remotely sensed data.

For further details on the use and restrictions of remotely sensed data for vegetation mapping see (Ahmad et al., 1992; Chica-Olmo and Abarca-Hernandez, 2000; Wyatt, 2000).

Multitemporal analyses

The use of Landsat scenes acquired at different seasons and/or years to improve land cover classification is not a new concept. Many studies have shown that classification results have improved with the use of multitemporal images rather than single time-shots. Having a reduced number of images however can give large savings in imagery cost and processing effort (Pax-Lenny and Woodcock, 1997). Among many other studies Pax-Lenny and Woodcock (1997) looked at agricultural lands in Egypt for calculating area estimates of non-productive and productive land. They assessed the effects of the number and timing of images on these estimates and found that the average overestimation of non-productive lands in the Nile Delta was around 5% when using a data set of 9 images, but over 300% with a data set containing only 2 images. Generally data sets that included more images from the peak of the growth season resulted in higher accuracies, although in some cases having a mixture of peak and low growth season gave greater accuracy.

Increasingly, advances in the fields of pattern recognition and machine learning have led to the application of decision tree and neural network classifiers, particularly with regards to land cover classifications at global to continental scale. de Colstoun et al. (2003) explored decision tree classifiers for multi-temporal satellite data from the ETM+ instrument to map 11 land cover types in a National Park near Milford, US. They used land cover classes already specified by the National Vegetation Classification Standard at the Formation level. Usage of ETM+ scenes acquired at multiple dates improved the accuracy over the use of a single date, particularly for the different forest types.

Classification

The Maximum Likelihood Classifier (MLC) quantitatively evaluates both the variance and covariance of a set of feature's spectral response patterns when classifying an unknown pixel which is an important quality of this particular classifier. The Minimum-Distance-to-Means classifier for example has problems classifying spectral classes that are close to one another in the measurement space and have high variance. The Parallelepiped classifier is sensitive to this category variance,

however it has problems dealing with spectral patterns that are highly correlated, this is a problem in classification with many classifiers (Lillesand et al., 2004).

Decision tree classifiers, for example, have been preferred to statistical classifiers for coarse-scale applications because they do not make any implicit assumptions about normal distributions in the input data, as a MLC would. Decision trees have been used in the global land cover classification algorithm for the MODIS (de Colstoun et al., 2003).

Decision tree classifiers successively partition the input training data into more and more homogeneous subsets by producing optimal rules or decisions, also called nodes, which maximises the information gained and thus minimises the error rates in the branches of the tree. These classifiers can also accept a wide variety of input data, including non-remotely sensed ancillary data, and in the form of both continuous and/or categorical variables. Decision trees have been shown to provide improved accuracies over the use of other more traditional classifiers however despite these proven benefits, the use of decision trees for applications with high spatial resolution data such as Landsat Thematic Mapper (TM) and ETM has not yet fully been explored (de Colstoun et al., 2003).

Hoersch et al. (2002) reported that advantages using an object-based technique arose especially for the indication of single dwarf shrub plants and agglomerations of species at their upper elevation limit. The extraction of nearly circular patches of dwarf shrubs was simplified in the object-based approach by the integration of object shape, compactness, texture and context/topology besides the raw spectral characteristics of traditional per-pixel classification.

An alternative approach in investigating vegetation canopies from remotely sensed data is to develop mathematical models of the interaction of electromagnetic radiation with the canopy (Millington and Alexander, 2000). An additional alternative method for classification of vegetation communities in Australia by (Lewis, 1998).

Kalliola and Syrjanen (1991) notes that manual interpretation of digitally enhanced images is superior to supervised classification procedures in many botanical works, because the former is free from operator-defined classes which may not necessarily be representative.

Cingolani et al. (2004) used firstly an enhanced MLC (done by analysing objective ways of selecting the best training sites) and secondly using Discriminant functions directly obtained from the statistical analysis of spectral signatures. Their study was carried out in a heterogeneous mountain rangeland in central Argentina using Landsat data and 251 field sampling sites. The comparison through field validation of both methods for mapping units showed that classification based

on Discriminant Functions produced better results than the traditional Maximum Likelihood method (accuracy of 86% vs. 78%)

Chapter 3

Data Sets

3.1 Satellite Images

Certain factors need to be taken into consideration when choosing which satellite sensor to use. These include spatial, spectral, temporal, and radiometric resolution, and not to mention price and availability. Optical satellite sensors were the most appropriate for this project as they have spectral resolutions that cover the visible and infrared bands which are good for detecting different vegetation types. The satellite would need to orbit over the study often as often as possible in order to acquire a good image from spring, summer, and autumn. The ideal satellite sensor for an individual application does generally not exist however, and compromises usually need to be made. Possible satellites for this project include Landsat and SPOT.

The Landsat satellite with both the Thematic Mapper (TM) and Enhanced Thematic Mapper (ETM)+ sensors on board was chosen for several reasons. Firstly because the Spot satellite with its High Resolution Visible (HRV) and High Resolution Visible IR (HRVIR) detectors only have multispectral bands covering the equivalent of green, red, near infrared (NIR) and short wave infrared (SWIR) (20m resolution). SPOT 4 satellite also has a low-resolution wide-coverage vegetation instrument however this product comes with $1km$ resolution which is too coarse for this project. The sensors TM and ETM+ on board the Landsat satellite however cover in addition the blue and Mid Infrared (MIR) bands. Secondly the Landsat satellite images are sold ”at cost” where as the SPOT satellite is a commercial venture and each image is sold from around $US\$1 - 10,000$ (USGS, 2006). Thirdly, the Norwegian Computing Centre already had a large archive of

Landsat images available.

Landsat 5 and 7, launched in 1984 and 1999 respectively are currently the only two operational Landsat satellites. The Landsat satellites are travelling in sun-synchronous orbits at an altitude of approximately 705 km, with a period of around 100 min and a repeat cycle of 16 days. On board Landsat 5 are two earth observation sensors the Multispectral Scanner (MSS) and TM, and on board Landsat 7 is the ETM+. Table (3.1) gives the wavelength bands and resolutions for Landsat TM and Landsat ETM+, the two sensors used in this thesis. For reference see the electromagnetic (EM) spectrum diagram in the background chapter, section 2.3.1. The original scene sizes were approximately 170 x 183km.

In a study by Clark et al. (2001) a comparison of satellite systems for mapping plant communities was done between Landsat TM and SPOT HRV. A Maximum Likelihood Classifier (MLC) was used to classify 6 native and 2 non-native inter-mountain plant communities in Reynolds Creek in western US. When results were compared to ground reference points, the overall accuracy of the maps generated by SPOT and Landsat were statistically similar. de Colstoun et al. (2003) decided on using Landsat ETM+ for mapping vegetation in US National Parks (aiming at a solution for national mapping) because it provided well-calibrated, synoptic, multitemporal imagery for every National Parks Service (NPS) park unit at a cost of less than 0.03 US cents per hectare.

Sensor	**Bands**	**Wavelength (μm)**	**Resolution (m)**
Thematic Mapper (TM)	Band 1	0.45-0.52	30
	Band 3	0.63-0.69	30
	Band 4	0.76-0.90	30
	Band 5	1.55-1.75	30
	Band 6	10.40-12.50	120
	Band 7	2.08-2.35	30
Enhanced Thematic Mapper (ETM)+	Band 1	0.45-0.52	30
	Band 2	0.53-0.61	30
	Band 3	0.63-0.69	30
	Band 4	0.78-0.90	30
	Band 5	1.55-1.75	30
	Band 6	10.40-12.50	60
	Band 7	2.09-2.35	30
	Band 8	0.52-0.90	15

Table 3.1: Wavelength regions and resolution corresponding to each original Landsat band for the TM and ETM+ sensors. (USGS, 2006).

The ideal dataset would have a cloud- and snow free image from spring, summer and autumn in order to cover the differences in the growing season. Trying to find a cloud free image over the mountains in Norway on the right date, however, is a

challenging exercise. Although the Landsat satellites can produce images over the same region every 16 days, the largest number of acceptable images found for the extended mountain area around Venabygd for a particular season was three. Even finding one clear image in an entire growing season was sometimes not possible, so collected images over several years were obtained. Table 3.2 lists the images used.

The scenes stem from various Landsat imagery providers, common to them all is that they were acquired in the L1G format as specified by the Landsat 7 Science Data Users Handbook, see NASA (2006). In this format the Landsat data are radiometrically and systematically corrected. Although the L1G products are georeferenced, the georeferencing applied was not based on the use of ground control points and typically resulted in residual positional errors on the order of 250m. This was unacceptable and manual georeferencing was done to improve this. This georeferencing was performed using ERDAS Imagine (version 8.7, by Leica Inc.). Ground control points were selected in the uncorrected images and were matched with points of known position and altitude in a water mask (water mask based on the M711 series of maps). The water mask was made by The Norwegian Mapping Authority and used in conjunction with a 25m resolution digital elevation model (DEM) (also made by the Norwegian Mapping Authority). The images were geometrically corrected to the UTM coordinate system (zone 32) using the WGS84 datum (a global reference frame for the earth defined by the World Geodetic System). Geo-referencing was necessary in order to establish a correspondence between the satellite image pixels and the physical positions on the earths surface (Aurdal et al., 2005b).

A warping and interpolation was then performed using the bilinear interpolation approach, in the resulting image the geographic position of the upper left pixel was known and coincided with a fixed 25m grid so as to allow for easy comparison between files (e.g. the 25m DEM). The residual error in these corrected images was on the order of 25m. In the L1G product, the contents of all spectral channels were represented as 8 bit digital numbers (range 0 to 255). Before using the images, these digital numbers were scaled back to 'at satellite radiance' (asr) values. This procedure is described in Chander and Markham (2003) and NASA (2006) for the Landsat TM and ETM data respectively.

A copy of the images was then converted to reflectance values using the calibration process described in Chander and Markham (2003) for converting Landsat radiance values to reflectance values. The images were also clipped to cover only the Venabygd area. All the pre and post processing of the images described here was done by the Norwegian computing centre (NR) in connection with other projects (Aurdal et al., 2005b).

Sensor	Date	Path	Row	Geometric correction	Resolution
TM	24.07.1994	198	17	UTM 33	25m
TM	25.06.1995	198	17	UTM 33	25m
TM	17.08.1997	198	17	UTM 33	25m
TM	29.07.1999	199	17	UTM 32: reprojected to 33	25m
ETM+	18.10.1999	198	17	UTM 33	25m
TM	23.05.2004	199	17	UTM 33	25m

Table 3.2: An overview of the Landsat TM and ETM+ images that were used in this thesis, along with their attributes. The wavelengths for each band of the TM and ETM sensors are described in the table above.

3.2 Digital Elevation Model

A 25m raster (i.e. grid) DEM made by "©Statens Kartverk", the National Mapping authorities, was made available by the University of Oslo. It had UTM coordinate system, zone 32-33 for all of Norway, and was made using the WGS84. The DEM was made in 2001-2002. It was made from a combination of 20m interval contour data from the 1:50,000 map series and height points from lakes, rivers, and roads. The DEM was originally created in a triangular irregular network (TIN) format and then interpolated into a raster (grid) format with 25m resolution. The elevation accuracy of the model is around 5-6m, although this varies with the slope and aspect. The smoother the slope, for example, the greater the height accuracy. The area corresponding to that of the satellite images and the Venabygd study area was clipped out of the main image (UTM zone 32).

3.3 Ancillary Data

Road networks, tractor networks, river networks, contour lines, lakes, housing locations, council borders and areas, were used as additional vector layers. These vector layers were obtained from Statens Kartverk (Norwegian state Mapping authorities) available through the University of Oslo. They were part of the N-50 series of SOSI standard maps for the Oppland County, Ringebu Community area. They had UTM zone 32 coordinate system using EUREF89 / WGS84 models. The contour lines had 20m intervals.

3.4 Aerial Photographs

The Aerial photos used were bought by the Norwegian Computing Centre from Terratec. They belong to series number 11833. Images A: (2, 3, 4, 5, 6, 7) B: (4, 5, 6, 7, 8, 9, 10), C: (4, 5, 6, 7, 8), and D: (5, 6, 7, 8, 9) were used. They were in paper format with an approximate scale of 1:22,000. The images are taken in infrared colour film and were all taken on the 25th of June 1995. This series was chosen because it had information from the infrared region and because it was closest in date to the main satellite image dated 24th July 1994.

3.5 NIJOS's Mapping Methods

The Norwegian Institute for Land Inventory (NIJOS) has mapped the vegetation of a $160km^2$ area of the Venabygd mountain area in Ringebu Community in Oppland county. The mapping was conducted using methods defined by NIJOS for mapping at a scale of 1:50,000. The vegetation map comes with 6 separate thematic maps on grazing animals (sheep, cattle, and reindeer), grazing impact, and species diversity. The map data over Venabygd will be used as the ground reference data for analyses and classifications made for mapping outfield grazing areas and their quality using satellite data.

The Vegetation mapping methods used by NIJOS was a combination of visual inspection in the field and analysis of aerial photos using colour and texture recognition as well as ecological knowledge. A stereoscope was used to look at the air photos in 3 dimensions and correct for errors in the image (from different photographic angles and flying heights). The field work for the Venabygd map was done in 2001. The field registrations, borders and signs were drawn on aerial photos from 1992 (series 11438 in scale 1:40,000) and digitised from the photos with the use of an analytical stereo-instrument. The topographic base for the map came from the National Mapping Authority's N50 map series. General overview maps are, more often than detailed maps, based on more use of binoculars for vegetation classification. On average a general overview map will have field workers working at aprox. $3km^2$ per day in forest landscape and $5km^2$ in mountains terrain, with a detailed map this is decreased to aprox. $0.5 - 1km$ per day (Bryn and Rekdal, 2002). The Venabygd vegetation map is an overview map.

Vegetation Attributes
The Venabygd area is divided into areas that have each been given a vegetation type. The definition of a vegetation type is a characteristic grouping of species

which find themselves in places with similar growing conditions. Many species appear therefore in more than one vegetation type. These species have a broad ecological living area but their abundance varies from perhaps the dominating species in a vegetation type to scarce in another. Other species are sensitive to certain environmental factors and can be an indicator to environmental conditions in an area. When the extensiveness of a vegetation type is mapped the dominant species and indicator species are used as the mapping features.

NIJOS uses two systems to map vegetation depending on whether the map is a detailed map ($1 : 5,000 - 20,000$) or an overview map ($1 : 50,000$). Larsson and Rekdal (1997) describes the methods used for overview mapping. The identification of vegetation types in an overview map is built more on the physical appearance of the vegetation, i.e. how it is distinguished or characterised by dominating species or species groups. The system divides the vegetation types into 10 groups. Under these there are 45 defined vegetation types and 9 land cover types. There are additional attributes in the form of symbols assigned for important information about the type definition, for example, % coverage of bare rock. When counting all the combinations of vegetation classes and attributes as unique, the Venabygd area has 362 unique labels of vegetation (Bryn and Rekdal, 2002).

In appendix B there is an excerpt from the attribute table of the Venabygd vector layer. It shows the attributes associated with each polygon. These include; area, perimeter, the dominant vegetation type (Veg1), the secondary vegetation type (Veg2), first additional attribute, second additional attribute and the map sign associated with that polygons vegetation type. An example is $2cx/2ex$, where $2c$ is the dominant vegetation type, x is the first additional attribute for this dominant vegetation type, 2e is the secondary vegetation type, with the x as an additional first attribute (they can also have secondary attributes). A secondary vegetation type is only named if makes up more than 25% of the area inside the polygon. The symbols for each vegetation class and their names are shown in figure 3.3 along with their percent coverage of the Venabygd area. The additional attribute symbols and their meanings are shown in appendix B.2. For a further description of these vegetation types see Bryn and Rekdal (2002).

Grazing Quality Map

At the moment NIJOS's only way of systematically mapping the outfield grazing quality is by assigning already mapped vegetation categories with a grazing quality category. Three categories are used to categorise the different grazing qualities for sheep and cattle; Less good (MG) (*Mindre godt*), Good (G) (*Godt*) and Very

	Vegetasjonstype	Dekar	%	Sau beitekvalitet
1b	*Grassnøleie*	196	0.1	*Godt*
2b	*Tørrgrasheier*	634	0.4	*Mindre Godt / Godt*
2c	*Lavhei*	18200	11.15	*Mindre Godt*
2d	*Reinrosehei*	179	0.1	*Godt-Mindre / Godt*
2e	*Rishei*	34798	22.1	*Godt*
3a	*Lågurteng*	388	0.2	*Svært Godt*
3b	*Høgstaudeeng*	2311	1.5	*Svært Godt*
4a	*Lav- og lyngrik bjørkeskog*	2773	1,8	*Mindre Godt*
4b	*Blåbærbjørkeskog*	36543	23.2	*Godt*
4c	*Engbjørkeskog*	3801	2.4	Svært *Godt*
4e	*Oreskog*	395	0.3	*Svært Godt*
4g	*Hagemarkskog*	415	0.3	*Svært Godt*
6a	*Lav- og lyngrik furuskog*	1202	0.8	*Mindre Godt*
6b	*Blåbærfuruskog*	580	0.4	*Godt*
7a	*Lav- og lyngrik granskog*	2358	1.5	*Mindre Godt*
7b	*Blåbærgranskog*	20623	13.1	*Godt*
7c	*Enggranskog*	4926	3.1	*Svært Godt*
8c	*Fattig sumpskog*	230	0.1	*Mindre Godt*
8d	*Rik sumpskog*	664	0.4	*Godt*
9a	*Rismyr*	7307	4.6	*Mindre Godt*
9b	*Bjønnskjeggmyr*	39	0.0	*Mindre Godt*
9c	*Grasmyr*	9185	5.8	*Mindre Godt / Godt*
9d	*Blautmyr*	947	0.6	Mindre Godt
9e	*Storr- og takrørsump*	247	0.2	*Mindre Godt*
11a	*Dyrka mark*	4935	3.1	
11b	*Beitevoll*	1760	1.1	*Svært Godt*
12b	*Ur og blokkmark*	1355	0.9	
12c	*Bart fjell*	448	0.3	
12d	*Bebygd areal, tett*	44	0.0	
12e	*Bebygd areal, Åpent*	118	0.1	
12f	*Anna nytta impediment*	147	0.1	
	Sum landareal	157813	100	
	Vann	3618		
	SUM TOTALT AREAL	161431		

Table 3.3: Vegetation types and their codes in the Venabygd area. The percentage of area coverage is listed and the type of grazing quality the vegetation type has for sheep. *Mindre Godt* = Less Good, *Godt* = Good, and *Svært Godt* = Very Good. Information from Bryn and Rekdal (2002).

Good (SG) (*Svært godt*). Figure 3.3 indicates the general grazing class for each vegetation class when not considering additional attributes.

The production of grazing plants varies a lot with growing conditions, and the nutrient content varies depending on which plant species are available, their growing

location, and harvesting time. Both production and nutrient content area important and measurable factors. The degree of utilisation is less easy to measure because it is largely associated with the particular grazing habits of the different animal species. The animals choice of grazing plants and areas are affected by factors such as access availability, distribution of vegetation in the peak growing season, vegetation diversity, grazing press, time of the year, weather conditions, shelter possibilities, and position of salt stones etc.

The assigning of grazing quality classes is a complex evaluation much of which is built on the knowledge of the analyst. The grazing quality results for each vegetation type were controlled by 3 factors (Bryn and Rekdal, 2002).

- Production of grazing plants (kg dry stuff per 1/4 acre)
- Nutrient content (feeding units per kg dry mass)
- Degree of utilisation (how large a part of the plant mass, gets taken up by the animals)

The grazing value was evaluated from ”normal” plant cover i.e. the potential value without the influence of previous grazing. From the vegetation map, grazing maps are made as discussed. The grazing quality assignment is based on the information in the vegetation map. Each vegetation type has a presumed grazing quality but with the addition of extra attributes this grazing quality can change e.g. areas with more than 50% open rock will have their grazing quality reduced. The grazing quality of the vegetation will of course vary throughout the season. Figure 2.5 shows the spread of these grazing classes over the Venabygd area as mapped by NIJOS.

Sources of Error in the NIJOS Data

The mapping system in scale 1:50,000 is a compromise between; the type of information one wants the map to show, how much the mapping itself will cost, and what is cartographically possible to display. The map should mirror the ecological relationships and properties as best as possible, but at the same time, the mapping should be completed at a pace that is economically feasible. Access to areas in the field also limits the mapping capabilities. The vegetation types are therefore often identified from certain criteria that can be recognised on an aerial photograph or with a pair of binoculars. The vegetation boundaries are as a rule gradual changes

from one type of vegetation to another, and the vegetation can be in a detailed mosaic pattern which is very difficult to map.

The cartography drawing method is complicated and contains the copying or movement of lines and figure signatures several times. For a detailed map this could be a potential source of error and sets large responsibility for routine checking and reading. Some vegetation types can lead to problems during classification (e.g. boundary definition). This is commented on in the detailed descriptions of each vegetation type in Bryn and Rekdal (2002).

All the problems that the cartographer meets can not necessarily be solved through a set of standard rules and must therefore be solved in a subjective manner. The vegetation analyst's assignment is then to determine the most dominating vegetation category for which to map. Detailed analyses of the polygons and borders without these issues in mind will lead to errors.

Chapter 4

Methods

4.1 Initial Class Separation

A flow diagram for the procedure followed during the initial class separation analyses is shown in figure 5.2.

4.1.1 Spectral Distribution

Grazing classes
The Venabygd vector layer containing attributes of vegetation type and grazing quality was used as an overlay to the satellite images. Figure 4.1 illustrates how the data values for each grazing class were extracted in order to plot the spectral distribution curves for each class. New vector layers were created in Envi 4.2 for each grazing class by doing an attribute query and creating a new vector from the resulting selection. Each of these vector layers were converted to singular region of interest (ROI) files (connected to one satellite image) which enabled the pixel values within each grazing class to be extracted and exported. The ROI files contained a list of all pixel values within the ROI, i.e. inside all polygons of a sheep class. The ROI files do contain any information about which polygon a pixel value was connected to or its position. The data was imported into Matlab for statistical and graphical representation. This procedure was done for 4 of the grazing quality classes: Less Good, Good, Very Good and Impermeable and in connection to 6 satellite images (with 6 radiometric bands each) ranging from Spring to Autumn.

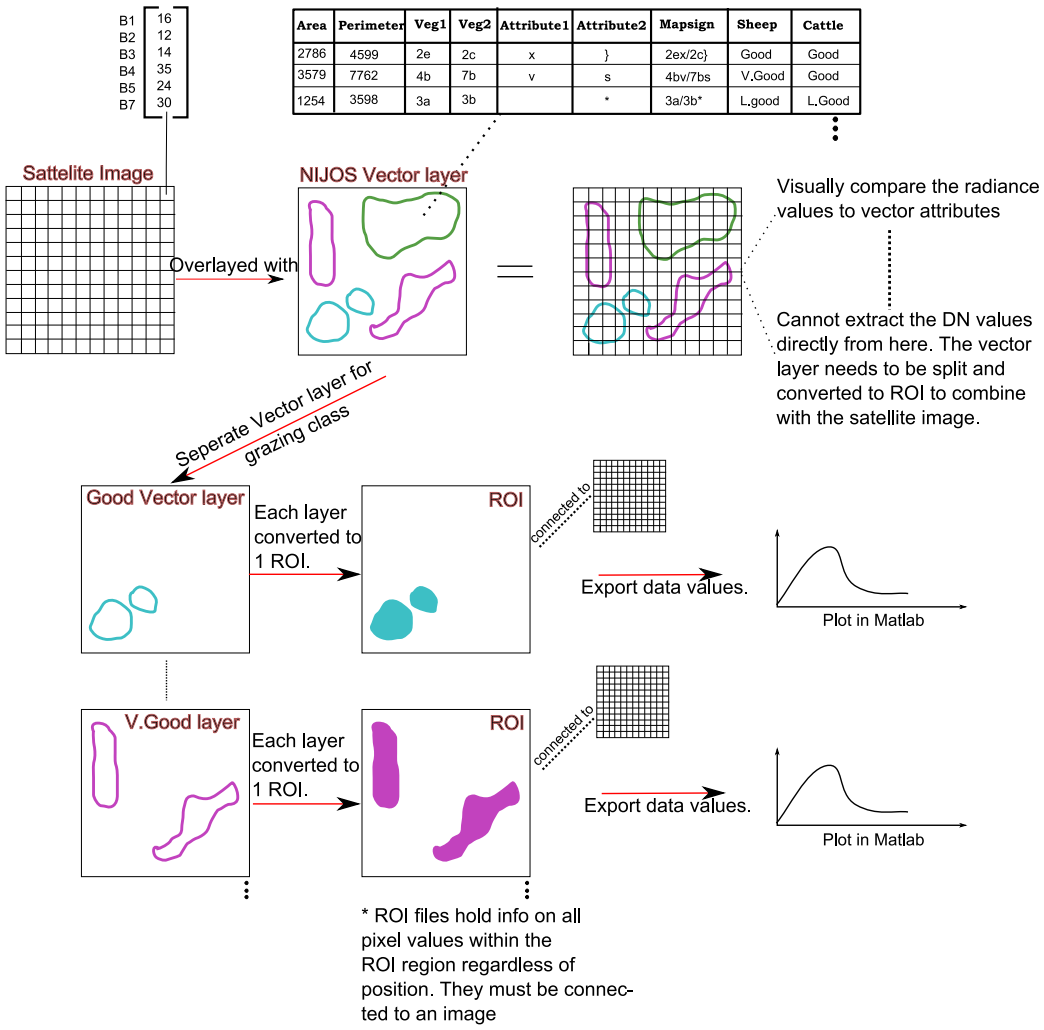

Figure 4.1: An illustration of the procedure used to extract the pixel data within a selected group of vector polygons of a certain grazing or vegetation class. The vector layer was overlaid onto a satellite image to give a visual impression of the radiance values within each polygon. In order to extract the data however, each grazing (or vegetation) class had to be selected through attribute queries on the main vector file and new vector layers made from each selection. These vector layers were then converted to ROI which were connected to the satellite image and contained the values for all pixels within the defined ROI area. The ROI values were exported and imported into matlab for graphical representation.

Vegetation classes

Plotting the spectral distribution of the vegetation classes followed the same procedure as for the grazing classes, see figure 4.1. A vector layer for each vegetation 1 class (i.e. the main classes) was created and then each layer converted to one ROI. In the Venabygd area there are 33 defined main groups of vegetation ranging

through alpine grasses, meadows, pines, spruce, marsh & moor lands, and birch.

4.1.2 Statistical Separation Algorithms

The ROI separation algorithms used were Jeffries-Matusita (JM), and Transformed Divergence. They are incorporated into Envi 4.2 software and give a statistical measure of separability between ROI pairs. Their values range from 0 to 2.0. Values greater than 1.9 indicate that the pairs have statistically good separation (ENVI, 2003). The following algorithm explanations closely follow the work from Richards (1986).

Statistical separation algorithms are an attempt to quantify the separation between a pair of probability distributions (as models of spectral classes) and their degree of overlap. The distance between the means of two distributions is an insufficient measurement, as overlap is also influenced by the standard deviations of the distributions. A combination of both the distance between means, and a measure of standard deviation is required. These must be vector-based measures to be applicable to the multidimensional subspaces in satellite images.

Jeffries-Matusita Distance

The JM distance, also known as Bhattacharrya distance, between a pair of probability distributions (spectral classes) is defined as: (Richards, 1986)

$$J_{ij} = \int_x \left\{ \sqrt{p(x|\omega_i)} - \sqrt{p(x|\omega_j)} \right\}^2 dx \tag{4.1}$$

where, $p(x|\omega_i)$ and $p(x|\omega_j)$ are the values of the two class probability distributions i and j at a position x. J_{ij} is the JM measure of the average distance between the two class density functions. For normally distributed classes this becomes:

$$J_{ij} = 2\left(1 - e^{-\alpha}\right) \tag{4.2}$$

in which

$$\alpha = 1/8(m_i - m_j)^t \left\{ \frac{\Sigma_i + \Sigma_j}{2} \right\}^{-1} (m_i - m_j) + 1/2ln \left\{ \frac{(\Sigma_i + \Sigma_j)^{1/2}}{|\Sigma|_i^{1/2} |\Sigma|_j^{1/2}} \right\} \tag{4.3}$$

where, m_i and $\sum_i$ are the mean and covariance of $p(x|\omega_i)$. m_j and $\sum_j$ are the mean and covariance of $p(x|\omega_j)$.

The first term in α (eq: 4.3) is akin to the square of the normalised distance between the class means. The presence of the exponential factor in equation 4.2 gives an exponentially decreasing weight to increasing separations between spectral classes. If this is plotted as a function of distance between class means, it shows a saturation behaviour, not unlike that expected for the probability of correct classification, see figure 4.2.

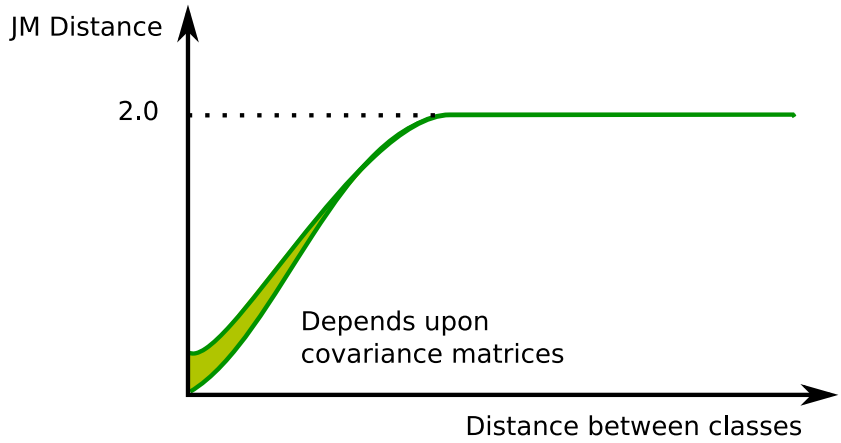

Figure 4.2: Jeffries-Matusita distance as a function of separation between spectral class means. The JM distance measure gives an exponentially decreasing weight to increasing class separations. When plotted it shows a saturating behaviour not unlike that expected for the probability of correct classification. Copied and modified from Richards (1986).

The JM distance approaches 2 asymptotically as the distances between classes increase. A JM distance of 2.0 between spectral classes would imply classification of pixel data into the 2 classes, (assuming there were only two) with 100% accuracy. This saturating behaviour is highly desirable (Richards, 1986).

Transformed Divergence

The Transformed Divergence is a modification of simple divergence (eqn: 4.4).

$$d_{ij}^{T} = 2\left(1 - e^{-d_{ij}/8}\right) \tag{4.4}$$

It has an exponential character which will have a saturating effect with increasing class separation, as the JM distance does. It is computationally more economical

and has been shown to be considerably better than simple divergence and is almost as effective as the JM distance measure (Richards, 1986). Because the JM distance is considered slightly more accurate it will be weighted higher in results discussion.

4.1.3 Composite Images

A layer stacking function in Envi 4.2 was used to combine 3 images from spring, summer and autumn. All images had the same co-ordinate system. No atmospheric or topographic correction was performed on the images before stacking.

4.1.4 NDVI

NDVI is a measure of ”greenness”. Equation 4.5 shows the simple mathematical expression to derive the normalised difference vegetation index (NDVI) using the near infrared (NIR) and red bands of a satellite image. The band ratio nature of the equation helps to compensate for changing illumination conditions, surface slope, aspect, and other extraneous factors (Lillesand et al., 2004). NDVI was calculated for the reflectance image of 24.07.94, and the values for each grazing class was plotted.

$$NDVI = \frac{NIR - RED}{NIR + RED} \tag{4.5}$$

4.2 Image Variation

The Image variation group of analyses takes a closer look at the dataset to understand what is varying, where, and why. The procedure for this group of analyses is outlined in the flow diagram in figure 5.11 and 5.16.

4.2.1 Polygon Variation

The procedure used to extract the pixel values within each polygon of a vegetation class is similar to that shown in figure 4.1. However, with only 1 ROI for a whole vegetation class there is no information in the ROI file to indicate which polygon

the pixel values came from. In order to accommodate for this an ROI for each polygon within each vegetation class must be made, see figure 4.3. Due to the time consuming nature of this process, the procedure was only carried out for 8 of the 33 vegetation classes.

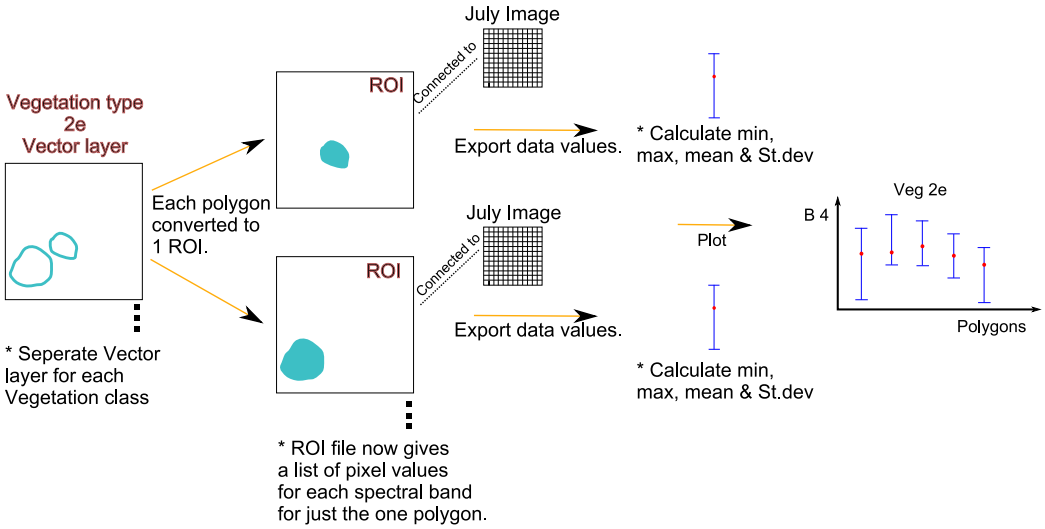

Figure 4.3: Procedure for extracting all the pixel values for each polygon separately and plotting their min, max, mean and standard deviation in order to analyse the between and within polygon variation in a single vegetation class.

4.2.1.1 Buffering

The original idea for negative buffering was taken from one of the basic mathematical morphology operations, erosion. The effect of this operator on a binary image is to erode away the boundaries of regions of foreground pixels (i.e. white) so that the areas of foreground pixels shrink in size, and the holes within those areas become larger (Soille, 2003).

ArcGIS AcrMap 9.1 was used to perform negative buffering i.e. inward area buffer on the vector layers. The vector layers for the individual vegetation classes were buffered by $-50m$ and $-75m$ separately. The two lengths were chosen for comparison.

Figure 4.4 shows an illustration of how negative buffering works around each polygon, the purple border indicates the area that is being taken away from the polygons, and the yellow areas show what remains of each polygon. Once the buffers were determined the new buffered layers were added to the satellite image layers and the values within each polygon extracted (for procedure see figure 4.3).

The data for the buffered polygons were plotted in the same manner as in the figure 4.3.

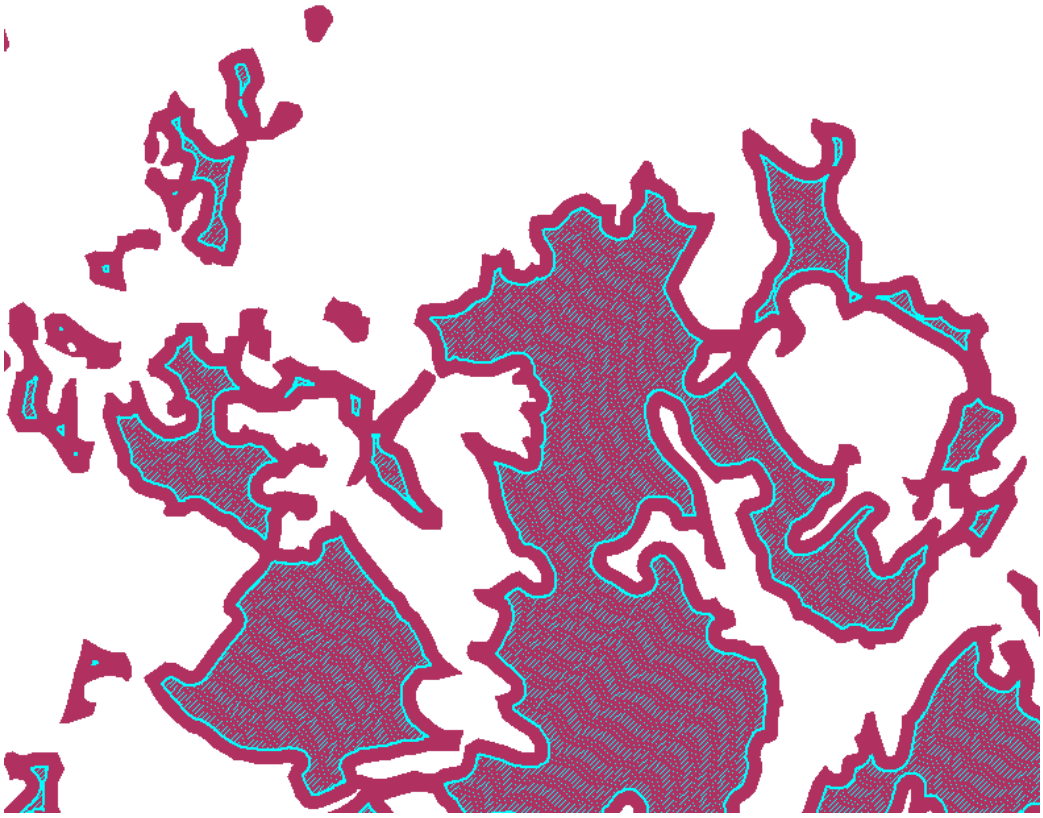

Figure 4.4: An example of buffering. Buffering is normally done to increase the border of an area to include its surroundings but here a negative buffering has been used to reduce the size of the polygons by 50m from all edges. This example is of the vegetation class 4b. The original polygons are in maroon and the new buffered polygons are shown in turquoise. Note that some of the polygons were too small to cope with a buffering of 50m, and nothing was left of them (i.e. just maroon coloured). Negative buffering was done to reduce the affect from neighbouring vegetation types. Buffering was also done at -75m for all polygons for comparison. This eliminated too many polygons however.

4.2.1.2 Measurement Space

The vector layers containing the polygons buffered by -50m were used for this step. These polygons had gone through a secondary selection process to exclude any polygons that had secondary vegetation types or additional attributes. This was done to select the most pure representation from each vegetation class. The buffered vector layers were converted to raster grids in ArcGIS 9.1 using the *Fea-*

ture to Raster tool. This tool converted the polygons into pixels, with each pixel representing a certain main (i.e. Veg1) vegetation code. The vector layer contained many columns of information of which only one could be used in the raster layer. A new field (i.e. new column) was added to the vector layer. Using the calculate values tool a numerical code was added to represent the main vegetation types (i.e. Veg1). This was the data that appeared in the raster layer. The satellite image and the vegetation grid were then joined together to form one raster and this was done using the *combine* tool. For example, having 2 input rasters, the combine tool gives an output with 4 columns. The first is a value column giving a value number (e.g. 1-10) for each unique combination that occurs between the two rasters. The second column gives the count, i.e. the number of times the unique combination has occurred. The last two columns give the values of the combination e.g. 4 & 5, or 6 & 5. Having this dataset made it possible to then plot the individual pixel values within each vegetation class in scatter plots of different band combinations.

4.2.2 Terrain Variation Calculations

4.2.2.1 Elevation

Elevation was extracted from a 25m raster digital elevation model (DEM) over the Venabygd area and was used to compare elevation to the reflectance values of pixels in an image. The DEM values were exported and imported to Matlab along with the reflectance data from the image (process described in figure 4.1). Scatterplots showing the relationship between one band of data and elevation for 2 vegetation types at a time were drawn.

4.2.2.2 Slope and Aspect

Slope is the steepness of gradient of a unit of terrain represented by the DEM at any given point, and is made up of two components: (1) gradient, the maximum rate of change of altitude; and (2) aspect, the compass direction in which the unit of terrain faces (Huggett and Cheesman, 2002). Algorithms in Envi 4.2 were used to calculate both aspect and slope. Aspect is expressed in positive degrees from $0°$ to $359.9°$, measured clockwise from north. Pixels in the input raster of zero slope (i.e flat) were assigned an aspect of -1. The slope was measured in degrees with the convention of 0 degrees for a horizontal plane (ENVI, 2003). The 25m raster DEM over the Venabygd area was used to calculate the slope and aspect angle for

every pixel.

Slope and aspect were calculated using a 3 x 3 window that passed over the DEM to determine a *best fit tilted plane* for the pixel at the center of the window. This allows the calculation of constants for the equation:

$$z = a + bx + cy \tag{4.6}$$

where z = height at the point of interest (the centre of the window), (x,y) = co-ordinates of the point at the centre of the window, and a, b & c are the constants. The slope and aspect for the centre cell can then be calculated (S = slope, A = aspect) using the formulae (Wood, 1996):

$$S = b^2 + c^2 \tag{4.7}$$

$$A = \tan^{-1}\left(\frac{c}{b}\right) \tag{4.8}$$

The raster layers slope, aspect, elevation, satellite image, and vegetation raster were combined together using the procedure described in section 4.2.1.2. This created a dataset that could be used for creating polar plots (in Matlab) to represent the relationship between aspect, slope, elevation, reflectance value and vegetation class. Hence, the dataset created here, was set up such that each row represented a unique combination of elevation, aspect, slope and reflectance values for each band with its number of occurrences in the count column. The vegetation raster contained a numerical code for each of the vegetation 1 classes, and the aspect and slope values were converted to integer values before the combination.

4.2.3 Atmospheric Corrections

It was not considered necessary to conduct an atmospheric correction on any images. Most analyses were conducted with only a single date image, see results section 5.3.2.3 for further description.

4.2.4 Topographic Corrections

An ideal slope-aspect correction removes all topographically induced illumination variation so that two objects having the same reflectance properties show the same

digital number despite their different orientation to the sun's position. The c-correction and the cosine topographic correction methods were the two used. The following closely follows Teillet (1986) and Meyer et al. (1993). The calculations for both methods were performed in matlab. The slope and aspect raster layers were derived in Envi4.2 using a 25m DEM over the area (see section 4.2.2.2 for procedure). The suns elevation angle and azimuth were given in the satellite image header information. The sun's zenith angle is calculated by subtracting the sun's elevation angle from 90. Topographic corrections were performed on one summer image dated 24.07.1994.

Cosine Correction Method

The amount of irradiance (radiation from the sun) reaching a sloping pixel is proportional to the cosine of the incidence angle i, where i is defined as the angle between the normal of the pixel in question and the zenith direction (the sun in this case) see figure 4.5. The cosine law takes the sun's position into account in the form of the sun's zenith angle (sz), but assumes the solar constant and the distance between the sun and the earth to be constant for all scenes. In this thesis an image from only one time period was used so the assumptions were correct.

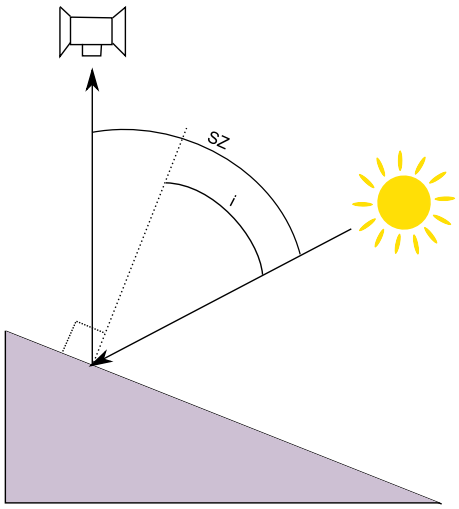

Figure 4.5: Diagram illustrating how the solar zenith angle (sz) and incidence angle (i) are measured. The inclined slope can be thought of as the earth's surface, with the satellite directly in the zenith and the sun at some other angle. Copied and modified from Teillet (1986)

The cosine correction is a strongly trigonometric approach based on a basic physical law assuming Lambertian reflection characteristics of objects and neglecting

the presence of an atmosphere. The cosine correction is represented by the following equations:

$$Lh = Lt\frac{\cos(sz)}{\cos(i)} \tag{4.9}$$

$$\cos(i) = \cos(sz)\cos(slope) + \sin(sz)\sin(slope)\cos(azimuth - aspect) \tag{4.10}$$

where, Lh = the radiance observed for a horizontal surface (i.e. the new corrected value), Lt = radiance observed over a sloped terrain (i.e. original value,,) sz = sun's zenith angle, and i = sun's incident angle in relation to the normal on a pixel.

The cosine correction method only models the direct part of the irradiance. In reality regions which are weakly illuminated by direct sunlight, receive a considerable amount of diffuse irradiance. In such areas, the cosine correction has a disproportional brightening effect (because the diffuse radiation is not taken into account). The smaller the $\cos(i)$ (Eq. 4.10), the stronger this over-correction is. For pixels in complete self-shadow (i.e. when $\cos(i) = 0$), and in faintly illuminated areas, the digital numbers (DNs) saturate and lead to artifacts in the corrected image.

A linear regression was calculated for the original and cosine correction method to understand the changes the topographic method had made with the data. A linear regression describes the relationship between 2 variables. A function in matlab *polyfit*, finds the coefficients of a polynomial $p(x)$ of degree n (in this case 1 -linear) that fits the data, $p(x(i))$ to $y(i)$, in a least squares sense. The result p is a row vector of length $n + 1$ containing the polynomial coefficients in descending powers (Matlab, 2005). These coefficients can then be plugged into the linear equation described in 4.11 and plotted.

C-Correction Method

The c-correction method is very similar to the cosine correction method but brings the original data into the form:

$$Lt = m\cos(i) + b \tag{4.11}$$

This corresponds to a regression line (also used in the statistical-empirical approach) with the original DN for a spectral band on the Y axis and $\cos(i)$ on the

X axis. This method is based on a significant correlation between a dependent and one or several independent variables. With the help of a regression function the influence of the independent variables can be corrected. The quality of such a correlation depends on the degree of explanation of the regression function. The c-correction method introduces a parameter c which is the quotient of b and m of the regression line. The c parameter was derived by calculating the regression line in matlab for data from the satellite image that represented the Good, Very Good, and Less Good grazing classes. All other areas were masked out to give the best possible regression function. These areas were then the areas that were topographically corrected and no other. The c parameter is built in to the cosine law as a additive term:

$$Lh = Lt\frac{\cos(sz) + c}{\cos(i) + c} \tag{4.12}$$

$$c = \frac{b}{m} \tag{4.13}$$

where, Lh = radiance observed on a horizontal surface (i.e. the new value), Lt = radiance observed over a sloped terrain (i.e. original value), sz = sun's zenith angle, i = sun's inclination angle in relation to the normal on a pixel, c = correction parameter, m = inclination of regression line (i.e. gradient), b = intercept of the regression line, and $\cos(i)$ is defined in equation 4.10.

According to Teillet (1986) the parameter c creates the effect of path radiance on the slope-aspect correction, however the physical analogies are not exact. Mathematically, the effect of c is similar to that of the minnaert constant i.e. that it increases the denominator and weakens the over-correction of faintly illuminated pixels as a consequence.

4.3 Unsupervised Classification

The "Iterative Self-Organising Data Analysis" (ISODATA) is an algorithm for determining the natural spectral groupings present in a dataset, similar to K-means. It accepts the minimum and maximum number of clusters from the analyst. The algorithm then arbitrarily "seeds" or locates, that number of cluster centres in the multidimensional measurement space. Each pixel in the image is assigned to the cluster whose arbitrary mean vector is closest. This algorithm permits the number of clusters to change from one iteration to the next, by merging, splitting, and

deleting clusters. In each iteration, following the allocation of pixels to the clusters, the statistics describing each cluster are evaluated. If the distance between the mean points of two clusters is less than some predefined minimum distance, the two clusters are merged together. On the other hand, if a single cluster has a standard deviation (in any one dimension) that is greater than a predefined maximum value, the cluster is split in two. Clusters with fewer than the specified minimum number of pixels are deleted. All pixels are then reclassified into the revised set of clusters, and the process repeats until either there is no significant change in the cluster statistics or some maximum number of iterations is reached (Lillesand et al., 2004).

ISODATA was run using Envi 4.2. 5 unsupervised classifications were run on the c-corrected reflectance image from the 24.07.1994, each with a different number of maximum classes; 10, 20, 30, 40, & 60. It is easy to visually illustrate the classification results with the vegetation polygons on top but to get hold of the combined data (i.e. which, and how much of each vegetation class appeared in each unsupervised cluster) was a complicated task.

To keep the individual class identifiers, separate masks of (0,1) were created for each vegetation / grazing class and these were then added together. The lake areas and those areas defined as not being outfield grazing areas were also masked out. An algorithm was made in matlab to give a numerical value to each of the masks e.g. (mask1 x1) + (mask2 x 2) so that the final mask layer contained an identifier for each class (i.e. the mask layer had values 0 & 1,2,3,4,5, etc). Discrepancies were noticed during this process that some of the pixels had more than one class value, i.e. the pixel had appeared in several of the masks. This is a result of the masking algorithm used by Envi. The problem lies in converting the polygon areas to raster format, where polygon borders run through sections of a pixel. Approximately 5% of the pixels were affected by this problem within the grazing class masks, and under 1% of pixels were affected within the vegetation classes. To make sure these pixels did not cause any unwanted problems in the comparison of the unsupervised clusters they were all removed from the test.

4.4 Airphoto Interpretation

The photos used were taken on the 25.06.1995. They were taken with infrared film and have a scale of approximately 1:22,000. They were in paper format and those examples shown in the report were scanned to 600dpi with equal light conditions. The photographs themselves, however, had varying exposures. The photos are not geometrically corrected in any way, but are considered representative for this

analysis. The photos were analysed manually using a basic stereoscope.

The digital copies of the photos were edited in the graphics program GIMP, where polygon borders were drawn on manually. The polygon borders were drawn in as much likening to the Norwegian Institute for Land Inventory (NIJOS) polygon borders as possible, but there are variations due to the difficulty of determining border positions using visual comparison and the slight distortion in the uncorrected paper images.

4.5 Supervised Classification

The Maximum Likelihood Classifier (MLC), used here, quantitatively evaluates both the variance and covariance of a set of feature's spectral response patterns when classifying an unknown pixel. For the MLC to evaluate both the variance and covariance of a class of spectral patterns an assumption has to be made, that the distribution of the training data point cloud (in the measurement space) is Gaussian (normally distributed), which is a reasonable assumption for common spectral response distributions (Lillesand et al., 2004).

Under this assumption the distribution of a set of pixels can be described by the mean vector and covariance matrix. These parameters enable the maximum likelihood algorithm to calculate the statistical probability of a pixel belonging to a certain class. Each spectral class has it's own probability density function see figure 4.6 . For each pixel, the probability density function is used to calculate the probability of belonging to each spectral class, and the unidentified pixel is assigned to the spectral class with the highest probability. A threshold can also be set by the analyst so that pixels with a probability value under that threshold will be classified as ”unknown” (Lillesand et al., 2004).

A maximum-likelihood classification was run on the topographically c-corrected image from 24.07.94. Envi was used to run the classification. The training data was chosen by visual inspection of the satellite image as well as aerial photos and comparisons with the unsupervised classification (60 clusters), to choose the most representative pixels for each class. The supervised classification was run for the 3 grazing classes; Less Good (LG), Good (G), and Very Good (VG).

Before the classification was run, additional map data was brought in and certain areas were masked out of the satellite image. The image had already been masked so that only the areas covered by the 3 NIJOS grazing quality classes LG, G and VG were available. The agricultural areas, lakes and non-permeable areas had

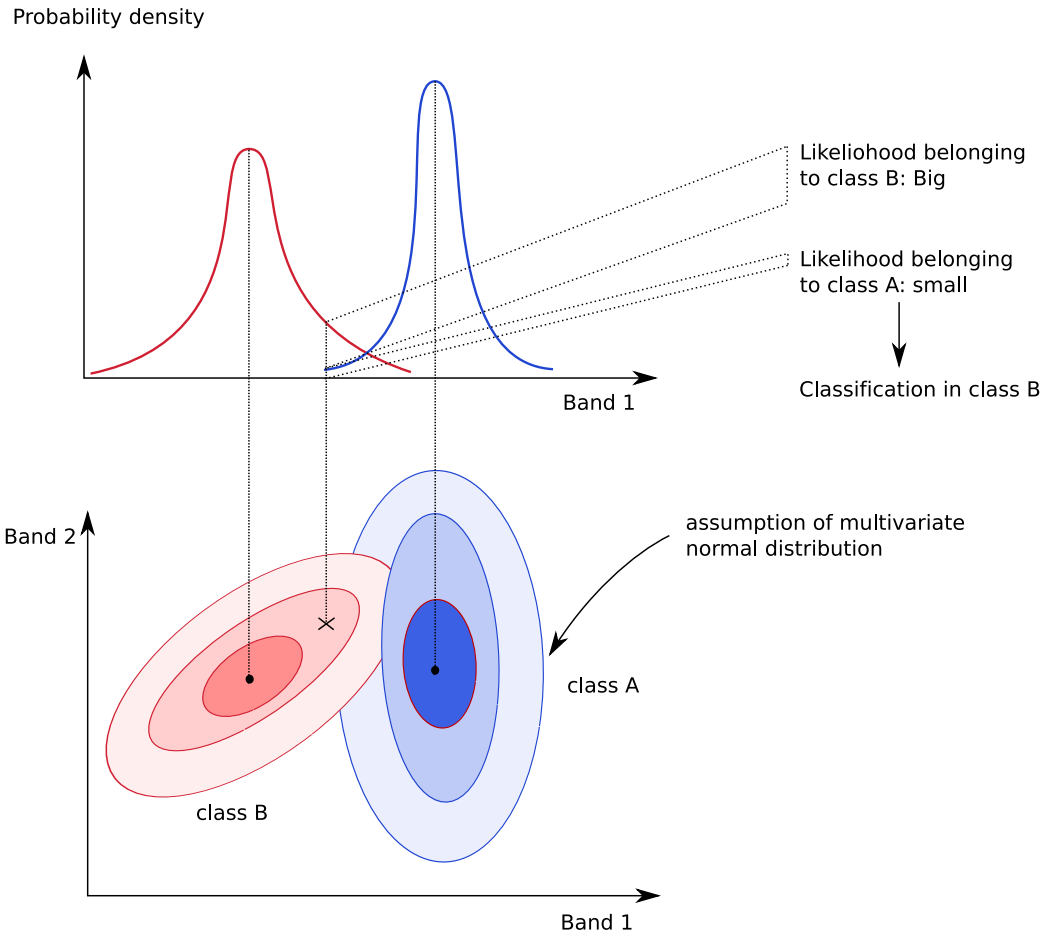

Figure 4.6: Illustrations of how the maximum likelihood classifier calculates probability distributions for a class, and assigns a pixel to the distribution with the highest probability. Copied from Hashimoto et al. (1993)

been masked out (process described in the section 4.2.4). Outlines for the stream network, road network, tractor road network, and houses (points), were added to the image and masked out. These areas greatly affected the classification results as they appeared in the middle of polygons classed as vegetation types. The layers brought in were from the N50 series over Norway and in the SOSI standard. They had UTM zone33, EUREF89 / WGS84 coordinate system and were converted by ENVI4.2 to zone 32 when they were put together with the satellite image.

Error Assessment

A confusion matrix was drawn to assess the accuracy of the classification. The confusion matrix expresses the number of sample units (i.e. pixels) assigned to a particular class relative to ground truth. The columns represent the ground truth data and the rows represent the classification generated from the remotely sensed data. The table indicates the accuracies of each category as well as the errors of inclusion (commission errors) and errors of exclusion (omission errors). The Producer's and User's accuracy were calculated. The producers error divides the total number of correct pixels in a class by the total number of ground truth pixels in that class (i.e. column number). The user's accuracy is calculated by dividing the total number of correct pixels in a class by the total number of pixels that were classified in that class (i.e. row) Congalton (1991).

Chapter 5

Results

This chapter is organised into the following sections; initial class separation, image variation, classification, and the visual inspection of aerial photographs. Flow diagrams presented at the beginning of each section illustrate the procedure taken for that group of analyses. The objective behind all analyses was to find a pattern that could relate the brightness values appearing in a Landsat image, to the grazing quality classes defined by the Norwegian Institute for Land Inventory (NIJOS).

5.1 Satellite Images Across Growing Seasons

Different plants dominate at different times of the year because of variations in the growing seasons of individual species. Having images from different parts of the growing season is therefore an asset when assessing vegetation spectral separability and can improve classification (de Colstoun et al., 2003; Pax-Lenny and Woodcock, 1997; Wolter et al., 1995).

The 6 satellite images used in this thesis are shown in figure 5.1. Three spectral bands from each image are visualised in red, green and blue. The distinction between the different land cover types (trees, low vegetation, bare rock, and snow) are clearest when shown in a false colour band composite including the Mid Infrared (MIR), near infrared (NIR), and the red band. Varying the band combination is a visual tool and does not affect the data in any way. The dark areas in the images represent small lakes. They appear black because the water both absorbs and specularly reflects all visible wavelengths away from the satellite sensor. The August image has a few scattered clouds which also appear as black in the image. There are additional dark areas in the October image representing shadow due to

a lower sun angle.

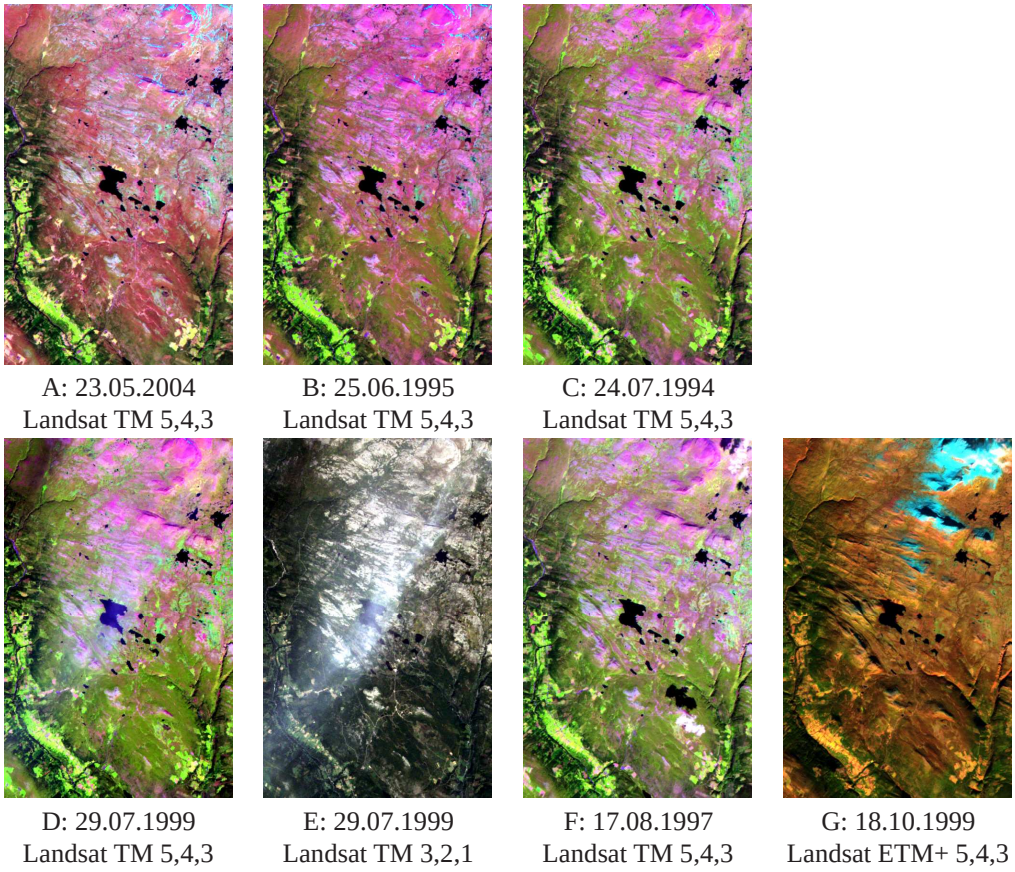

Figure 5.1: The Landsat images used ranged from spring to autumn. Images A, B, C, D, F & G are displayed in a band 5,4,3 combination which means MIR=red, NIR=green and red band=blue. Image E is shown in a true colour combination. Image E & F have the same image data but are displayed in different band combinations. Notice how the thin cloud in the image is more visible in a true colour combination. Notice also the change in vegetation coverage from May - October (i.e. increase in green area from May - July, and decrease in green area from July - October).

The blue colour is represented by the red spectral band in all the images in figure 5.1, except E. The chlorophyll in healthy plants absorbs most of electromagnetic (EM) radiation in the red region. This means that little radiation is reflected back and recorded at the satellite sensor (see figure 2.11) (Lillesand et al., 2004). This is why there is very little blue in most of the images in figure 5.1. Those small areas in the images (e.g. image G) that are blue, however, are from areas that are either covered in bare rock or by snow or ice.

Green is represented by band 4, the NIR band. Healthy plants in this wavelength region have high reflection. The pixels that are strongly green in the false colour

images are those that contain dense vegetation. This includes most of the tree covered areas, which in addition, have considerable undergrowth.

Red is represented by band 5, the MIR band. The alpine heath and bog areas reflect in this wavelength and hence are represented in the red and pink areas in the images. The green areas (trees) cover the lower altitudes, while the pink and red areas cover the higher altitudes (grasses & shrubs). The images cover scenes from May through to October and illustrate a change in vegetation coverage across growing seasons. The June and July images (B, C, & D) have considerably larger greener areas than those in May and October. The October image (G) shows a considerable reduction in green area. The deciduous vegetation has clearly lost its leaves and the reflection pattern has changed. The evergreen vegetation consisting of Pines and Spruces are found in the narrow valley that skirts the bottom of the study area. These areas appear as dark green in the October image. Snow and ice have started to form in the higher regions, appearing as bright blue (see fig 2.3 for topographic map). The October image presents little information on the vegetation types present, but has been incorporated to illustrate all phases of the growing season which are not covered by snow.

Images D and E in figure 5.1 are the same image, but shown in different band combinations. Image E is in a true colour composite. This combination shows the thin cloud cover more clearly than the false colour image (D). Having cloud covering an image distorts the reflectance values of the ground cover and makes accurate analysis more difficult. The scene shown in D and E was originally used for the first separation analyses but was not used further on due to concerns about the cloud coverage. The mid summer image from the 24th of July was used instead (C).

5.2 Initial Class Separation

The vegetation map produced by NIJOS recorded grazing quality for both sheep and cattle (see chapter 3 for details). This thesis focused on the grazing quality of vegetation for sheep only, as there is more demand from sheep grazing in the mountainous outfield areas than there is from cattle. If a satisfactory method for classifying sheep grazing quality were found, the procedure could be extrapolated to cattle grazing.

Tests for initial class separation involved plotting the spectral distribution of the grazing quality and vegetation classes, for each band of the different images. In addition a composite image of different dates was created and the normalised

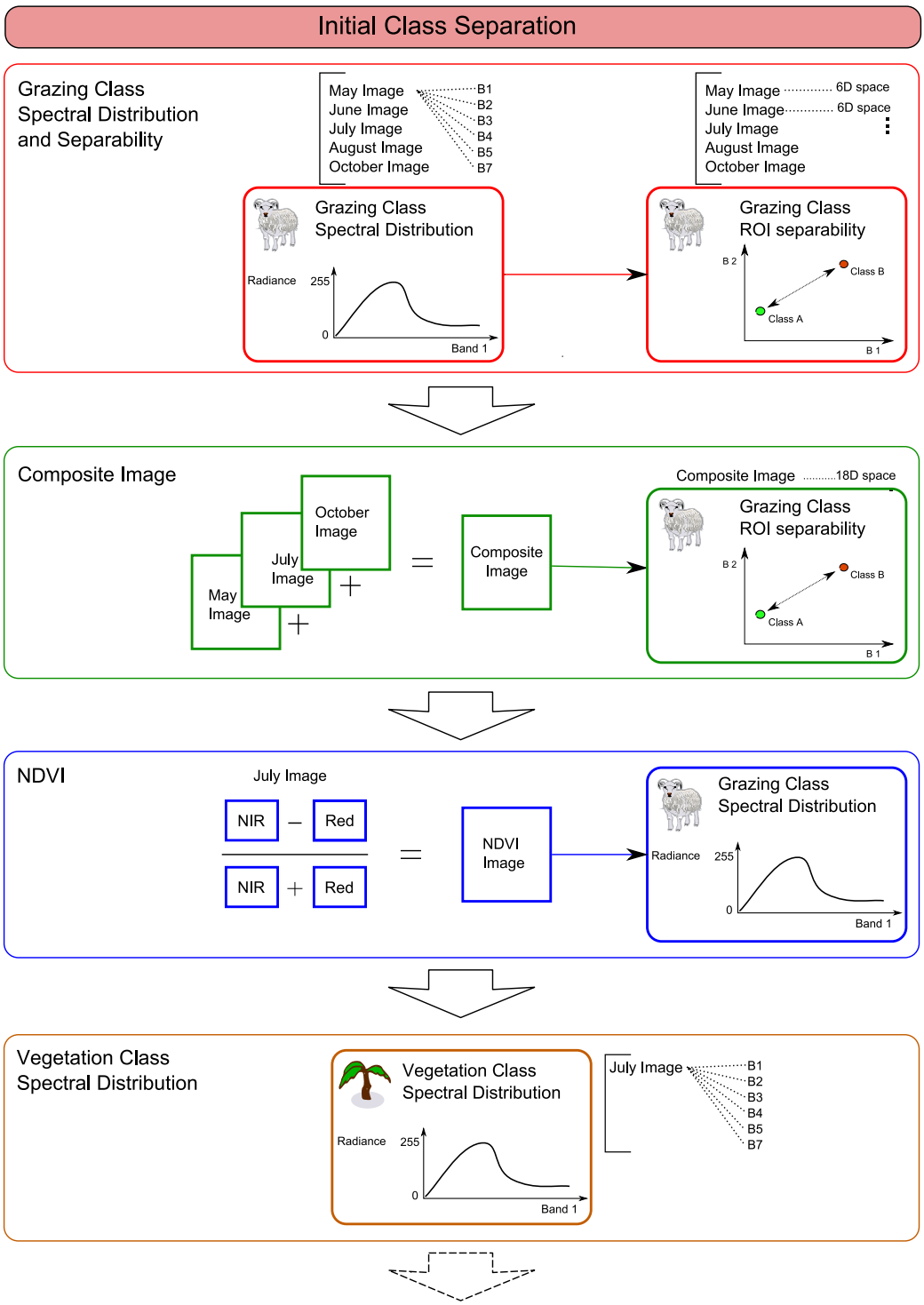

Figure 5.2: Flow diagram illustrating the process followed in the initial class separation analyses. This is the first flow diagram in a series of 4. These analyses were done to illustrate if it was possible to separate between the grazing quality classes that NIJOS had defined. The plant symbol indicates those analyses done on the individual vegetation types. The sheep represents all those analyses performed on the sheep grazing quality classes. The analyses were tested on images from May, June, July, August and October, each with spectral bands in the blue, green red, NIR and MIR regions of the EM spectrum. Figure 5.11 presents the next flow diagram.

difference vegetation index (NDVI) was used. Figure 5.2 illustrates the procedure followed for this group of analyses.

Grazing Classes

Initial analysis involved analysing how separable the NIJOS grazing quality classes were by using histogram plots and statistical separation algorithms. Figures 5.3 to 5.5 show 3 of the 5 histograms, plotted to visualise the data from each image. The images from May (spring), July (mid-summer) and October (late autumn) are shown. They illustrate the change in 'at satellite radiance' (asr) values for each grazing class, across each band.

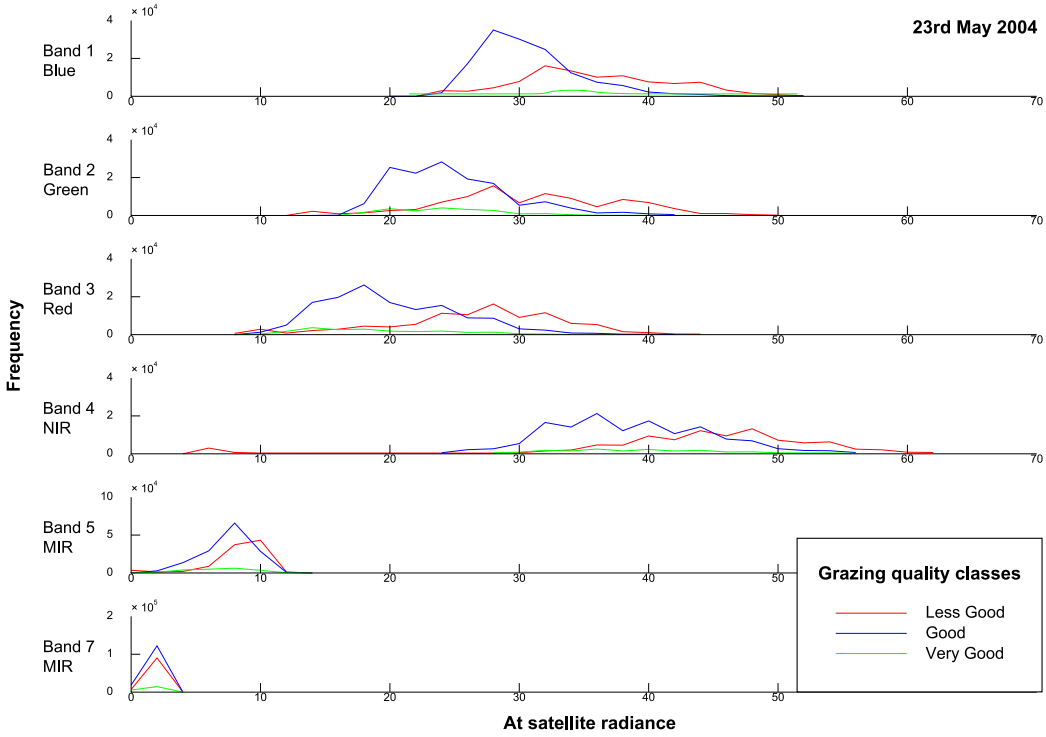

Figure 5.3: Histogram of sheep classes. asr image - 23rd May 2004. Shows the distribution of the grazing classes within each band. The NIR band has the highest radiance values. The blue band has often the lowest radiance values for vegetation, but not here. This could be due to increased atmospheric scattering in this band. The same pattern is seen in the next two histograms, with blue having slightly higher radiance values than the green band. The grazing quality classes overlap considerably and there is no visual points of separation between classes.

In each of the 3 plots (figures 5.3, 5.4 & 5.5) the blue band had slightly higher radiance values than the green band. This is atypical of vegetation, which usually

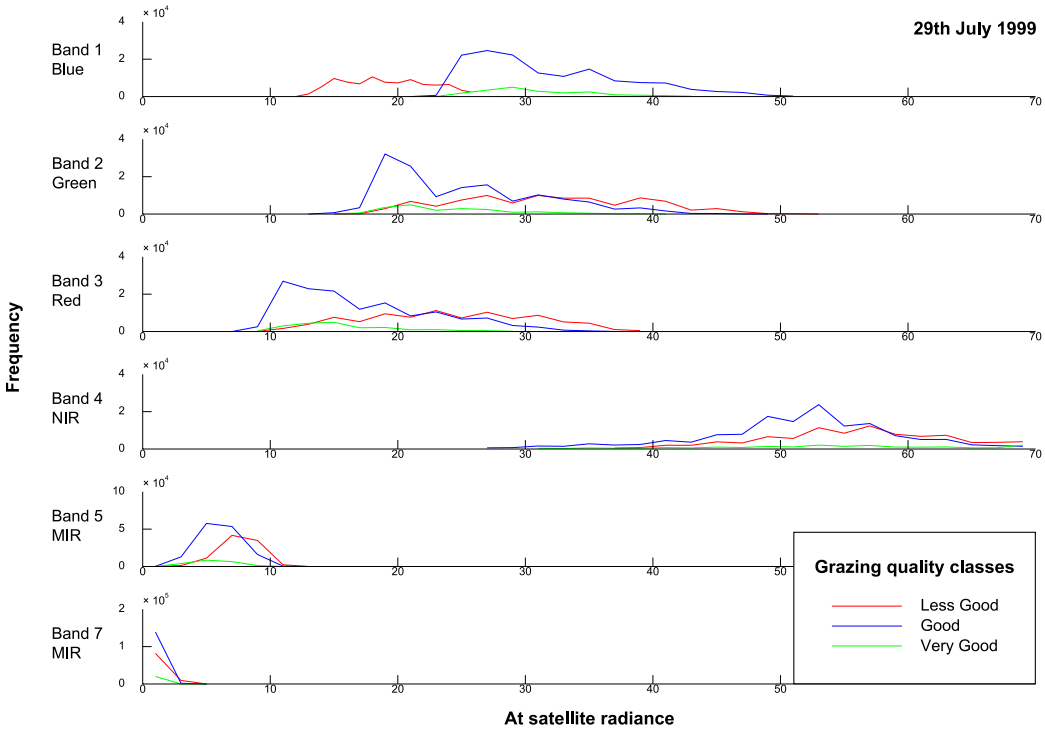

Figure 5.4: Histogram of sheep classes. asr image - 29th July 1999. Notice that there is now a greater difference between values in the red, and NIR bands compared to the May image. This is because the vegetation is more mature in mid summer than in early spring. Notice also the difference in radiance values in the LG class compared to the G class in the blue band.

has the highest values, within the visible spectrum, in the green band. This could be explained by Rayleigh scattering. The affect of Rayleigh scatter is inversely proportional to the fourth power of the wavelength (Lillesand et al., 2004). Hence, there is a much stronger tendency for shorter wavelengths to be scattered by this mechanism than longer wavelengths (i.e. the blue band is more affected).

Data in the green band for all three images had higher radiance values than the red band. This is to be expected as vegetation absorbs more in the red and blue bands than in the green band (refer to section 2.3 for further descriptions). Bands 3 and 4 of figures 5.3 and 5.4, illustrate the known relationship between the reflection in the red and NIR bands for vegetation. Vegetation has high absorption in the red band and high reflection in the NIR band (Fiella and Penuelas, 1994). The ratio is strongest in the July image. The May image shows similar radiance values in band 3 to the July image indicating that there is abundant chlorophyll absorption at that time.

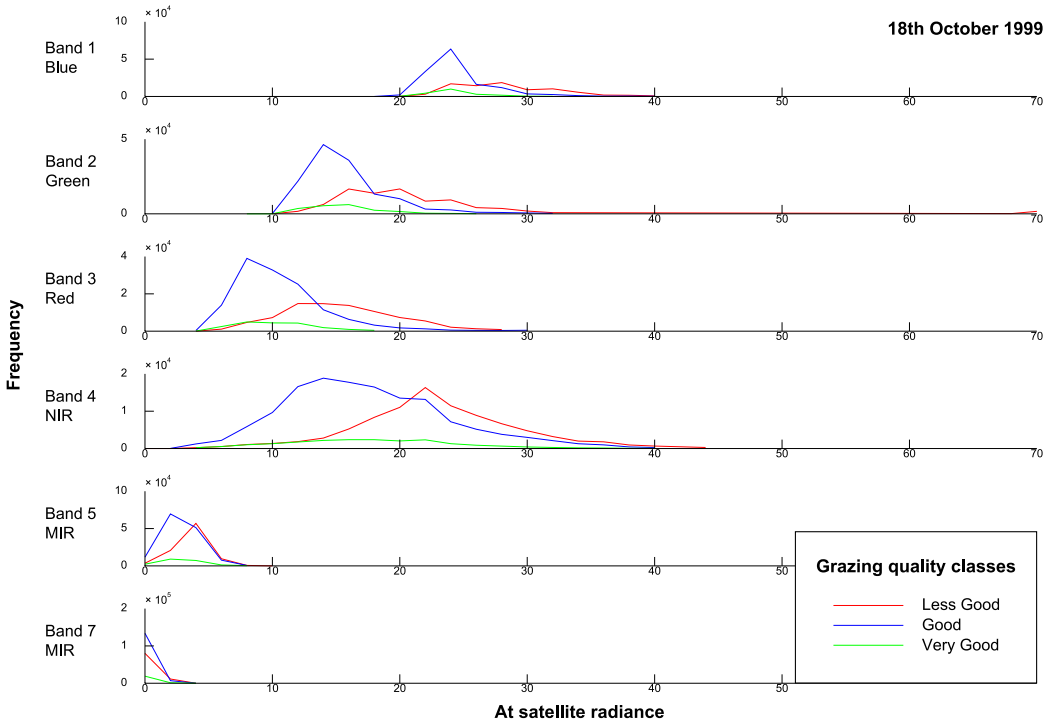

Figure 5.5: Histogram of sheep classes. asr image - 18th October 1999. This is late in the growing season so the difference in radiance values between the red and NIR bands is very small. Most deciduous plants will have lost their leaves. This drastically reduces reflection in the NIR band. The data in bands 2 and 3 have also reduced in radiance when compared to the spring and mid-summer data.

It is interesting to note the changes in the radiance values from band 4 (NIR) from May to July. The May image shows maximum values around 30-40, whereas the July image shows maximum values around 50-60. This suggests that the vegetation is not as mature as during July. Reflection values in the NIR spectrum are not only an indication of the presence of vegetation but also the amount, healthiness, water content, leaf age, and vegetation type of the plant (Lillesand et al., 2004).

The October image (fig 5.5), shows very low radiance values in the NIR band and reduced values in the red band compare to the May and July images. The satellite image in figure 5.1 G, shows a reduction in green area compared to the summer, indicating less green leaf vegetation. The valley areas at the bottom of the Venabygd area do contain dark green areas and these represent the conifers and spruce trees that are found there. The conifers and spruce vegetation types (6a, 6b, 6c, 7a, 7b, 7c) are only found below 1000m a.s.l in the study site.

In terms of separability between grazing quality classes, the histogram plots gave

no clear indication of this in any of the 5 images studied. There were large overlaps between the different grazing classes, in each band. The July image showed the greatest difference between bands 3 and 4 but all grazing classes within those bands covered similar radiance values.

The LG and G grazing quality classes dominated the frequency in the histogram plots. They had varying distributions from each other with a difference in their maximum values and standard deviations. Their radiance values still overlapped too much for any simple clear separation. The Very Good (VG) grazing class is only just visible on the graphs in green because it represents a much smaller % area than the other two classes, and hence lower frequency.

The data shown in tables 5.1 to 5.6 gave a more numerical and statistical indication of the separation possibilities between grazing classes for each of the 6 satellite images. The numbers represent the average statistical distance between region of interest (ROI) pairs. As described in section 4.1.2, values over 1.9 in both the Jeffries-Matusita (JM) and transformed divergence methods, gives a statistically good separation. The JM method is more reliable and will be given a heavier weighting in the discussion of results (Richards, 1986).

The results are listed in order of separation from least to most. Those numbers highlighted in yellow indicate a reasonable separation ($>\approx 1.65$) and those in green have very good separation with values above (> 1.9). The separability statistics were calculated between the classes VG, G, LG, and impermeable. Impermeable surfaces are typically built areas that include surfaces such as bitumen and concrete. This class was included to show the contrast between a very different spectral class to the vegetation classes.

Grazing Quality Classes	Jefferies Matusita	Trasformed Divergence
Good & Very good	0.43	0.51
Less Good & Good	0.58	0.63
Less Good & Very Good	0.95	1.18
Less Good & Impermeable	1.13	1.30
Good & Impermeable	1.51	1.79
Very Good & Impermeable	1.63	1.94

Table 5.1: ROI separability. (asr) image - 23.05.04. Those highlighted as green are separable and those in yellow have reasonable to good separation. It is intuitive that pairs of ROIs in the VG and impermeable classes have the greatest separability.

Following the changes in separation between classes from month to month (i.e. May - October) there is a slight increase in the separation between the G & VG, the G & VG, and LG & G classes. This starts to decrease again from July to August, and again to October. Overall the separation is very low between grazing

Grazing Quality Classes	Jefferies Matusita	Trasformed Divergence
Good & Very good	0.47	0.60
Less Good & Good	0.66	0.71
Less Good & Impermeable	1.02	1.24
Less Good & Very Good	1.069	1.28
Good & Impermeable	1.50	1.79
Very Good & Impermeable	1.66	1.93

Table 5.2: ROI separability. asr image - 25.06.95. Note the poor separation between all grazing quality classes. LG and G have the highest separation of the grazing quality pairs, although they are not separable

Grazing Quality Classes	Jefferies Matusita	Trasformed Divergence
Good & Very Good	0.47	0.54
Less Good & Impermeable	0.78	0.91
Less Good & Good	0.79	0.95
Less Good & Very Good	1.21	1.60
Good & Impermeable	1.38	1.69
Impermeable & Very Good	1.61	1.91

Table 5.3: ROI separability. asr image - 24.07.94. Note that the G and VG classes are hardest to separate between. This is reflected in all other images except the August data.

Grazing Quality Classes	Jefferies Matusita	Trasformed Divergence
Good & Very Good	0.34	0.38
Less Good & Good	0.61	0.65
Less Good & Impermeable	0.79	0.92
Less Good & Very Good	0.96	1.06
Good & Impermeable	1.21	1.57
Very Good & Impermeable	1.44	1.79

Table 5.4: ROI separability. asr image - 29.07.99. Note that the LG and VG class pairs have the best separation between the grazing quality classes even though their separation is still not good.

Grazing Quality Classes	Jefferies Matusita	Trasformed Divergence
Less Good & Good	0.52	0.55
Good & Very Good	0.55	0.69
Less Good & Impermeable	0.73	0.83
Less Good & Very Good	1.05	1.28
Good & Impermeable	1.13	1.38
Very Good & Impermeable	1.45	1.68

Table 5.5: ROI separability - asr image - 17.08.97. Note that the LG grazing quality class is closest (i.e. least separable) from the impermeable class, of the three grazing quality classes.

Grazing Quality Classes	Jefferies Matusita	Trasformed Divergence
Good & Very good	0.27	0.32
Less Good & Good	0.42	0.44
Less Good & Very Good	0.79	1.08
Less Good &Impermeable	0.91	1.13
Good & Impermeable	1.29	1.65
Very Good & Impermeable	1.49	1.86

Table 5.6: ROI separability - asr image - 18.10.99. Note the pattern of least to best separation between classes for all images stays almost the same.

quality classes when using single date images. Separation between the LG and G classes was highest with the 24.07.1994 data. Between G and VG, the best results were with the 17.08.1997 data. Between LG and VG the highest separation statistics were found with the 24.07.1994 data.

Table 5.4 (July 29) shows slightly less promising results than table 5.3 (July 24). This could be accredited to the slight cloud cover over the July 29 image. The images were taken in different years however, and the results could reflect differences in growing seasons or changes in vegetation constitution. For a single image, the 24.07.1994 image date showed the most promising separation values for all classes.

The LG & VG class pair gave the highest separation of the three grazing quality class combinations as they are the furthest apart spectrally. This makes sense in that the VG grazing class represents lusher vegetation, which has much stronger values in NIR region than the LG class. The pattern of least to most combinations kept almost the same from May through to October with the G & VG classes being the hardest to separate between. The VG grazing class was most separable from the impermeable class. Vegetation has spectral values far apart from houses, concrete and roads, and would naturally be easier to separate from than the other vegetation types (refer to figure 2.7).

After these initial grazing class separation analyses it was not possible to see any straight forward separation between any of the three grazing quality classes when using a single date multispectral Landsat image.

5.2.1 Composite Image

If it was not possible to separate between grazing classes with a single image, it could be possible when combining images together. To test the potential for between class separation when using a time series, a stack of images from different

parts of growing seasons was created. Three images were used: Landsat Thematic Mapper (TM) 23.05.2004 (spring), Landsat TM 24.07.1994 (summer), and Landsat Enhanced Thematic Mapper (ETM)+ 18.10.99 (late autumn). This multitemporal data merging was done by combining images of the same area taken on more than one date to create a product useful for visual interpretation.

Merging various combinations of bands from the different dates to create colour composites can aid the interpreter in discriminating the various vegetation types present (Lillesand et al., 2004). Figure 5.6 shows a combination of the three NIR bands from the three different image dates.

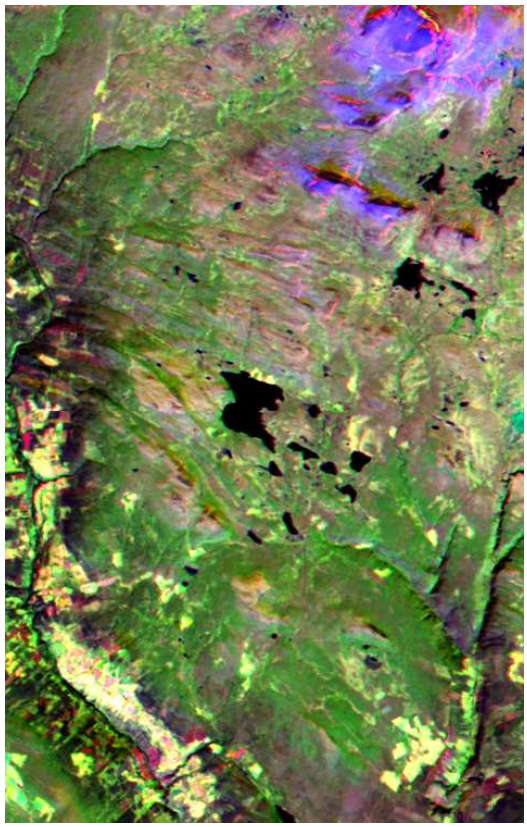

Figure 5.6: A composite 3 date image created from a data-stack of 3 dates. The NIR band from each date is shown in; red: 23.05.04, Green: 24.07.94 and Blue: 18.10.99. The composite image shows that the high NIR values are the most dominant feature in the July image, appearing as green and representing vegetated land cover. The blue areas, corresponding to snow and ice, are the most dominant in the October image. The dominating feature in the May image (visualised in red) are reflections from bare rock and soil in the image.

Visualised as green in the figure 5.6, are the areas that dominate the radiance values in the 24th of July image. Those areas are known to be covered in vegetation.

This can indicate that a mid summer image is a good choice for the classification of vegetation using a single date image. Visualised as bright blue, are the radiance values from the 18th of October image. These corresponds to areas with snow and ice (see original image in fig 5.1G). The more exposed areas of Venabygd are covered in alpine grasses, lichen and bare rock. These are appearing as the dominating radiance values from the 23rd of May image (i.e. in red).

ROI separability statistics were calculated from all 18 bands in the image stack, see table 5.7. When comparing these results with those from the single date images (shown in tables 5.1 to 5.6) there has been a considerable improvement in the separability between all grazing classes pairs. LG and VG received 1.88 using transformed divergence, and G and VG were clearly separable from the impermeable class.

Grazing Quality Classes	Jefferies Matusita	Trasformed Divergence
Good & Very Good	1.02	1.19
Less Good & Good	1.07	1.21
Less Good & Impermeable	1.57	1.75
Less Good & Very Good	1.66	1.89
Good & Impermeable	1.85	1.98
Very Good & Impermeable	1.94	1.99

Table 5.7: ROI separability. asr images (i.e. 18 bands): 23.05.04, 24.07.94, 18.10.99

Further improvements could be made by adding additional dates or trying other date / image combinations from various parts of the growing season. Despite the promising results obtained from the time series analysis, proceeding analyses in this thesis focused on one mid summer image. This was to reduce the complexity of the situation and make the process more manageable. An image from the middle of the summer was chosen. The image was from the 24th July 1994 as it had the best separation results between grazing quality classes. More importantly, a summer image ensures that all vegetation types are present and are a part of the signal recorded in the image.

5.2.2 NDVI

The normalised difference vegetation index (NDVI) gives a measure of ”greenness” of the land cover which ranges from -1 to +1, with +1 representing very ”green” land cover types. The NDVI for the mid summer image was calculated and compared to the grazing class polygons. Figure 5.7 shows the results in a histogram.

As expected all the grazing classes have values above 0. The maximum value for the classes lay at around 0.7. Each class had fairly high standard deviations, but the peak values for each class were distinct from each other. The VG grazing quality class had the highest NDVI peak value, followed by the G grazing quality class. The LG class peaked at the lowest value of the three classes, at around 0.35.

The pasture class (*beitevoll*) was a very small class in the Venabygd area and was not represented clearly in the range of frequencies. It however had a peak similar to that of the VG class. Pasture is made of lush green grass and was expected to have NDVI values closest to the VG class. It was incorporated to give a comparison for very ”green” vegetation. In terms of using NDVI a feature to separate the grazing classes, there was too much overlap between them for this to be used as a separator alone, but did show positive results.

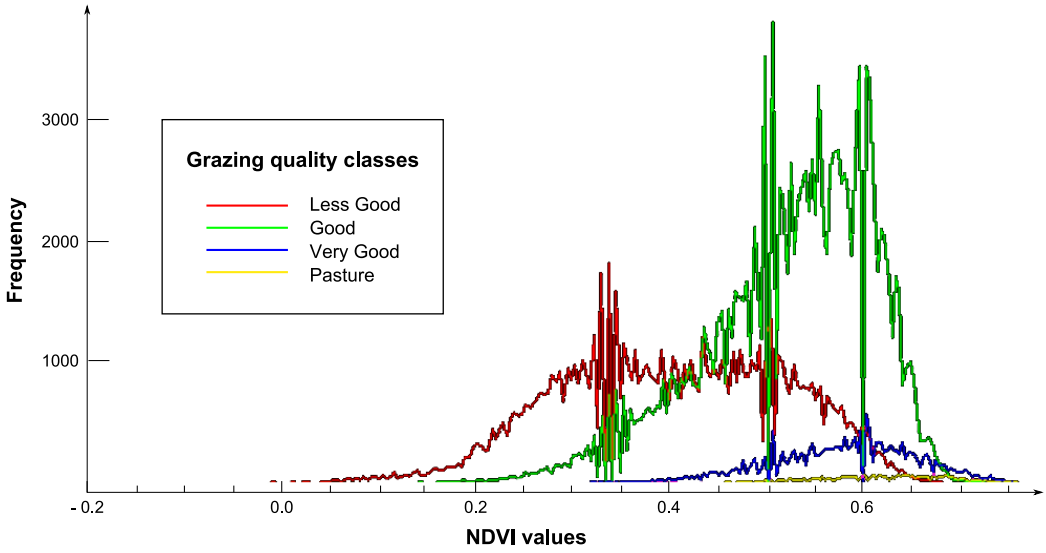

Figure 5.7: NDVI plotted for each grazing quality class. The NDVI gives a measure of ”greenness” which ranges from -1 to +1, with +1 representing very ”green” land cover types. Each class had a fairly high standard deviation, but the peak values for each class were distinct from each other. The VG grazing quality class had the highest NDVI peak value, followed by G grazing quality. The LG class peaked at the lowest value of the three classes around at 0.35.

Vegetation Classes

The initial grazing class separation results did not shed any strong light on the possibility for separation. The next phase was then to Break the grazing classes into smaller units to try and improve separation. These units corresponded to the

individual vegetation types defined by NIJOS.

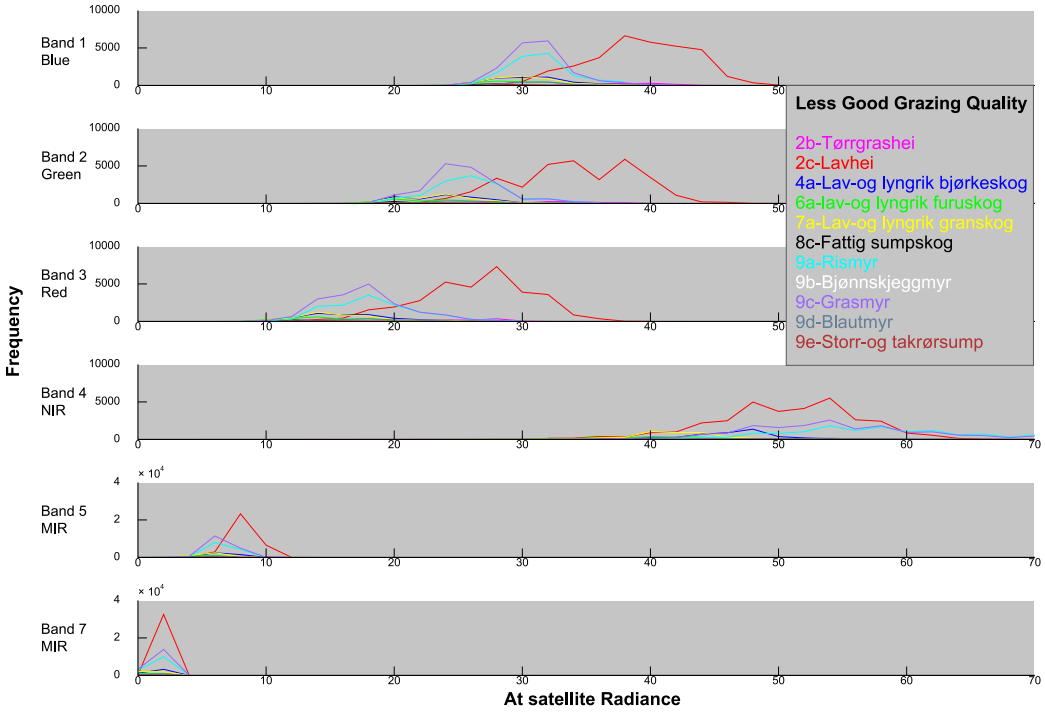

Figure 5.8: Histogram plot for each vegetation class within the LG grazing quality class. Lavhei (2e) has a distribution slightly outside the average for all the others in bands 1,2, & 3 for the LG grazing class. This could be leading to some of the problems in separating between the grazing classes.

Each vegetation type has its own number and letter code which will be used regularly throughout the results chapter. See chapter 3 for a full list of conversions. The following three histogram plots from fig 5.8, to 5.10 show the spread of each vegetation type grouped into the three grazing quality classes. Data is shown for each band of the mid summer image dated 24.07.1994.

In the LG grazing quality class (fig 5.8), 2c-*Lavhei* has a distribution that is slightly different from the others in bands 1, 2, and 3. In band 4 it has a similar distribution to the other vegetation types. Vegetation classes 9c-*grasmyr* and 9a-*rismyr* show very similar distributions in all bands. In band 4 it is a different vegetation type 7b that changes the distribution to the other two seemingly dominate classes.

Having a class with a distribution differing from the majourity can drastically alter the radiance mean of a grazing quality class. Illustrating the data in this way can give an indication of where the problem areas lie with the separation between grazing classes, making them not as visible on the plots. The frequencies

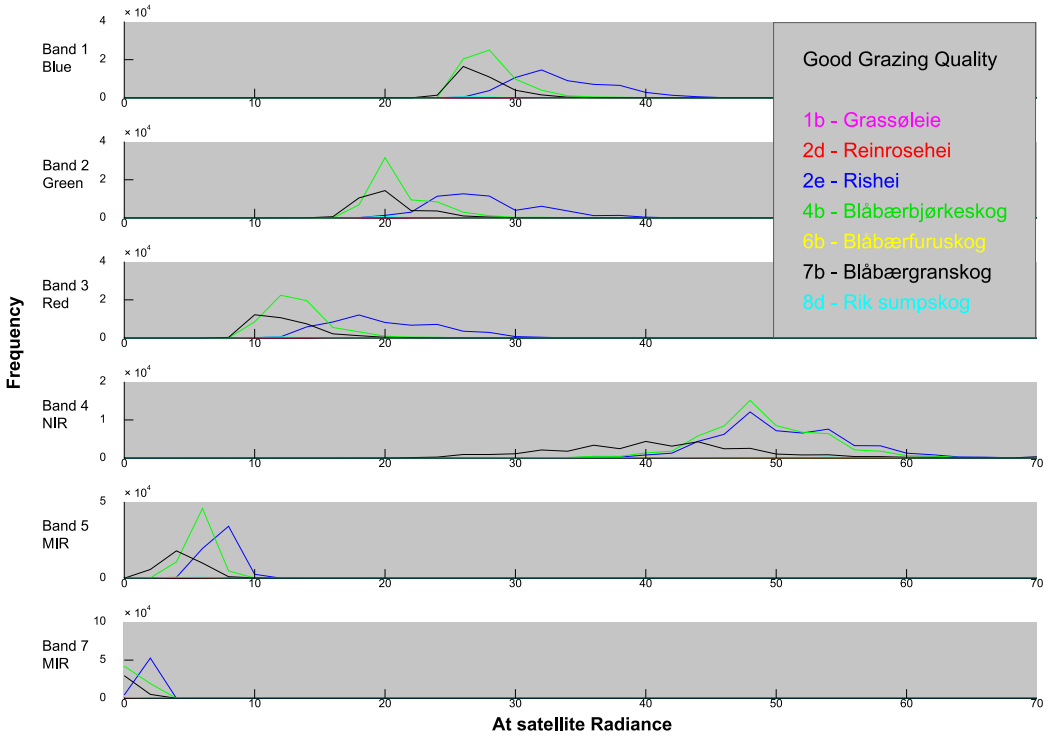

Figure 5.9: Histogram plot for each vegetation class within the G grazing quality class. 4b and 7b have similar distributions in bands 1, 2, 3, 5, and 7, but varying distributions in band 4. 7b has its radiance peak at a lower value in band 4 than that of 2e and 4b.

of many of the vegetation types are very small compared to the dominating classes. Good separation between grazing quality classes is important, but not between vegetation types of the same grazing class.

In the G grazing quality class (figure 5.9), the dominant vegetation types are 2e-*Rishei*, 4b-*Blåbærbjørkeskog* and 7b-*Blåbærgranskog*. 4b and 7b have similar distributions in bands 1, 2, 3, 5, and 7, but varying distributions in band 4. 7b has its radiance peak at a lower value in band 4 than that of 2e and 4b.

The VG grazing class in figure 5.10, has vegetation types with similar frequencies. 7c-*Enggranskog* and 4c-*Engbjørkeskog* have similar distributions but are slightly aside from the other vegetation types. Band 4 has a large range of radiance values. 11b and 4g are defined in their own grazing quality class called pasture (*beitevoll*), but are included here for comparison.

No vegetation type singled its self out completely from the rest in any of the grazing quality classes. Separation between any single vegetation classes did not become apparent from these plots.

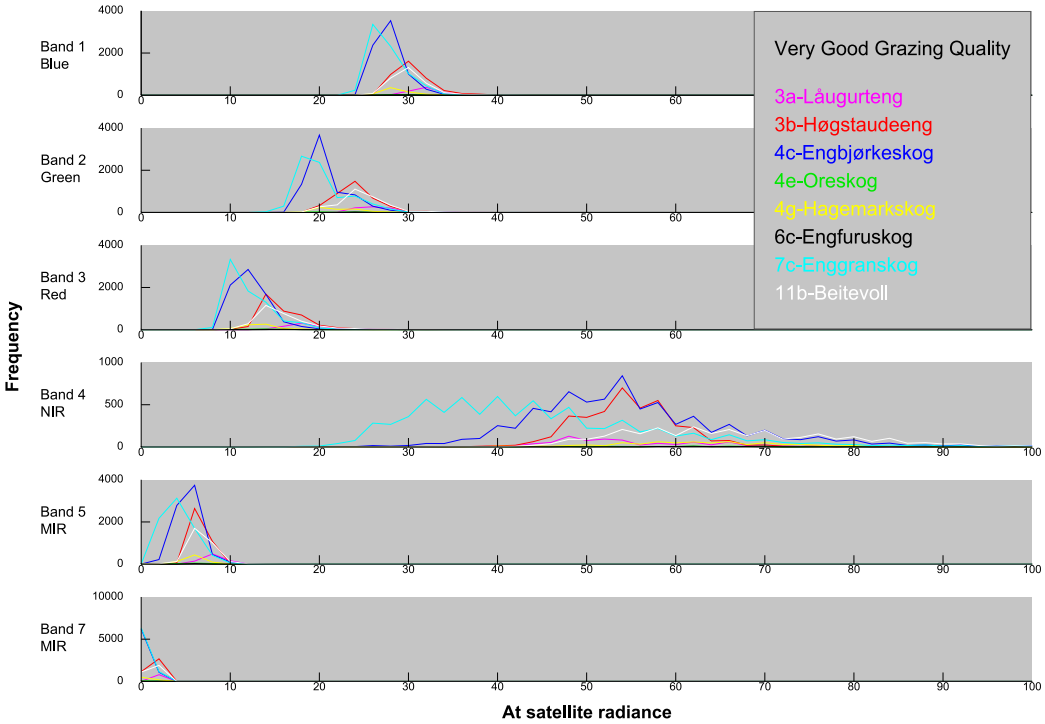

Figure 5.10: Histogram plot for each vegetation class within the VG grazing quality class. Vegetation types have fairly similar distributions. Distributions in band 4 cover a large range of radiance values.

5.3 Image Variation

The next set of analyses followed on from the initial separation results which illustrated that the defined grazing and vegetation classes did not have spectral properties that made it easy to separate between them. The second group of analyses therefore, looked closer at the dataset to try and understand what was varying in the image and why. Anaylses looked at what lies behind the variation within individual vegetation and grazing classes. This section covers analyses and discussions that look into:

- Spectral variation,
- Terrain variation,
- Terrain variation,
- Atmospheric variation,

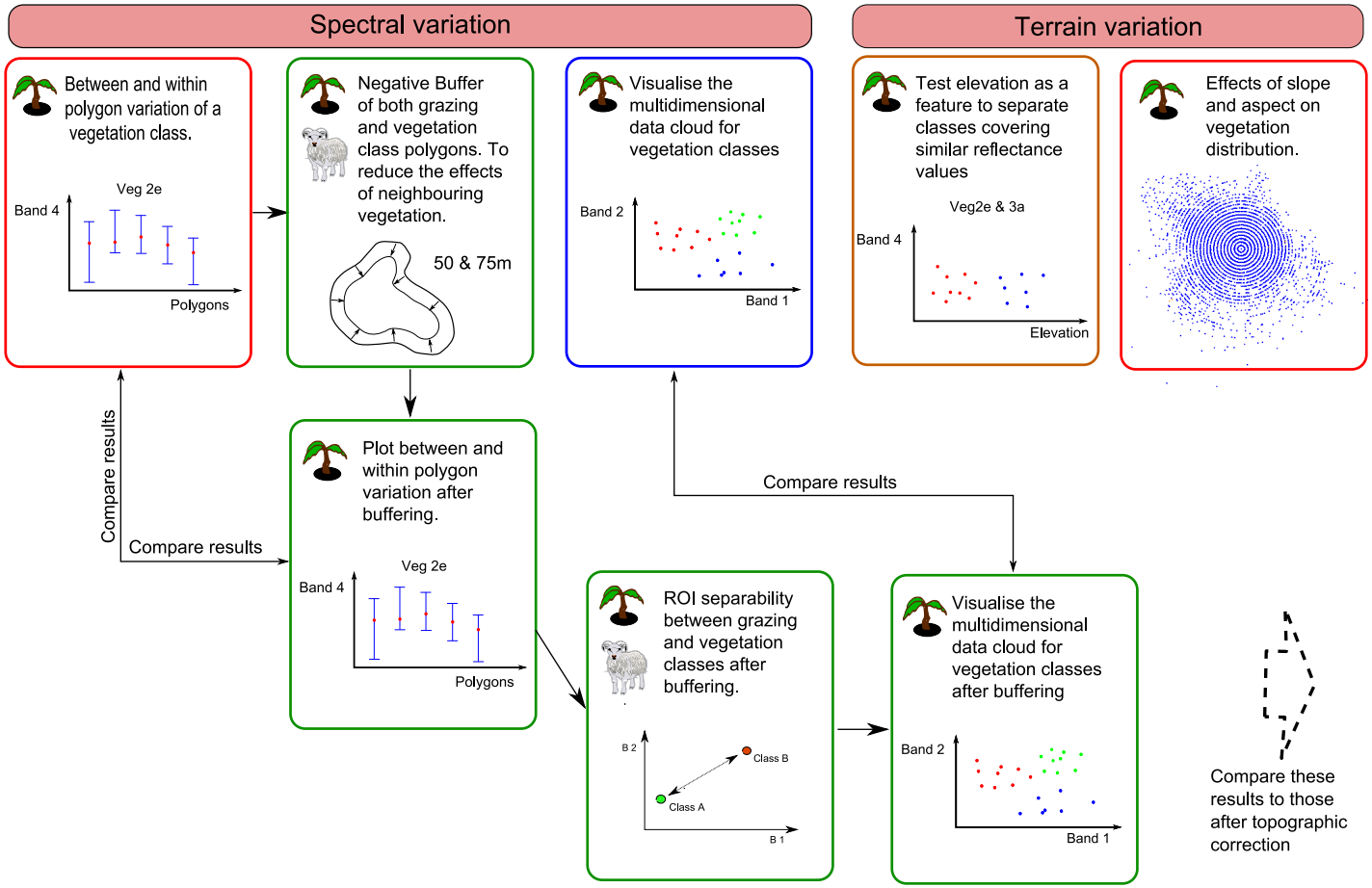

Figure 5.11: Flow diagram to indicate the procedure taken during analyses of terrain variation and spectral variation. This flow diagram follows on from figure 5.2. The next flow diagram is figure 5.16.

- Illumination variation and
- Effects of NIJOS mapping methods (section 5.4)

Figures 5.11 and 5.16 illustrate the procedures followed for these analyses with flow diagrams.

5.3.1 Spectral Variation

The reflection values for the Landsat TM 24.07.1994 image were used in this analysis and all proceeding analyses instead of at satellite radiance values. The following figures are an illustration of the distribution of the reflectance values in band 4 of image 24.07.94, for each polygon in a vegetation class. They were drawn to illustrate the within and between polygon variance of a vegetation type and to try and picture what was happening in the dataset. The results for the original, buffered, and topographically corrected data are shown in figure 5.12. The mean for each polygon was plotted in the middle of the line with a red dot, with its minimum and maximum drawn at each end in blue lines. The standard deviation for each polygon was shown at the bottom of the plot with black dots.

Eight vegetation types were chosen for this analysis, shown in table 5.8. Those chosen had the greatest area coverage and spread of polygons over the Venabygd area. Some of the vegetation types contained a small amount of polygons making them unsuitable for this analysis. There were at least 2 vegetation types for each grazing quality class.

Code	**Vegetation type**
2c	*Lavhei*
2e	*Rishei*
4b	*Blåbærbjørkeskog*
7b	*Blåbærgranskog*
7c	*Enggranskog*
9c	*Grasmyr*
11b	*Beitevoll*
9a	*Rismyr*

Table 5.8: This table lists the vegetation types included in the buffering and measurement space analyses. Those chosen had the greatest area coverage and spread of polygons over the Venabygd area. There were at least 2 vegetation types for each grazing quality class.

The results for vegetation type 2e (*Rishei*), an alpine heath, are those displayed in figure 5.12. The variation between and within polygons in the original reflectance data is shown in the top left hand plot. The variation within this one vegetation class is large, with reflectance values ranging from 2-40. A number of individual polygons are slight outliers to the majority. This can cause problems for finding pure vegetation class representations (i.e. training data) for classification. Similar properties of large variation and outliers were common to all of the 7 other vegetation types.

The polygons with larger variations could have also been problem areas during the classification by NIJOS. These could be polygons with strong influence from other vegetation types within, and around the polygon. The border definition of the polygon could have been difficult, allowing for more neighbouring vegetation types to sneak into the classification and make additional noise to the spectral reflectance information assumed to belong mostly to *Rishei*.

These are natural characteristics of vegetation, but make classification more difficult. Vegetation types mostly occur in mosaics, where changes from one vegetation grouping to the next occur gradually over a distance (Cingolani et al., 2004). Such characteristics are hard to map on paper and must therefore be estimated as best as possible. These factors are influential and must be taken into consideration when looking at satellite images and using such a map as ground truth. Some of these factors and their consequences for analysis will be looked at in detail when inspection the aerial photos and the mapping methods of NIJOS (see sections 5.5 & 5.7).

5.3.1.1 Buffering

Assuming that neighbouring vegetation types greatly affect the variation within polygons of a vegetation type, a test was run to see if by eliminating the border areas of a polygon, this would show a reduction in the within polygon variation of a vegetation class. If the hypothesis was right, the results would represent a more pure picture of the natural variation within a vegetation class.

The results from the -50m inward buffering for vegetation type 2e is shown in figure 5.12. As hypothesised the variation within and between each polygon was drastically reduced after buffering. The distributions between each polygon became less varied (i.e reduced standard deviation). Reducing the borders of each polygon meant many of the polygons disappeared completely (i.e. they were too small). The results left larger more homogeneous polygons which gave a more pure representation of the vegetation type's spectral properties.

The polygons were also buffered by -75m. These results showed that the within and between variation of the polygons did not decrease significantly from the 50m buffering, but rather there became fewer polygons. The 50m buffering had been effective enough so the discussion of results focuses on the 50m buffering. The plots showing polygon variation after topographic correction will be discussed in section 5.3.3.

Seven other vegetation classes were plotted for polygon variance as mentioned (see table 5.8). Several of these classes didn't make it through the buffering process such as 11b (*Beitevoll*-pasture), and 2c (*Lavhei*). The polygons that were included in the buffering process for this analysis were also selected for being pure (i.e. only had a main vegetation class, no secondary vegetation type). This means that the types that didn't make it through the buffering process had a small number of polygons with pure vegetation attributes and / or polygons smaller than $50m^2$. This analysis can indicate vegetation types that are harder to find pure spectral responses for. These vegetation types occur in small patches (i.e. small polygons) and are therefore likely to be more influenced by surrounding vegetation types.

The classes 2e, 4b, 7b, 7c, and 9c all showed similar results after buffering. Their within and between polygon variation of the same vegetation class had been reduced. This reduction did not increase significantly after a -75m buffering but rather reduced the number of polygons.

Measurement Space

The histograms shown previously (figures 5.8, 5.9 and 5.10) show the distribution and separation possibilities for vegetation types within individual spectral bands. This did not provide an understanding of where the data was in the multi-dimensional space (6 dimensions) however. The ROI separability statistics for grazing and vegetation classes were calculated between pairs in this 6 dimensional space.

Because it is not easy to visually interpret data plots with more than 2 dimensions, scatter plots of 2 band combinations for selected vegetation classes were drawn up. Scatter plots were drawn for all 15 possible band combinations, with each plot showing a selected group of vegetation classes (see table 5.8). The pixels used in the scatter plots were from the -50m buffered and pure selected polygons. One band combination example is shown for the buffered, cosine corrected and c-corrected data, see figures 5.13, 5.21 and 5.23. The scatter plots for the topographically corrected data will be discussed in section 5.3.3.

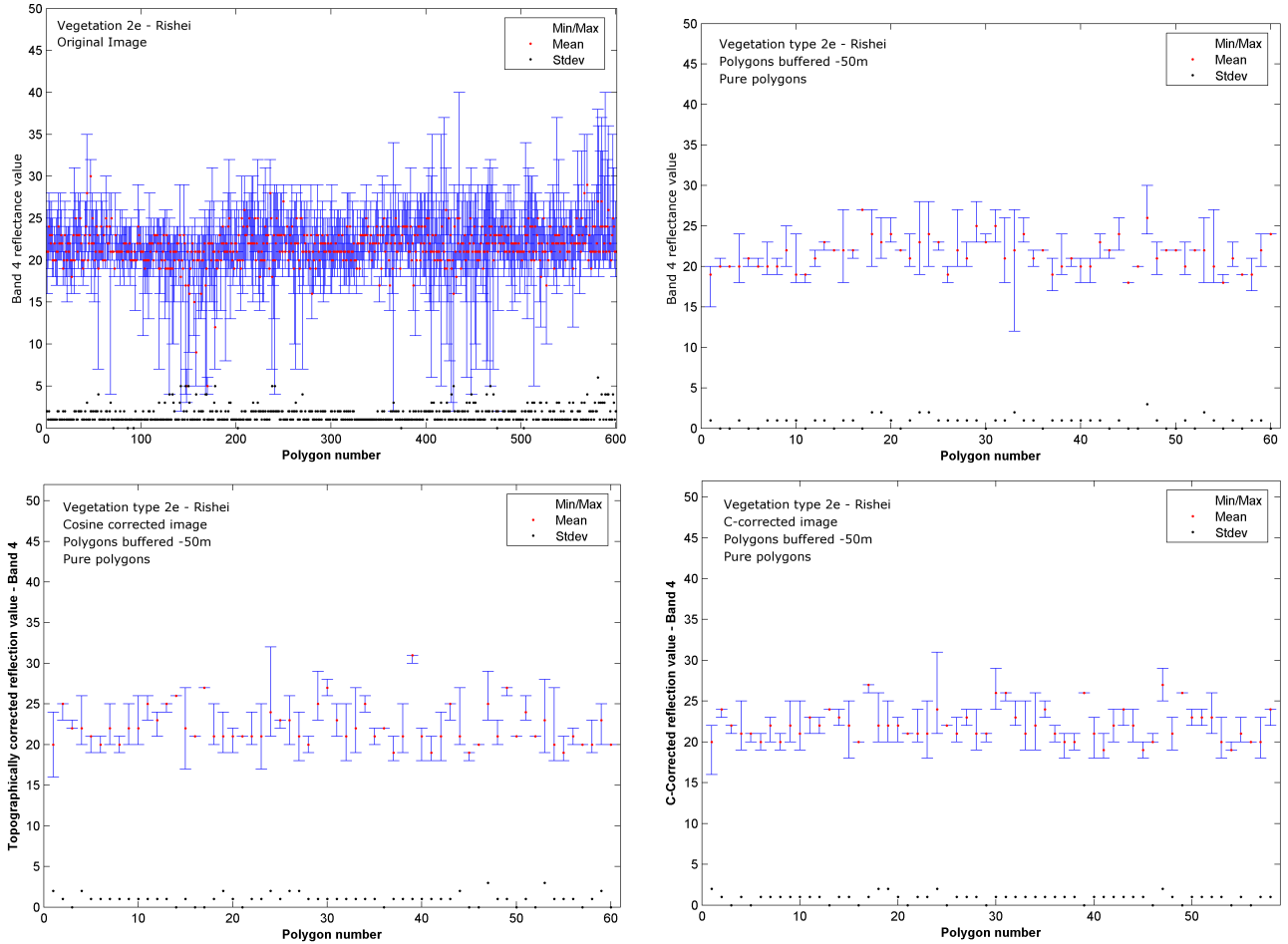

Figure 5.12: Within and between polygon variation for the original image, after buffering, pure selection & topographic corrections. Note the reduction in between and within polygon variation after buffering.

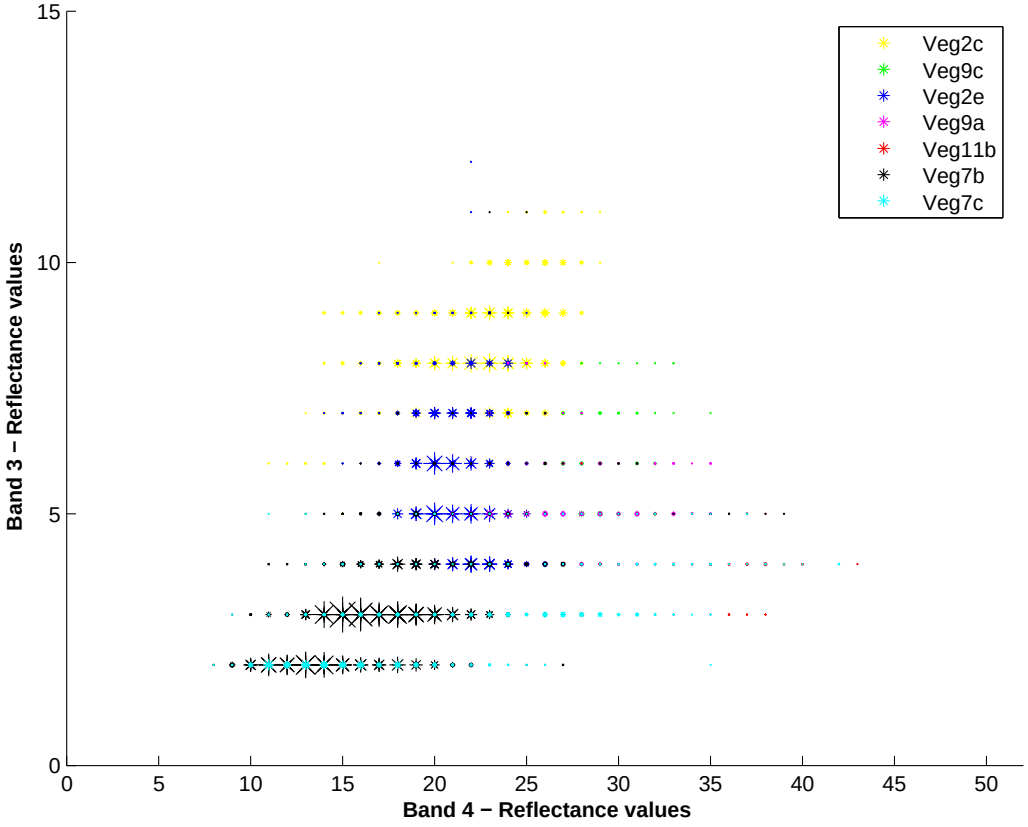

Figure 5.13: Scatter plot of original reflectance data after being buffered by -50m and the vegetation polygons selected for purity. Each vegetation type is shown in a different coloured star, where the size of the star represents the frequency of that data value. Combination of Band 3 and 4. Note the difficulty in visually separating between vegetation types.

Figure 5.13 has very spread out values in the NIR band (from 7-42% reflection). Note that the some of the NIR values are quite low. In the red band (3) the values range from 1-10% reflection. Having high reflectance values in the NIR band and lower reflectance values in the red band is typical of most vegetation types (Lillesand et al., 2004). Vegetation type 7c (Enggranskog, a spruce type), has reflectance values that cover the whole range of the scatter-cloud in the NIR band. Other types such as 2c, the green dots (lavhei, alpine grass), cover a smaller, more compact ranges. From this scatter-plot, none of the majour vegetation types shown appear to be separated from the rest of the group.

The other 14 band combinations showed varying shapes and sizes but they all followed the same trend of overlapping vegetation types. These being seven of the main vegetation types, if these classes can not be separated, then the classification results would not be good enough.

5.3.1.2 ROI Separability after Buffering

Tables 5.9 and 5.10show the results of ROI separation statistics after the polygons have been buffering.

After having buffered the polygons and theoretically reduced a lot of the influence from neighbouring vegetation types, it is now possible to separate between LG and VG, and LG and Pasture classes, which is very positive, see table 5.9. When compared to those ROI separability results without buffering, there is a huge improvement (see section 5.2). The LG and VG combination received 1.21 (JM), (table 5.3), whereas here this pair had a value of 1.85. This has implications for choosing areas as representations for classification. i.e. whole polygons of a particular class should not be chosen for training data, the centre of large homogeneous polygons are more likely to give a better representation.

Grazing Quality Classes	Jefferies Matusita	Trasformed Divergence
Good & Very good	1.00	1.18
Very Good & Pasture	1.16	1.35
Less Good & Good	1.46	1.84
Good & Pasture	1.49	1.77
Less Good & Pasture	1.79	2.00
Less Good & Very Good	1.86	2.00

Table 5.9: ROI separability - reflectance image 24.July.94. Buffered 50m but not pure polygons.

The second table, figure 5.10, shows results from selected pure and then buffered vegetation polygons (7 types). This table shows a large difference between the JM method and the Transformed Divergence method. The last 5 combinations had very good separation. These include pairs of vegetation types that are quite different from each other, e.g. 2e (*Rishei*) and 7c (*Enggranskog*).

The most important aim in this project is to separate between the very different vegetation types as they mostly represent different grazing qualities. Similar vegetation types often represent the same grazing type. Although these tests give an indication of the separability between pairs of vegetation types they do not indicate whether a single type can be separated from all the others. Vegetation class 2e (Rishei-Good quality) for example can be well separated from classes 7c (VG), perhaps separated from 7b (G), and 11b (VG) and not separated from 9a (LG), 4b (G), and 9c (LG).

For class 2e the most important is to be able to separate itself from 9a, and 9c which are LG and then from 7c and 11b which are VG, which it managed to do.

Class 2e (Rishei) is the second most dominating vegetation type in Venabygd, covering 22.1% of the total area. 4b (*Blåbærgranskog*) covers the largest proportion with 23.3%. Further analysis is needed to understand what lies behind the difficulty in separating between grazing qualities and vegetation types.

Vegetation Classes	Grazing Quality Classes	Jefferies Matusita	Trasformed Divergence
9a & 9c	LG & LG	0.74	0.81
7b & 7c	G & VG	0.79	0.87
2e & 4b	G & G	1.08	1.17
2e & 9a	G & LG	1.26	1.77
2e & 9c	G & LG	1.27	1.78
4b & 7b	G & G	1.35	1.65
4b & 9c	G & LG	1.48	1.95
11b & 9a	VG & LG	1.53	1.90
4b & 9a	G & LG	1.63	1.95
11b & 2e	VG & G	1.63	1.920
2e & 7b	G & G	1.68	1.94
11b & 9c	VG & LG	1.71	1.98
7b & 9c	G & LG	1.72	1.96
11b & 4b	VG & G	1.75	1.96
4b & 7c	G & VG	1.75	1.90
11b & 7c	VG & VG	1.79	1.85
11b & 7b	VG & G	1.85	1.96
7b & 9a	G & LG	1.87	2.00
7c & 9c	VG & LG	1.94	2.00
7c & 9a	VG & LG	1.95	2.00
2e & 7c	G & VG	1.96	2.00

Table 5.10: ROI separability - vegetation classes - reflectance image 24.07.94. Polygons are pure and buffered 50m.

5.3.2 Terrain Variation

5.3.2.1 Elevation

Elevation was plotted against reflectance values for a number of vegetation class pairs to determine if it could be used as a separation feature. Figure 5.14 illustrates one example of these. The vegetation classes 7c (*Enggranskog* VG) and 9c (*Grasmyr* LG) show that it is fairly possible to separate between these two types in the NIR band using elevation, even though they both cover similar reflectance

values. Elevation is a good attribute to add for separating vegetation types occurring in the valley with those higher up on the slopes, but that both cover similar reflectance values. 7c and 9c had a JM distance of 1.94 after buffering. Of the 10 plots for elevation using the selection of vegetation types in figure 5.8, only 2 were separable. The second pair was 7b and 2e, but most of the polygons in these classes belong to the same grazing quality class.

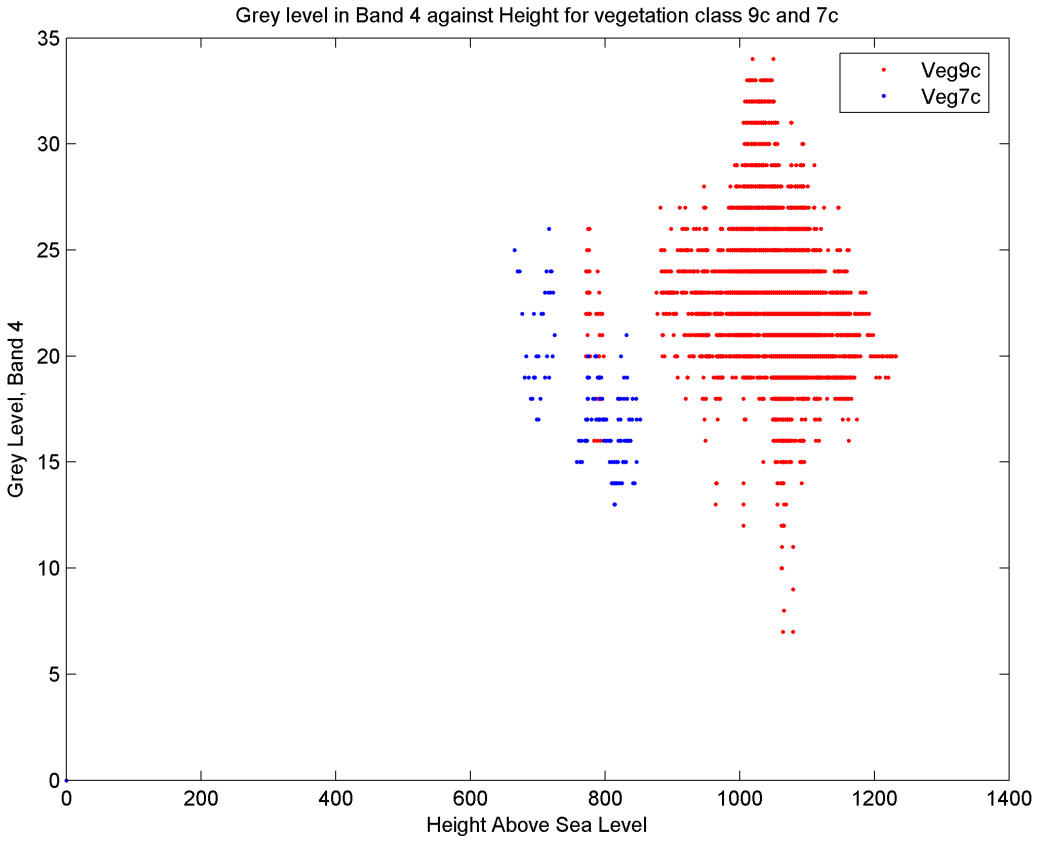

Figure 5.14: Scatter plot, elevation of 2 vegetation classes against the NIR band. Image 24.07.94

5.3.2.2 Slope & Aspect

The affects of slope and aspect on different vegetation types was illustrated through polar plots. Each dot was placed in a position on the polar plot depending on its slope and aspect value. A colour code represents the reflectance value range. The distance from the centre represents the slope of the pixel. Slope was recorded in whole integer numbers, which gives rise to the ring appearance of the plot (i.e.

each ring representing a degree of slope). The further out the data point is lying, the higher slope value. The angle measured from the centre represents the aspect. North is to the right and continues in a clockwise direction. There are 6 plots one for each Landsat TM band of data.

Figure 5.15 shows the data for vegetation type 7b (spruce with blueberry undergrowth). This type covers 13% of the Venabygd site and is categorised as having potentially good grazing quality. Those data points having a slope of approx. 6° or less appear to lie in a complete circle around the centre. This means that pixels with a low slope angle show no directional preference (i.e. specific aspect). This seems intuitive, as relatively flat ground would receive approximately the same amount of sun and water. When the slope angle increases however, the way in which the slope is facing becomes more important. Data points with slope values greater than 6° show more of a directional preference. From the plots of vegetation type 7b it appears that most of the vegetation lies in areas that have aspects ranging between north and southwest. The majourity of the data was lying on slopes that are $\approx 20^\circ$ or less.

Each plot represents a distinct reflectance value category. Band number 1, the blue band, has reflectance values that range from 5-17%, so it has a navy blue colour with a few orange spotse. Band numbers 2, 3 and 7 are red and hence have reflectance values from 0-5%, but there are also several blue and orange spots, indicating that some points have reflectance values up to 15%. Band 4 on the other hand is mostly green, in the 16-20% range. When looking closely there are also circles of red, blue, orange, gold, sienna and pink. In this band, for vegetation type 7b, the reflectance values range from 1-37%.

Similar plots were drawn for vegetation types 7b, 4b, 2e, 2c, 9c, 9a, 11b and 7c. Vegetation types 2e, 2c, 9c, and 9a, showed a fairly circular pattern meaning that as the slope increased they did not show any signs of being distributed on a particular slope direction (i.e. aspect). These vegetation types are alpine grasses, heath and swamp vegetation. 11b, 4b, and 7c however, showed more direction choice. 11b is pastures, and had a south, south-west direction on all slope angles although the slope angle range only went up to $\approx 10^\circ$. 7c, another spruce type showed fairly similar results to the 7b (spruce) plots (fig 5.15), with the vegetation lying mostly on slopes that faced in a west, south-west direction. The notable point in this plot was that there were almost no points towards the middle of the graph indicating that this vegetation type occurred at angles greater than 5° (but less than 10-12). 4b, a birch type, covered a large range of aspect angles especially in very low slope angles. Above $\approx 9^\circ$ most of the points were found in a south-west through to northerly direction. Each vegetation type had unique reflectance colour combinations for the different bands.

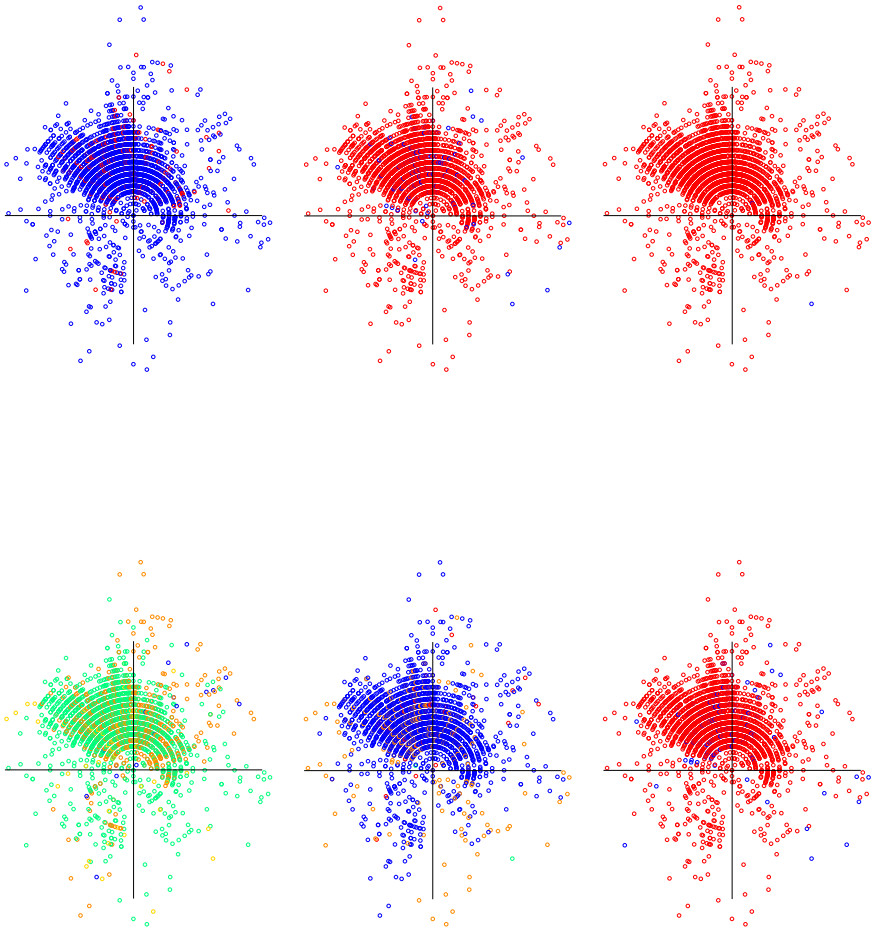

Reflectance Category	colour
0-5%	Red
6-10%	Navy Blue
11-15%	Dark Orange
16-20%	Spring Green
21-25%	Gold
26-30%	Sienna
31-35%	Deep pink

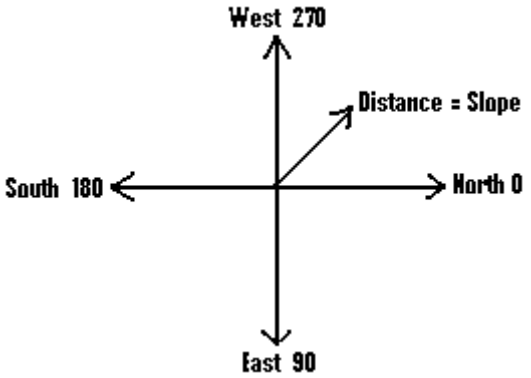

Figure 5.15: Vegetation type 7b. Band: 1, 2, 3, 4, 5, & 7, from left to right. Slope is given as the distance from the middle. Aspect as the angle from the centre, see north diagram. The reflectance value is represented in a series of colours. The size of the data point represents the frequency of the data value combination.

5.3.2.3 Atmospheric Variation

The electromagnetic radiation signals collected by satellites in the visual spectrum are affected by scattering and absorption by gases and aerosols as they pass through the atmosphere. When and how to correct the atmospheric effects depend on the remote sensing and atmospheric data available, the information desired, and the analytical methods used to extract the information. In many applications involving classification and change detection, atmospheric correction is unnecessary, as long as the training data and the data to be classified are in the same relative radiometric scale. Corrections are necessary however if multi-temporal datasets are to be used (Song et al., 2001). Due to the fact that an image from only one time period has been used in most analyses, no atmospheric corrections were performed. Cingolani et al. (2004) also agrees that it was unnecessary with atmospheric correction when a single image is to be used for classification.

5.3.3 Illumination Variation

Figure 5.16 illustrates the procedures taken to analyse the variation in illumination in the image. These follow on from those analyses on spectral and topographic variations in the image.

An ideal slope-aspect correction would remove all topographically induced illumination variation, so that two objects having the same reflectance properties show the same digital number (DN) despite their different orientation to the sun's position. Teillet (1986) subdivides the radiometric effects on an image into two major categories:

- Sensor induced effects - includes technical aspects such as the calibration of detectors, filtering, and platform and system stability, etc.
- Scene related effects - include the influence of topography, atmosphere, viewing angle, adjacency effect, position of the sun and the reflectance properties of objects.

The sensor induced effects were not considered here as they are calibrated for and delivered with the Landsat images. the scene related effects will be dealt with in this section through the correction of illumination variation. The position of the sun does not need to be corrected for when only working with one image, but when scenes from multiple dates are used then this becomes a factor.

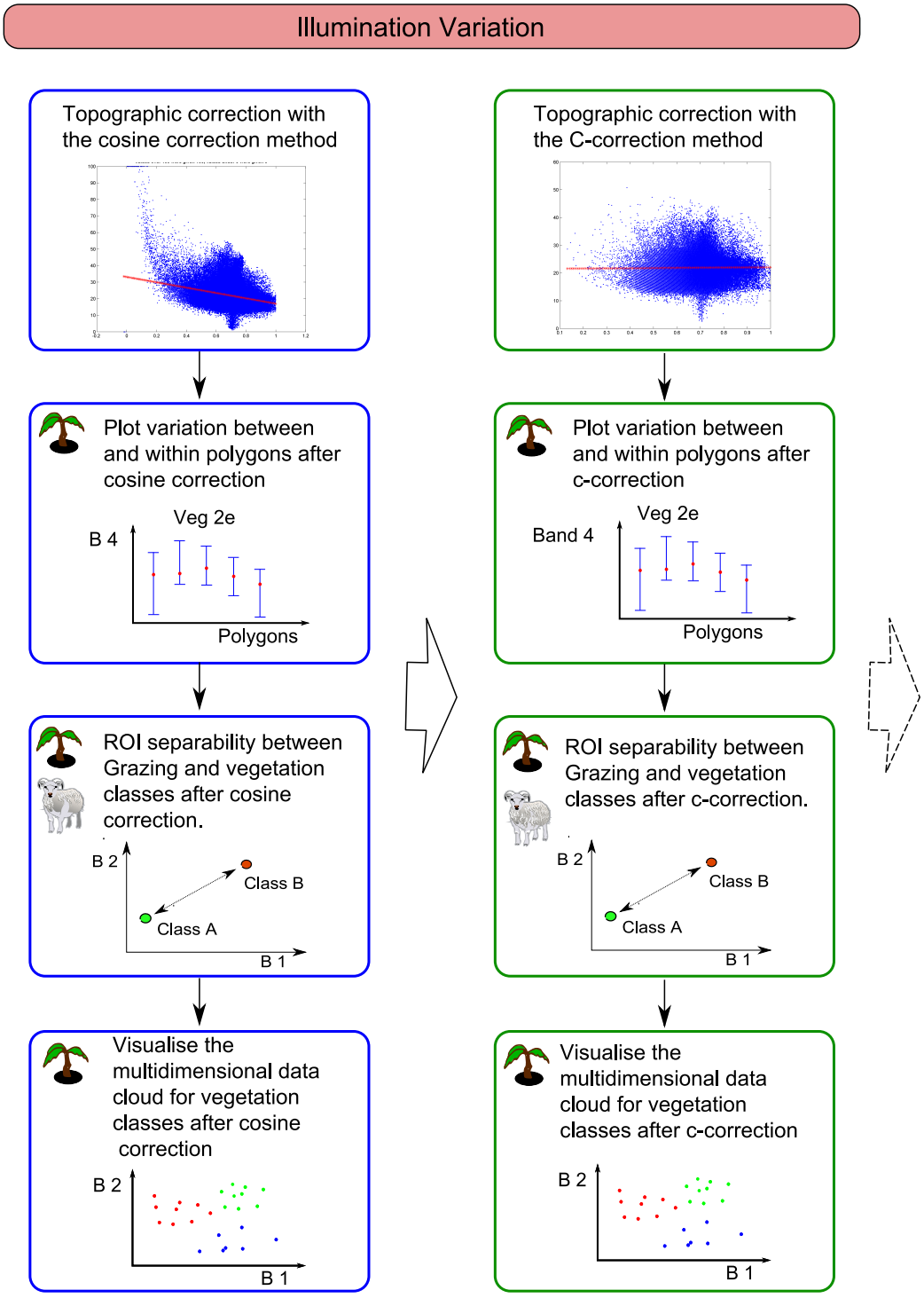

Figure 5.16: Flow diagram to indicate the procedure followed for analyses on illumination variation, more specifically topographic corrections. The results from these are compared with those from terrain variation and spectral variation analyses. The next flow diagram is shown in figure 5.24 which deals with classification of the image and the analysis of aerial photographs.

Cosine Topographic Correction

The cosine correction method models the direct part of the irradiance. In reality regions which are weakly illuminated by direct sunlight, receive a considerable amount of diffuse irradiance. In such areas, the cosine correction has a disproportional brightening effect (because the diffuse radiation is not taken into account). The smaller the $\cos(i)$ the stronger this over-correction is (Eq. 4.10). For pixels in complete self-shadow (i.e. when $\cos(i) = 0$), and in faintly illuminated areas, the DNs saturate and lead to artifacts in the corrected image.

Figure 5.17 shows the calculated illumination $\cos(i)$, for the reflectance image of 24.07.94. The lighter areas are areas that received mostly direct illumination (values close to 1) and the darker areas are those that received very little direct illumination or are even in complete self shadow (values close to 0). Very few areas have low $\cos(i)$ values, giving a good chance for the success of this method.

A first order linear regression of the image data before and after the cosine correction method illustrates how the data has been changed by the correction method. The regression was calculated on the 3 grazing quality classes only, to give the best possible regression line.

Figure 5.18 shows a scatterplot of the original uncorrected data, with band 4 on the Y axis and $\cos(i)$ on the X axis. The red line running through the data cloud is the regression line. The regression line illustrates that as the illumination increases for a pixel so does the reflectance value recorded back at the satellite. This is what is happening in the nature i.e. that the greater the illumination on an object the greater the reflectance. What we are trying to achieve, is a correction for this, so that irrespective of the illumination, an object of the same type will reflect the same amount of radiance.

The data plotted after the cosine correction is shown in figure 5.19. The cosine correction has lead to a regression line that is not flat, as was aimed for. The method has highly overcorrected the the lower illumination pixels to have very high reflectance values. In reality, these areas would receive a considerable amount of diffuse irradiation and would not be corrected so extremely. The values in this plot have been adjusted. The values that were given after the cosine correction method are shown in figure 5.20. The pixels that were overcorrected had been given values that were far above 100 and below 0 reflectance. These large numbers drowned out the variation in pixels within 0-100. In order to correct for this, all pixels that were given a reflectance value over 100, were given the value 100 and all pixels under 0, were given the value of 0. In figure 5.19 there is a small line of pixels having the value 100 and 0.

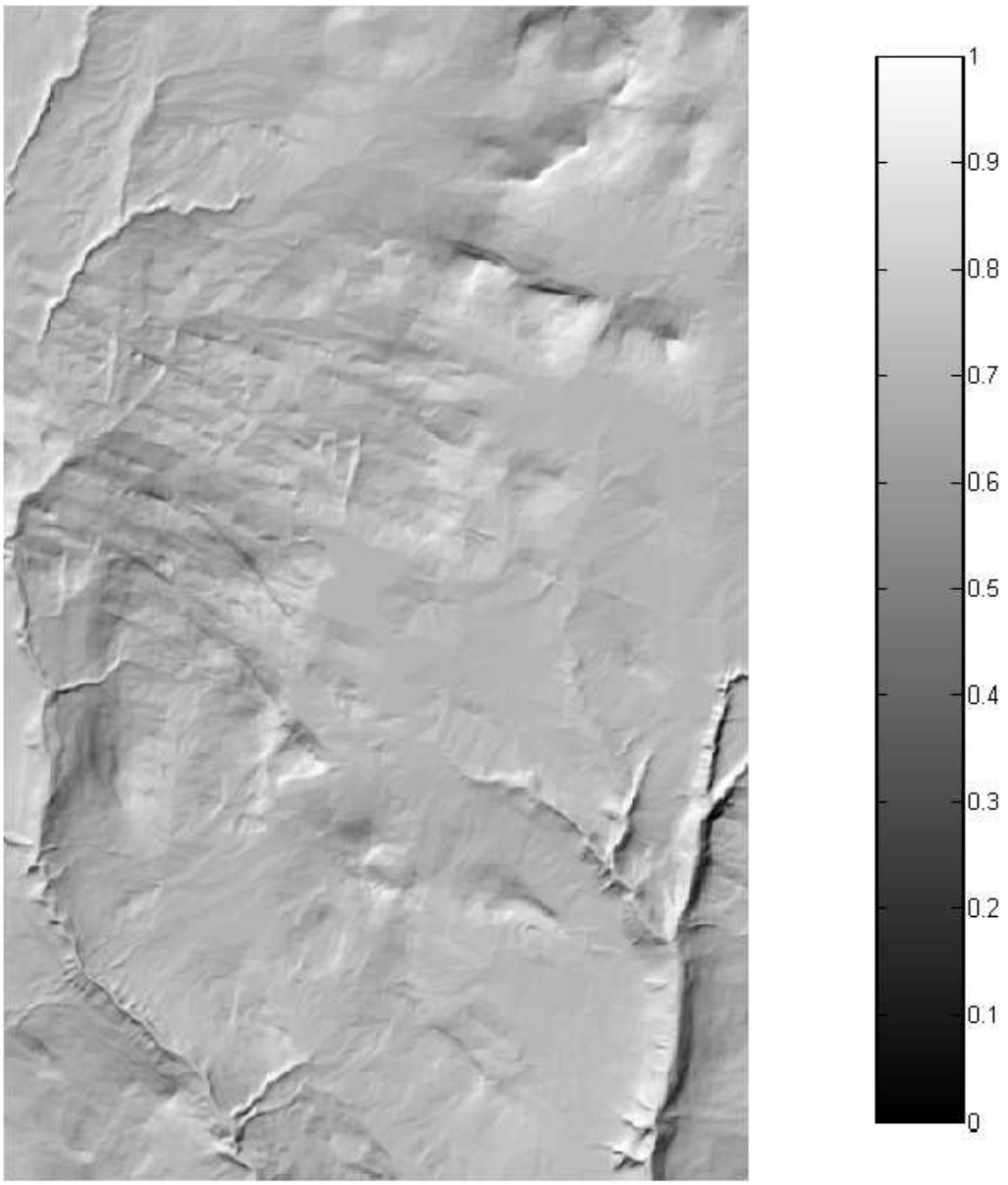

Figure 5.17: This image shows the illumination $\cos(i)$, calculated from the reflectance image 24.07.94. It is calculated taking the suns zenith angle, slope and aspect in to account. $\cos(i)$ determines the strength of a pixels illumination. A value of 1 indicates direct illumination. A value of 0, indicates no direct illumination. In this image from July there are only a few pixels which have poor direct illumination. There is a ridge that runs along the bottom right hand side of the image. On the far side of that (right hand side) there are some very dark areas. These areas have received poor direct sunlight in this image. Areas in deep shadow can give miss-representative reflectance information about the ground cover.

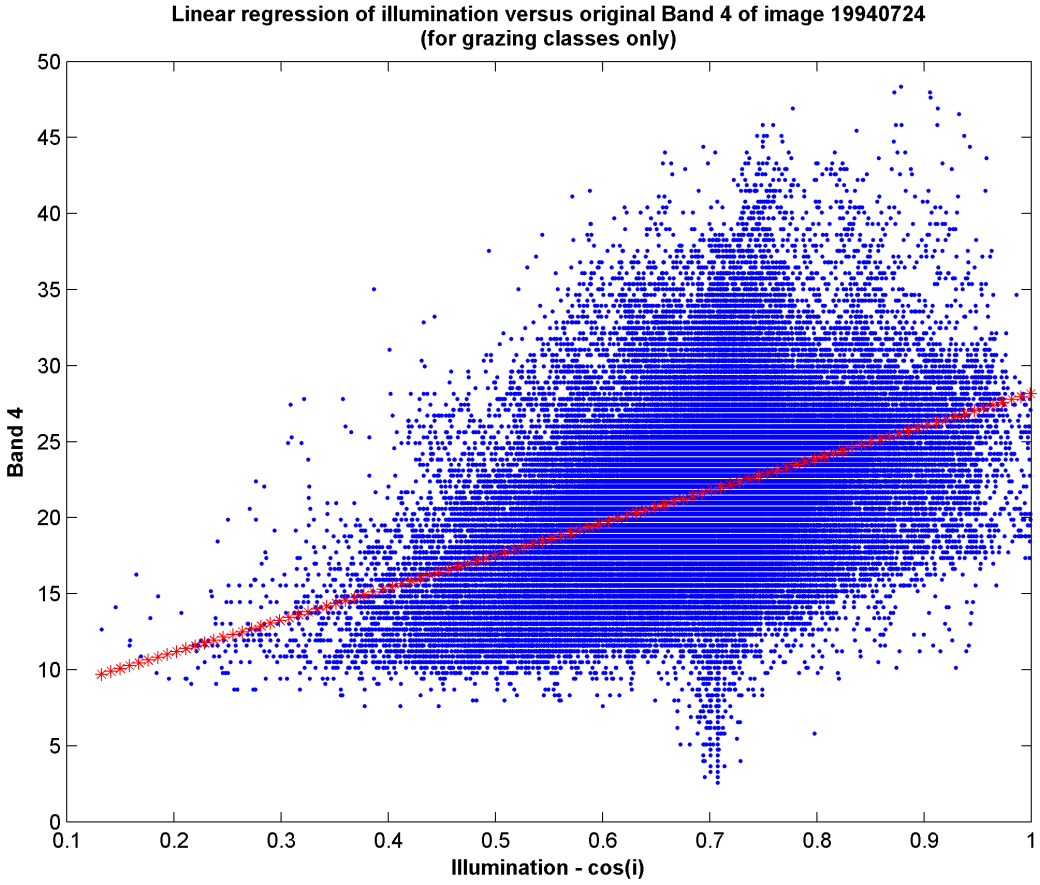

Figure 5.18: This plots represents the spread of data in band 4 of the image 24.07.1994 against illumination $\cos(i)$, before any topographic correction. The data belongs only to the 3 grazing quality classes, all other land cover types have been masked out of the image. The red line is a regression line for this data. It shows the trend in the data which indicates that the less direct illumination a pixel has, the less reflectance is recorded at the satellite. This is a normal situation, however, when analysing the reflectance values for land cover types the aim is to have a dataset which shows specific reflectance values for a given land cover type, irrespective of illumination. Topographic corrections can improve this situation.

A scatter plot of showing the data cloud in a 2 dimensional space after cosine correction is shown in figure 5.21. No significant changes were seen from the scatterplot of the original data (shown in figure 5.13) to that of of the cosine corrected data in a band 4 & 3 combination. The data did appear to have spread out slightly and there were now points dotted around the outside of the scatter-cloud. This is partly a result of the over-correction that occurs with the cosine method (see section 4.2.4). All 15 band combinations were drawn. Those band combinations with band 1 tended to have the greatest change from the original image and had more outliers around the edges of the cloud, making the plots look more

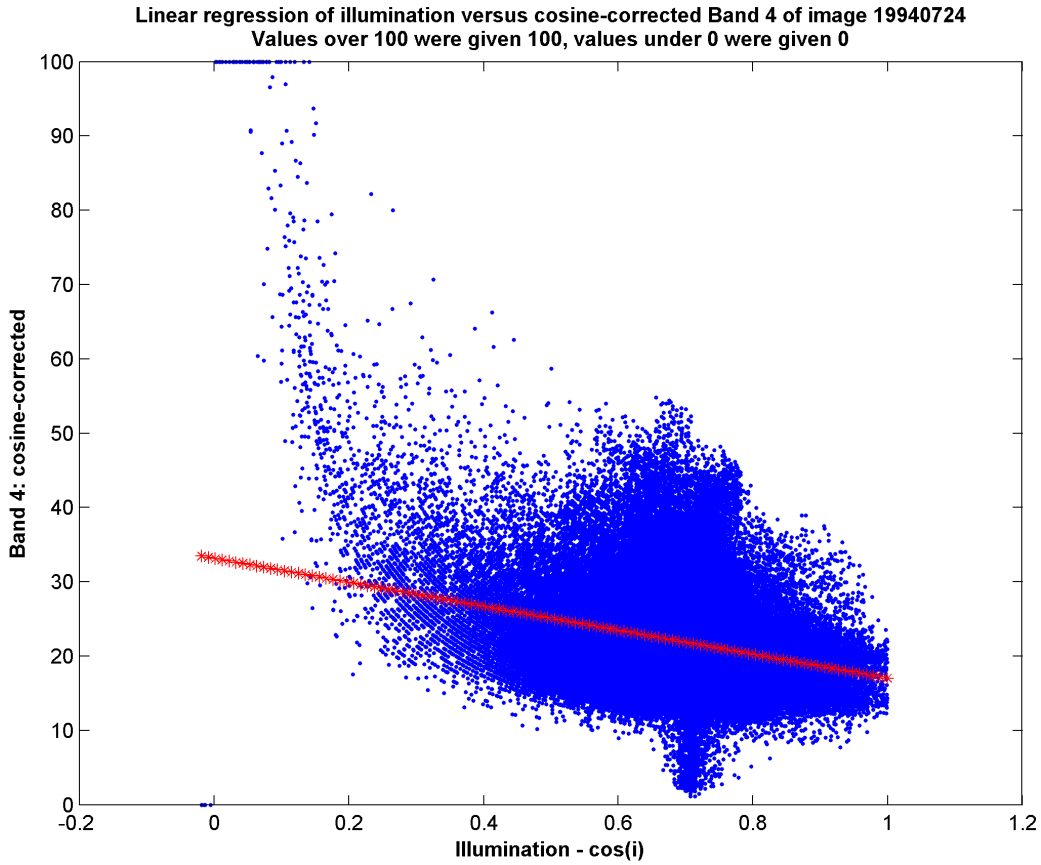

Figure 5.19: This plot represents the spread of data in band 4 of the July image against illumination $\cos(i)$ after a cosine correction. The regression line, shown in red, indicates that with decreasing illumination, there is an increase in reflectance. This is not ideal and is the result of the over-correction of illumination by the cosine method because it does not take any diffuse illumination into account.

fuzzy. As with the data before topographic correction none of the plots showed any clear separation between vegetation types.

Tables 5.11 and 5.12 show the results of the ROI separability tests. Table 5.11 shows the results from the grazing classes. See tables 5.1 to 5.7 for a comparison of values from the original images (may-oct), those from the composite images (table 5.7), and those from buffered and pure polygons, tables 5.9 to 5.10.

The results after the cosine correction look fairly good in comparison to the original images. The combination of LG & VG was 1.2 (JM) in the original image from this date. The separation values were higher than those shown from the composite image. The best results so far have been shown after having buffered all polygons, but this is a technique that can not be applied to a virgin area with

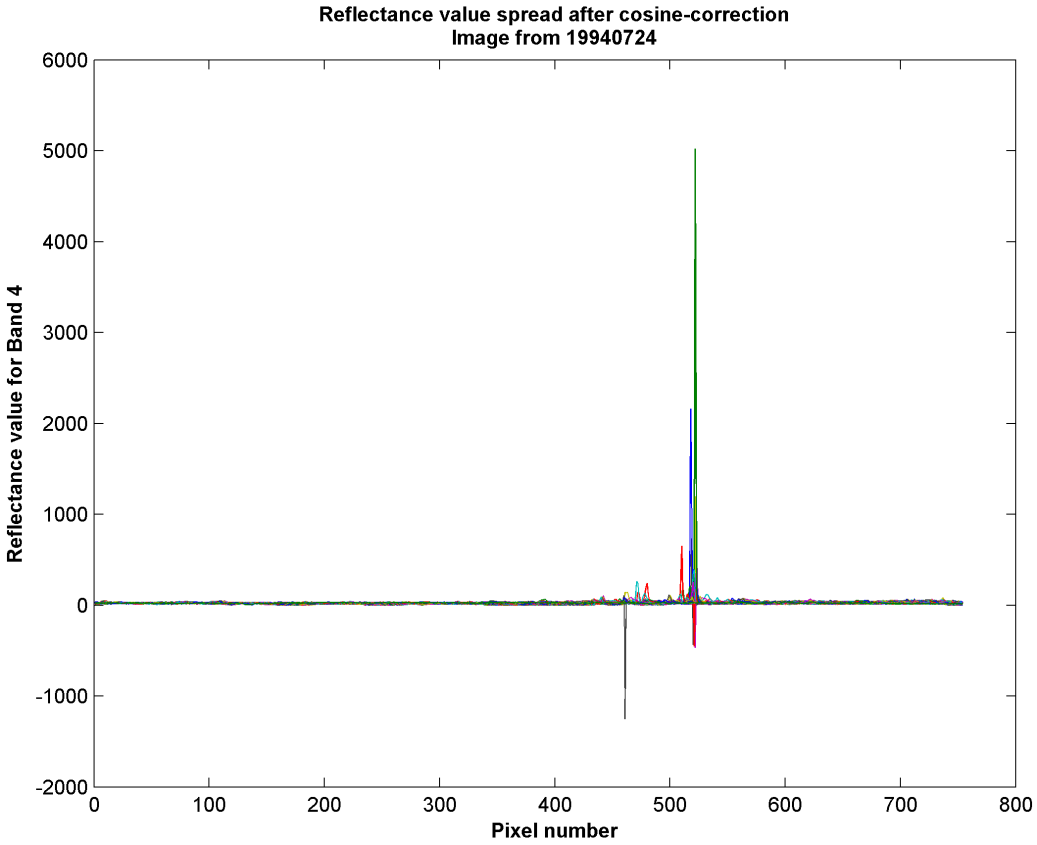

Figure 5.20: This plot shows the data value and frequency after the cosine correction. The variance between $0-100$ is totally drowned out by the over-correction in this method.

no predefined vegetation classes.

Grazing Quality Classes	Jefferies Matusita	Trasformed Divergence
Good & Very good	0.92	1.10
Very Good & Pasture	1.23	1.49
Less Good & Good	1.29	1.60
Good & Pasture	1.63	1.84
Less Good & Very Good	1.74	1.96
Less Good & Pasture	1.77	1.92

Table 5.11: ROI separability - grazing classes - after cosine correction - 24.07.94. Buffered 50m.

In respect to the vegetation classes, the results after a cosine correction (table 5.12) show a number of improvements when compared to the original buffered data (table 5.10). The ROI separability statistics for the vegetation classes after cosine correction were calculated on selected pure polygons and those buffered by 50m.

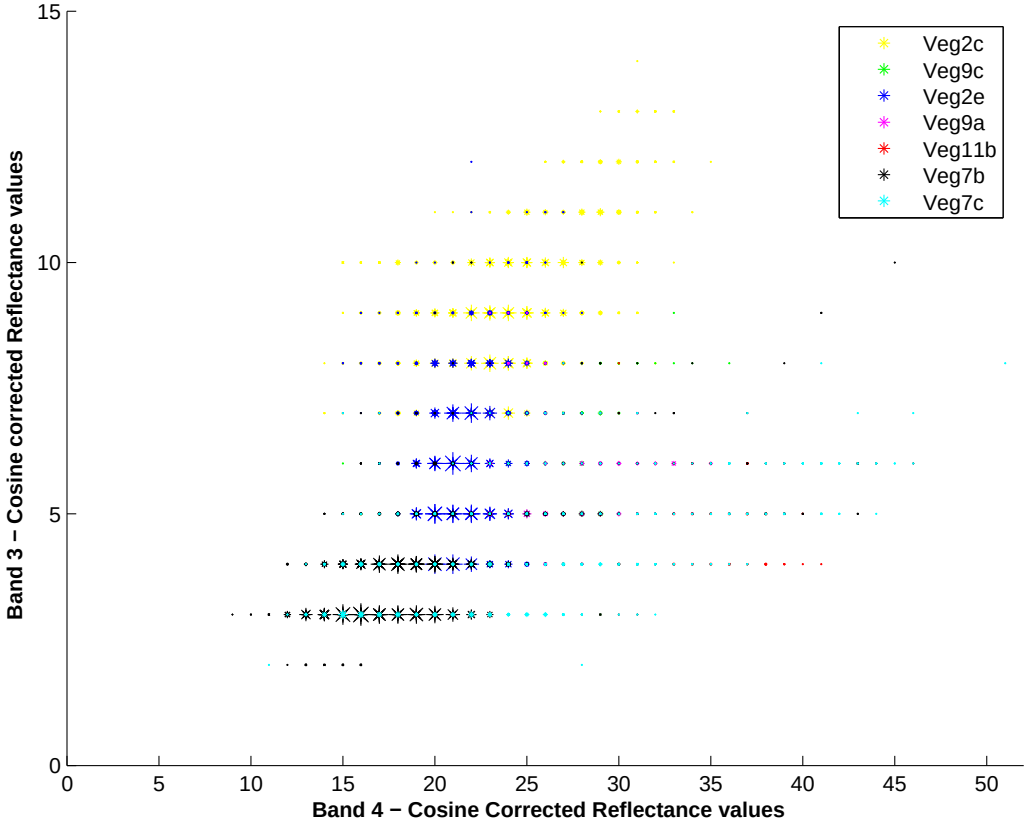

Figure 5.21: Scatter plot of band 3 and band 4 data of the cosine corrected image. The size of the star represents the frequency of that data value. Topographic correction has not changed the difficulty in separating between vegetation types. The results look very similar to those of the uncorrected image. See figure 5.13 for comparison.

An interesting observation was that the order (least to most) of separation changed considerably after this correction. The vegetation types 11b & 4b improved from 1.74 - 1.95 and 11b & 2e improved from 1.63 - 1.93. Some pairs reduced in separability after correction such as 7b & 9c which reduced from 1.72 - 1.59 and 4b & 9a which reduced from 1.62 - 1.47. There were some improvements and some reductions, giving no straight forward conclusion to if the cosine correction method was significantly better.

C-Correction

Figure 5.22 shows the data cloud after a c-correction has been applied. The regression line shows the relationship we were aiming for, in that with an increase

Vegetation Classes	Grazing Classes	Jefferies Matusita	Trasformed Divergence
9a & 9c	LG & LG	0.59	0.65
2e & 4b	G & G	0.79	0.83
7b & 7c	G & VG	0.84	1.01
2e & 9c	G & LG	1.07	1.52
2e & 9a	G & LG	1.24	1.68
4b & 7b	G & G	1.33	1.78
4b & 9c	G & LG	1.36	1.77
4b & 9a	G & LG	1.47	1.86
2e & 7b	G & G	1.49	1.91
7b & 9c	G & LG	1.59	1.86
11b & 7c	VG & VG	1.72	1.96
11b & 9a	VG & LG	1.72	1.86
4b & 7c	G & VG	1.76	1.98
7b & 9a	G & LG	1.76	1.97
11b & 9c	VG & LG	1.86	1.92
7c & 9a	VG & LG	1.86	2.00
7c & 9c	VG & LG	1.87	1.99
2e & 7c	G & VG	1.92	2.00
11b & 2e	VG & G	1.93	2.00
11b & 7b	VG & G	1.95	1.99
11b & 4b	VG & G	1.95	1.99

Table 5.12: ROI separability - vegetation classes after cosine correction - 24.07.94. Pure polygons, buffered 50m.

in illumination there is no increase in reflection. From the scatter plot of band 4 it appears that the c-correction method has been very effective at topographically correcting the image. Plots of the other bands showed similarly very positive results when plotting a regression line to the data.

In figure 5.23 the c-corrected data is represented in a scatterplot of band 3 vs band 4. There was very little change to the data compared to the original and cosine correction data. No visible distinction can be made for any of the main vegetation classes illustrated. This trend was also seen in all of the 15 other band combinations that were analysed.

Table 5.13 shows the results of grazing class separation after c-correction. Compared with the cosine correction, the results have improved for every combination except for VG & Pasture. When compared with the original image (table 5.3) the results have improved significantly in all classes. When compared to the buffered uncorrected image (table 5.9), the results varied with some improvement and some worsening. Topographic correction with the c-correction method shows promise

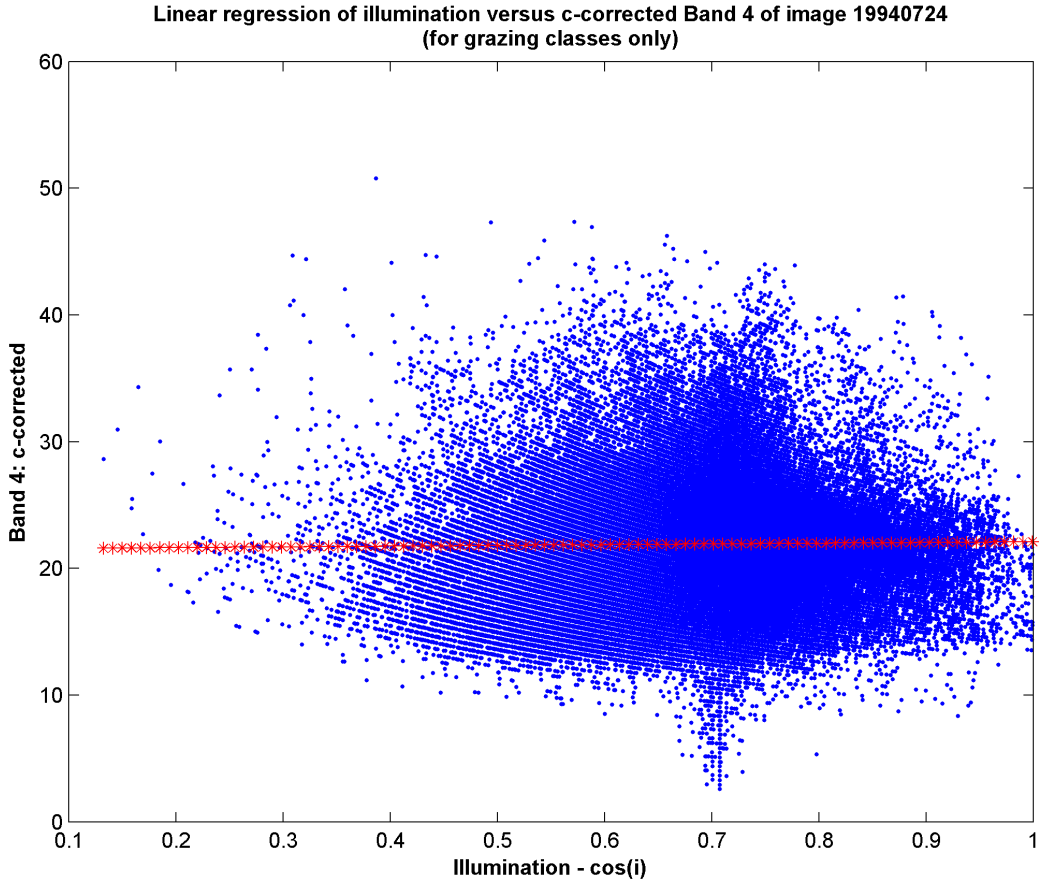

Figure 5.22: The regression line for this spread of data from band 4 of the July image against $\cos(i)$ after a c-correction, shows that the relationship between reflectance and illumination is now ideal. It illustrates that irrespective of illumination the reflectance for grazing classes is fairly equal.

for virgin areas.

Grazing Classes	Jefferies Matusita	Trasformed Divergence
Good & Very Good	0.86	1.02
Very Good & Pasture	1.30	1.51
Less Good & Good	1.35	1.73
Good & Pasture	1.69	1.89
Less Good & Very Good	1.74	1.99
Less Good & Pasture	1.82	1.99

Table 5.13: ROI separability - grazing classes - c-corrected - 24.07.94. Buffered by 50m, not pure polygons.

The vegetation classes showed a change in order again of least to best separated

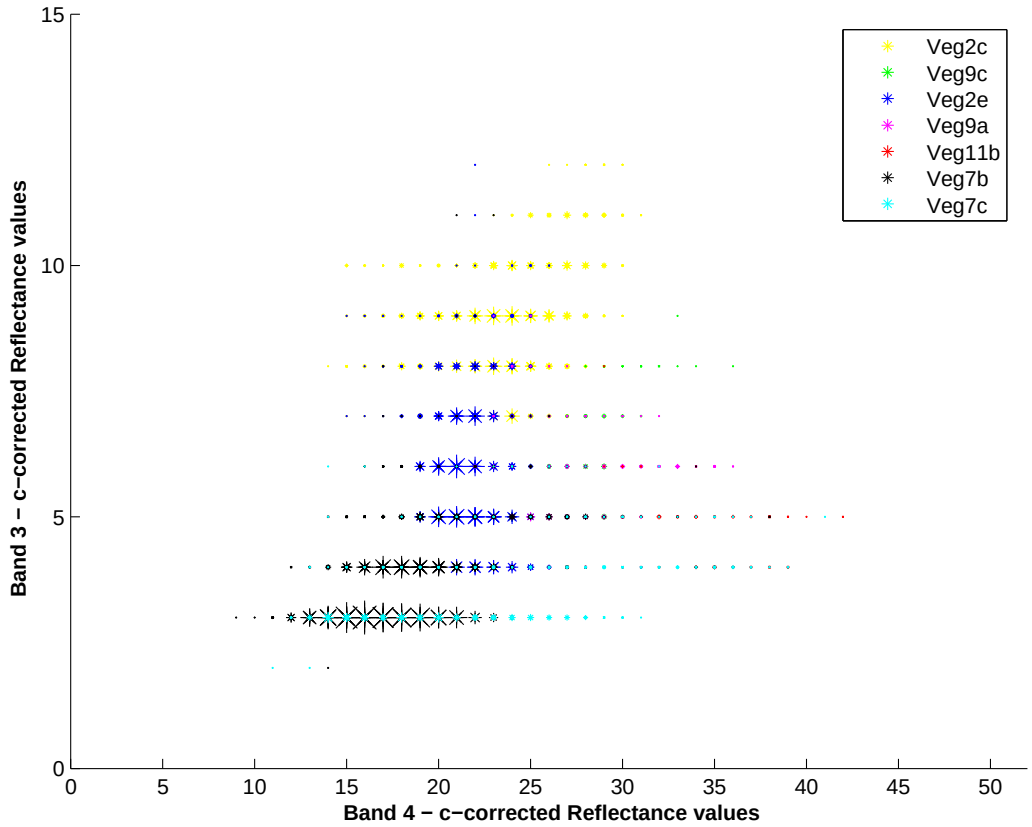

Figure 5.23: Scatter plot of bands 3 and 4 from the c-corrected image. The size of the star represents the frequency of that data value. The results are very similar to those of the uncorrected image and cosine corrected image. No visual separation can be between vegetation types.

pairs as was seen after the cosine correction method. The c-correction method showed a similar order to the cosine correction, but a slight variation from the original buffered image. The comparison of results from the cosine correction showed some improvements and some decreases.

Table 5.15 shows the difference between the original buffered and pure dataset from the 24.07.94, compared with the same dataset (i.e. buffered and pure) that has been topographically corrected with the cosine and c-correction methods. The summary is done for the JM difference method and registered to 2 decimal places. The results show that there are both decreases and increases from the original data after both topographic corrections (as discussed). The summed difference for the different comparisons are also included. These show that the original data is actually slightly better. When excluding those vegetation pairs that come from the same grazing quality class however (i.e. we don't want to separate between

Vegetation Classes	Grazing Classes	Jefferies Matusita	Trasformed Divergence
9a & 9c	LG & LG	0.61	0.66
7b & 7c	G & VG	0.67	0.81
2e & 4b	G & G	0.94	1.02
2e & 9c	G & LG	1.07	1.55
2e & 9a	G & LG	1.22	1.70
4b & 7b	G & G	1.239	1.68
4b & 9c	G & LG	1.43	1.89
2e & 7b	G & G	1.48	1.82
4b & 7c	G & VG	1.50	1.85
4b & 9a	G & LG	1.57	1.94
7b & 9c	G & LG	1.59	1.90
11b & 9a	VG & LG	1.63	1.76
11b & 7c	VG & VG	1.70	1.95
7c & 9a	VG & LG	1.74	1.98
7b & 9a	G & LG	1.76	1.98
2e & 7c	G & VG	1.79	1.95
7c & 9c	VG & LG	1.80	1.95
11b & 9c	VG & LG	1.83	1.98
11b & 2e	VG & G	1.92	1.99
11b & 7b	VG & G	1.96	1.99
11b & 4b	VG & G	1.97	2.00

Table 5.14: ROI separability - vegetation classes - c-corrected 24.07.94. Polygons buffered 50m and pure.

them) then the cosine method has the best results. As discussed in the methods, the cosine method is not optimal as it grossly over-corrects some of the pixels that lie in low illumination areas. The differences between methods are only slight and even though the cosine correction method comes out best in this analysis, the c-correction method is far more optimal.

The JM data values that were $\approx > 1.65$ are coloured in yellow and those that were > 1.9 are coloured in green. Reductions in pairs are not significant if the reduced value is still high enough for good separation. The values are coloured to give an indication of this. The c-corrected dataset will be used in further analyses as the results from the correction itself (see fig 5.22) show a much better regression relationship. Other studies have found the c-correction method to improve an image from its original state, and it is recommended in any mountainous area (Teillet, 1986).

Vegetation classes	Grazing classes	Original (O)	Cosine - O	C-corr. - O	C-corr. - Cosine
9a & 9c	LG & LG	0,73	-0,14	-0,12	0,02
7b & 7c	G & VG	0,79	0,05	-0,12	-0,17
2e & 4b	G & G	1,09	-0,30	-0,15	0,15
2e & 9c	G & LG	1,27	-0,20	-0,20	0,00
2e & 9a	G & LG	1,26	-0,02	-0,04	-0,02
4b & 7b	G & G	1,35	-0,02	-0,12	-0,10
4b & 9c	G & LG	1,48	-0,12	-0,05	0,07
2e & 7b	G & G	1,68	-0,19	-0,20	-0,01
4b & 7c	G & VG	1,75	0,01	-0,25	-0,26
4b & 9a	G & LG	1,62	-0,15	-0,05	0,10
7b & 9c	G & LG	1,72	-0,13	-0,13	0,00
11b & 9a	VG & LG	1,52	0,20	0,11	-0,09
11b & 7c	VG & VG	1,85	-0,13	-0,15	-0,02
7c & 9a	VG & LG	1,95	-0,09	-0,21	-0,12
7b & 9a	G & LG	1,87	-0,11	-0,11	0,00
2e & 7c	G & VG	1,95	-0,03	-0,16	-0,13
7c & 9c	VG & LG	1,94	-0,07	-0,14	-0,07
11b & 9c	VG & LG	1,71	0,15	0,12	-0,03
11b & 2e	VG & G	1,63	0,30	0,29	-0,01
11b & 7b	VG & G	1,85	0,10	0,11	0,01
11b & 4b	VG & G	1,74	0,21	0,23	0,02
Sum of differences between all pairs			-0,68	-1,34	-0,66
Sum of differences between unlike grazing pairs			0,10	-0,60	-0,70

Table 5.15: Comparison between topographic corrections using JM distance. All datasets have been buffered (50m) and are pure - 24.07.94

5.4 Unsupervised Classification

Unsupervised classifiers involve algorithms that examine the pixels in an image and aggregate them into classes based on the natural spectral groupings or clusters present in the image values. The basic premise is that values within a given cover type should be close together in the measurement space, whereas values in different classes should be comparatively well separated. The resulting classes must be compared with some form of reference data (ground truth) to determine the identity and information label of the spectral classes. In a supervised classification approach information categories are defined first and then their spectral separability is examined. This thesis has followed a primarily supervised approach of trying to address the separability of predefined information classes. The advantage

of an unsupervised classification is that, classes not apparent to the analyst may be found (Lillesand et al., 2004). See figure 5.24 for an overview of the procedures taken in this analysis section.

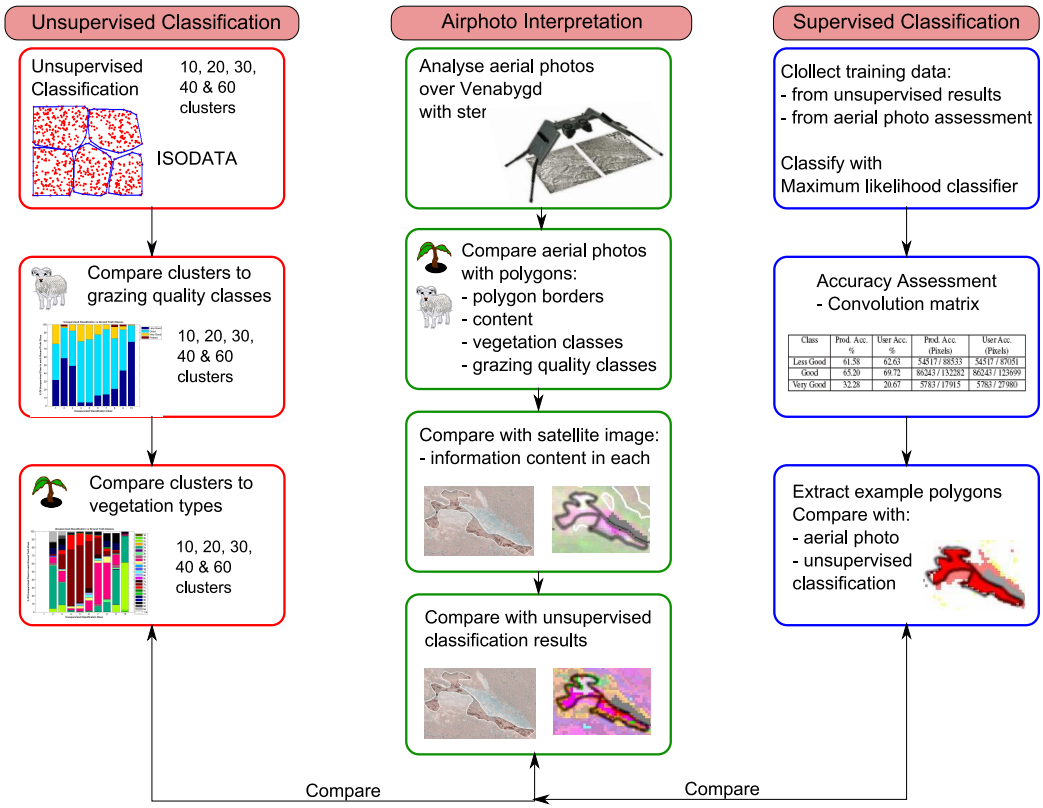

Figure 5.24: This flow diagram outlines the procedure followed for the unsupervised classification and supervised classification of the c-correction image. It also indicates the steps taken in the inspection or airphotos, and their comparison with the results of the classifications. This flow diagram leads on from that shown in figure 5.16.

Grazing Classes

Figures 5.25 to 5.27 show 3 of the 5 bar graphs created to illustrate the relationship between the unsupervised clusters and the grazing quality classes.

Figure 5.25 shows the plot for 10 unsupervised clusters. It shows that every cluster contains, parts of, at least 3 of the grazing quality classes. None of the clusters were spectrally representative of a single grazing class, however there were some that come close. Clusters 4, 5, 6 & 7 were fairly dominated by the G grazing class.

The VG & Pasture grazing classes were not dominant in any of the 10 clusters. The LG class was most dominant in the unsupervised cluster number 10.

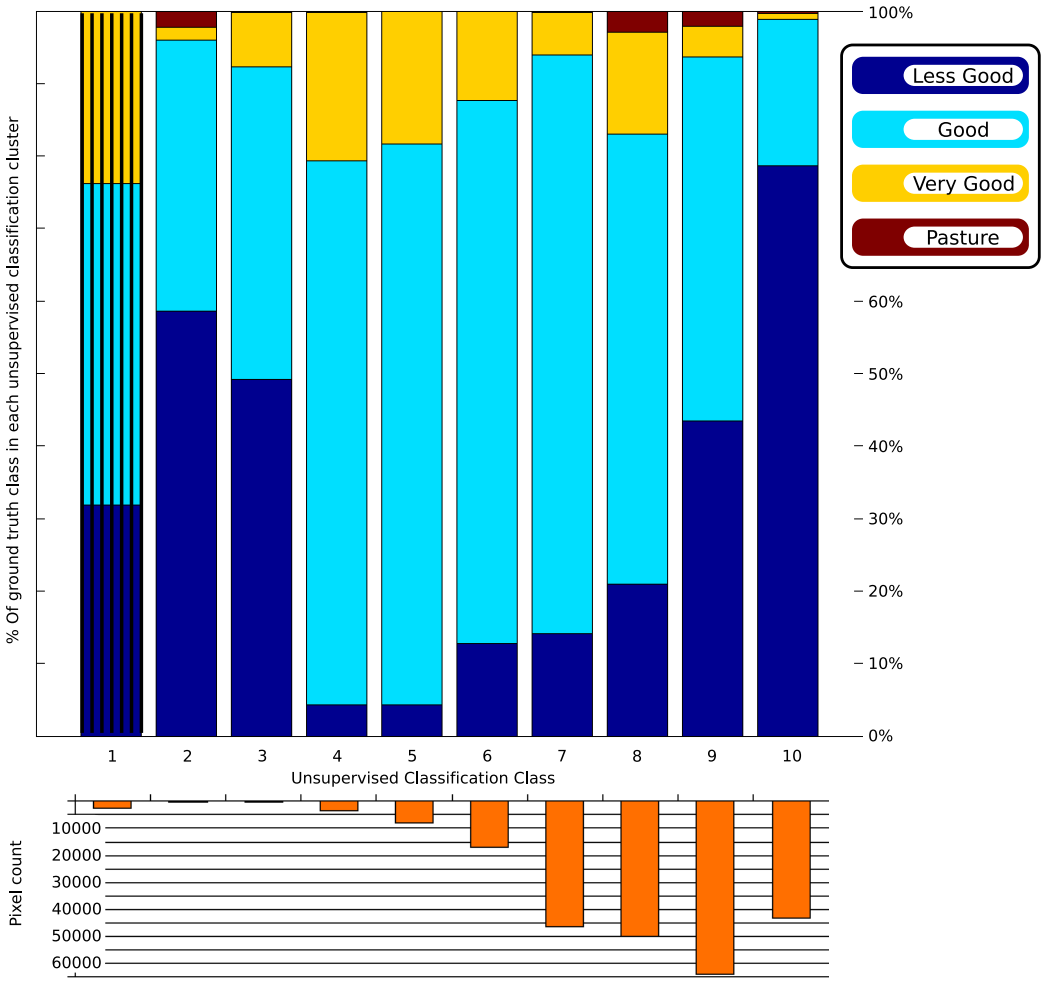

Figure 5.25: Unsupervised clustering with 10 classes. Bar plot comparison to grazing quality classes. Cluster number 1 contains all the masked pixels of the image and does not give any meaningful results. None of the clusters were spectrally representative of a single grazing class, however there were some that come close. Clusters 4, 5, 6 & 7 were fairly dominated by the G grazing class. The VG & Pasture grazing classes were not dominant in any of the 10 clusters. The LG class was most dominant in the unsupervised cluster number 10.

An interesting result appearing from the unsupervised classifications was that they all followed a similar distinct pattern. All the plots with 20, 30, 40, & 60 clusters followed the same pattern which was initiated with the 10 class clustering. As more clusters were allowed, those clusters defined in the 10 class unsupervised classification were subsequently split up further, creating several clusters for the initial 1 cluster. This can be seen clearly by comparing the 3 plots.

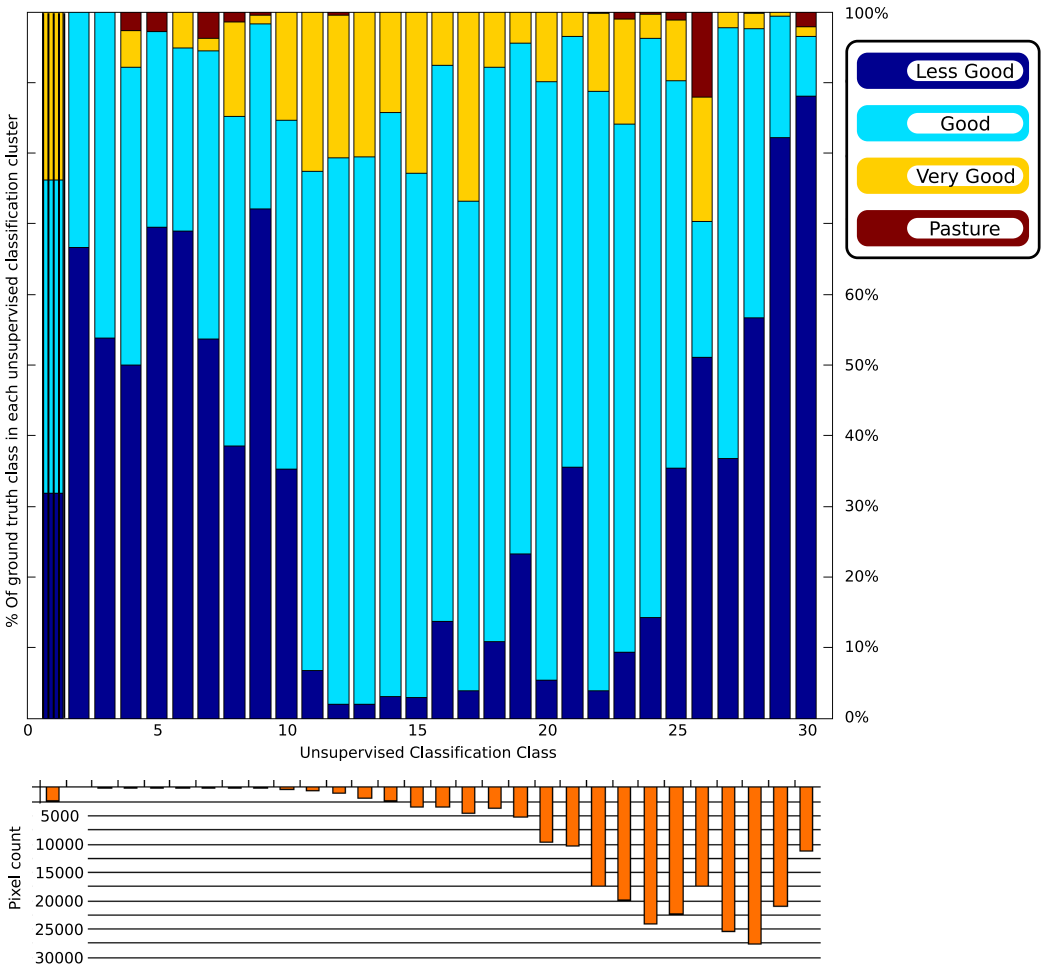

Figure 5.26: Unsupervised clustering with 30 classes. Bar plot comparison to grazing quality classes. An interesting result appearing from the unsupervised classifications is that they all followed a similar distinct pattern. All the plots with 20, 30, 40, & 60 clusters followed the same pattern that was initiated with the 10 class clustering. As more clusters were allowed, those clusters defined in the 10 class unsupervised classification were subsequently split up further, creating several clusters for the initial 1 cluster.

In figure 5.26 with 30 clusters, and similarly in all the other plots, the first group of clusters represented noise in the image. These clusters were much smaller (by numbers of pixels) than the remaining clusters (see graph at bottom of bar graph for the number of pixels in each cluster). The first cluster in all the unsupervised classifications contained the masked vales, those that had been given a value of 0 (i.e. all the edges around the Venabygd area, and all lakes etc). That is why this cluster contains almost an equal amount of each grazing quality class. The next set of clusters contained edge pixels around the borders of the lakes, shadow

pixels found in the deep part of the valley, and other random singular noise pixels that were scattered around the image. After these initial clusters, for example after cluster 9, in the 30 class clustering, the clusters then started to represent the grazing quality classes in the image. Each cluster was viewed separately, on top of the satellite image and polygon borders for the grazing quality classes, in order to make these assessments.

The following observations are from the 30 class results on a subset of the c-corrected image. Clusters 10, 11, & 12 represented the grazing classes situated in the valleys. They were mixed in terms of which classes were included. Cluster 11 & 12 showed over 70% of the pixels belonged to the G grazing class. Clusters 13, 14, 15, 16, 18, 19, 20, 22, 23, & 24 showed a dominance of the G class, with all these clusters having over 75% dominance. Cluster 17 appeared to represent a similar distribution to the VG grazing class when comparing the groups to the satellite image and grazing polygon distribution, but the pixel statistics show again that the G class dominated.

Those clusters that had a considerable mix of all grazing classes appeared illustrative of LG Grazing even though that class did not dominate the statistics. They indicate some kind of noise or disturbance that is similarly affecting all the clusters. Cluster 29 & 30 show a dominance of LG, having over 82% of pixels in that class.

From these observations, training data was selected to represent the G, LG and VG grazing quality classes. These were run through a Maximum Likelihood Classifier (MLC) on a subset of the c-corrected image (24 July 1994). Table 5.16 shows the error matrix derived from the classification. The overall accuracy for this supervised classification was 59.8 % (43949 / 73483 pixels).

The producers accuracy divides the total number of correct pixels in a class by the total number of ground truth pixels in that class (i.e. column number). This indicates the probability of a ground truth pixel being correctly classified. It is called the producer's accuracy because the producer of the classification is interested in how well a certain area can be classified. The user's accuracy is a measure of reliability and is indicative of the probability that a pixel classified on the image actually represents that category on the ground. It is calculated by dividing the total number of correct pixels in a class by the total number of pixels that were classified in that class (i.e. row) (Congalton, 1991).

81.65% of the ground truth pixels in the LG class were classified correctly as LG. There was a 60.14% probability that those pixels classified as LG in the image represented LG on the ground. The G class had a high user accuracy of 80.05% and a low Producers accuracy. The VG class did poorly in both error assessments.

Ground Truth (Pixels)				
Class	LG	G	VG	Total
LG	21484	13424	809	35717
G	4375	21614	1013	27002
VG	454	9459	851	10764
Unclassified	0	0	0	0
Total	26313	44497	2673	73483

Class	Producers Accuracy	Users Accuracy
Less Good	81.65%	60.14 %
Good	48.57 %	80.05 %
Very Good	31.84 %	7.91 %

Table 5.16: Error matrix showing the results after a maximum likelihood classification. The training data was selected by comparison with the 30 class unsupervised classification. This classification was run only on a subset of the c-corrected image.

In comparison to the unsupervised classification results, these results also indicate that the LG class is the hardest to identify and classify. This has also been verified through many of the ROI separability results.

The 60 class clustering (fig 5.27) showed the same pattern as described for the 30 class distribution; where the first set of clusters were very small and indicated the pixels with noise, shadow or masked values. The next group of clusters showed a spectral representation of the G grazing class, followed by a group illustrating the LG. The clusters that followed (the last few) appear to show a new representation that was not seen in the other figures (10 & 30 clusters) which show a mixture of classes dominated by LG, as well as mixed classes. Again the VG class did not have a strong representation in any of the clusters. It appears mostly in those clusters dominated by the G class, indicating that it has spectral values closest to this class. Pasture occurred in clusters that contained mixtures of VG, G and LG.

In summary of this analysis, the unsupervised clustering showed very interesting results with a clear pattern of similarity as the number of clusters were increased. The LG and G grazing classes were represented well by the spectral clustering and these clusters could be used to find clear representations in the image for training data for a supervised classification. The VG and Pasture classes were not well represented by this spectral grouping and this supports the results that have shown the difficulty of separation.

Trying to separate all three NIJOS grazing classes might not be possible with a Landsat image. The spectral values of the VG class are not distinct enough from the other classes. Newly defined grazing classes may have to be defined. These could represent a more general Good and Not Good grazing quality, which could

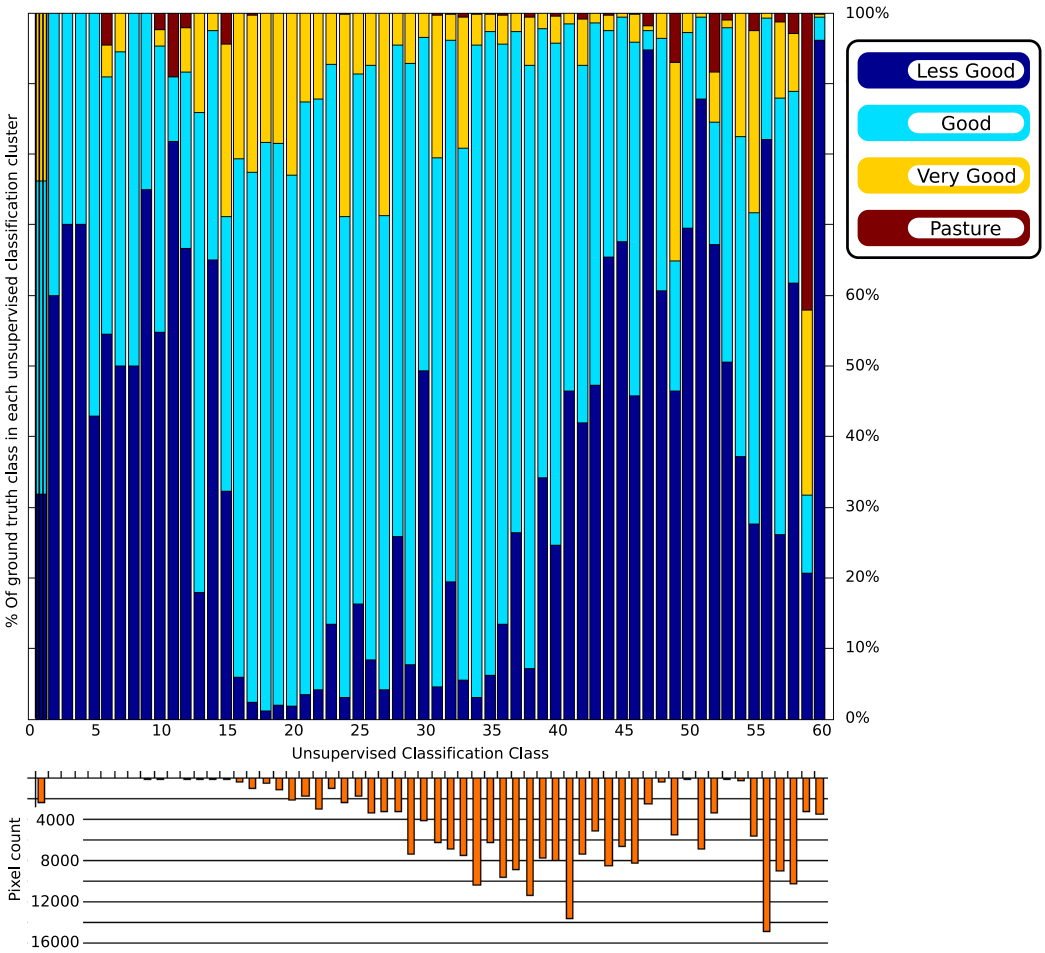

Figure 5.27: Unsupervised clustering with 60 classes. Bar plot comparison to grazing quality classes

then could then be linked back to the NIJOS classes.

Vegetation Classes

Following on from the comparison of grazing classes to the unsupervised clustering results, was a comparison with the vegetation classes. The results from this analysis were very interesting and explained a great deal about the spectral groupings in the image. The same plotting procedure used to compare the grazing classes was used here. Each unsupervised cluster is shown as a bar with the percentage of each vegetation type represented in that cluster. Plots were drawn for 10, 20, 30, 40 & 60 clusters, but only 3 of the 5 are shown here. See figures 5.25

to 5.27.

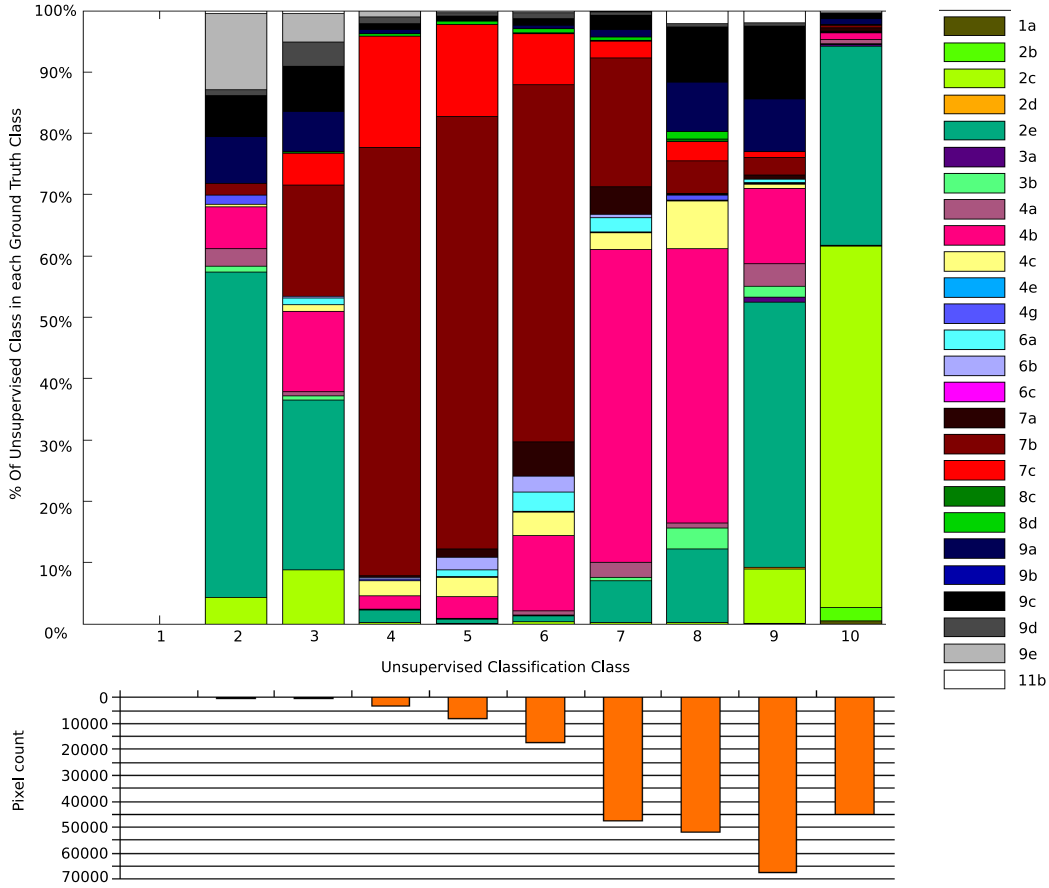

Figure 5.28: Unsupervised clustering with 10 classes. Bar plot comparison to vegetation classes. These results show a fairly course view of the spectral distribution. Clusters 4, 5, & 6 show almost entirely Spruce vegetation types; clusters 7 & 8 are dominated by Birch tree types, and clusters 9 & 10 are dominated by alpine grass and heath types.

Similar to the comparison results with the grazing classes, a distinct pattern was noted in the distribution of clusters from the different unsupervised classification runs. The 20, 30, and 40 clusterings showed a very similar pattern to each other and to the 10 class clustering. They appeared to show finer detail for each of the original 10 clusterings as more clusters were allowed.

The 10 class clustering (fig 5.28) shows a fairly course view of the spectral distribution. Clusters 4, 5, & 6 show almost entirely Spruce types; clusters 7 & 8 are dominated by Birch tree types, and clusters 9 & 10 are dominated by alpine grass and heath types. This is a strong trend for such few clusters.

As discussed in the previous section (comparing results with the grazing classes)

Figure 5.29: Unsupervised clustering with 30 classes. Bar plot comparison to vegetation classes. Similar to the comparison results with the grazing classes, a distinct pattern was noted in the distribution of clusters from the different unsupervised classification runs. The 20, 30, and 40 clusterings showed a very similar pattern to each other and to the 10 class clustering. They appeared to show finer detail for each of the original 10 clusterings as more clusters were allowed.

the first few clusters contain mostly noise and are comparatively small. Cluster 1 has been eliminated from all the vegetation plots as it contained only the masked pixels in the image.

The classifications with 20, 30, 40, and 60 clusters all show the same pattern with increasingly finer detail. In figure 5.30 the clusters clearly represent a grouping of 3 main vegetation types Spruce, Birch, and Heath / Alpine grasses. The clusters don't represent the individual vegetation types under each of the umbrella classes, however, e.g. 2e. They show clusters with the same mix of vegetation classes, all belonging to the same umbrella class. Clusters 16-20 are dominated entirely by Spruce types (veg 7a, 7b, & 7c) which are a mixture of *Lav og Lyngrik granskog*,

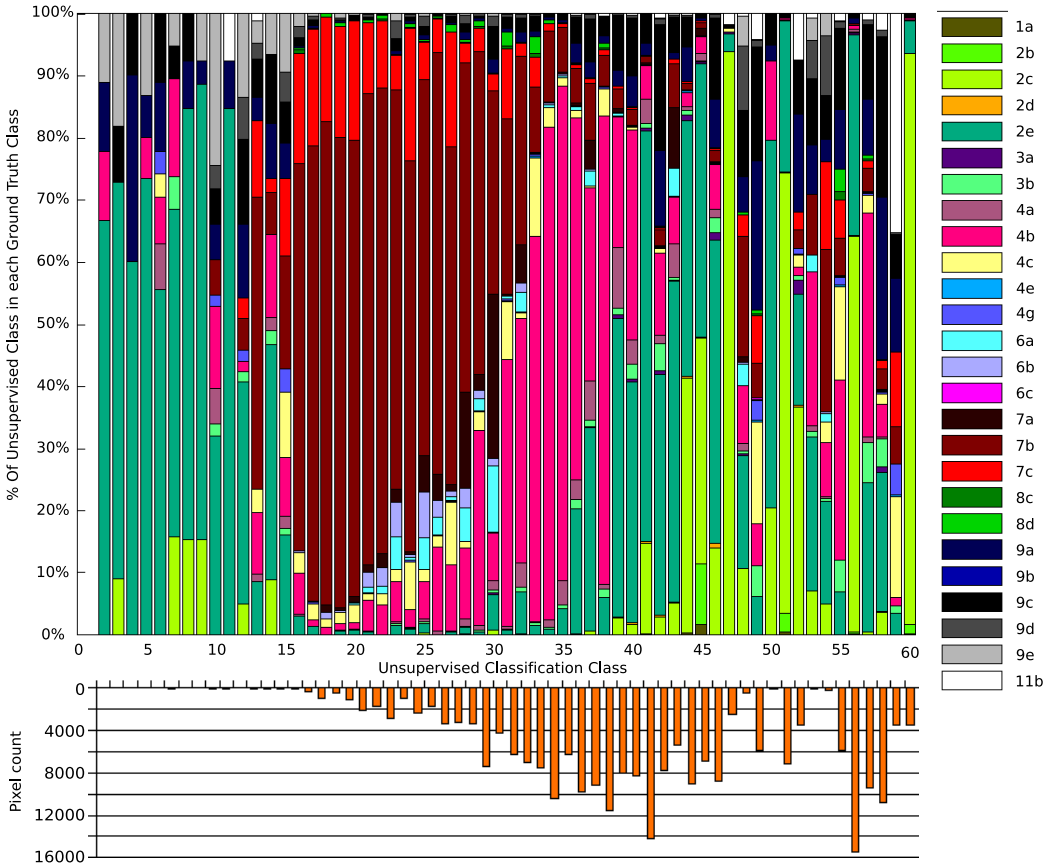

Figure 5.30: Unsupervised clustering with 60 classes. Bar plot comparison to vegetation classes. The classifications with 20, 30, 40, and 60 clusters all show the same pattern with increasingly finer detail. The 60 clusters represents the grouping of 3 main vegetation types Spruce, Birch, Heath / Alpine grasses. The clusters are not representing the individual vegetation classes under the umbrella classes, however.

Spruce with Blueberry undergrowth (*Blåbærgranskog*), and *Enggranskog*. Vegetation type (7b) is the dominating type in this group, most likely because it is such a dominant species, covering 13% of the total Venabygd area.

Clusters 21 to 30 are strongly dominated by spruce, but also become more mixed with the spectral values of birch trees as one follows the clusters to the right. From clusters 30 to 38 the dominance then becomes more birch trees (types 4a, 4b, & 4c). Vegetation type 4b (*Blåbærbjørkeskog*) is the dominant of these three types, however, each of these clusters are still a mix of types under the umbrella tree type birch and not a representation of a spectral cluster for each individual vegetation type underneath this umbrella.

From the birch tree dominated clusters, the spectral clusters then start to contain

mostly alpine grasses and heath types (2e, 2c, 2b, 1b) with *rishei* and *lavhei* being the most dominant of those. This is the case for clusters 39, 41 ,43-47 ,50-52, 56 & 60. In between these clusters are a few that have a mix of many of the umbrella classes.

The swamp and marsh vegetation classes are best represented in cluster groups 49 & 59, but they only amount to 50% of the spectral values. The Pine tree types (6a, 6b & 6c) were very poorly represented and did not dominate any of the spectral clusterings. They occurred primarily in a small minority in the clusters that were dominated by Spruce. This gives a good indication of where the problem lies in separating Pine.

Figure 5.31 is coloured in such a way that it is easier to see the groupings of the umbrella vegetation classes that have been discussed (Birch, Spruce and Alpine grasses / heath). In summary, the following trends were observed:

- The swamp and marsh group of vegetation classes were not well represented in the cluster groups.
- The Pine tree group of vegetation classes were not well represented.
- The Spruce tree vegetation types were shown as a distinct group of spectral values.
- The *Hei* group of vegetation classes were well represented together.
- The Birch tree vegetation types were shown as a distinct group of spectral values.
- Even with 60 spectral clusters none were dominated by an individual vegetation type (i.e. sub-umbrella types)

5.5 Airphoto Interpretation

This section looks at how some of the mapping methods used by NIJOS can affect the analysis of ground truth data and classification results. The aerial photos used in the following analyses were taken on the 25.06.1995 on infrared film. The scale of the photos is approximately 1:22,000. Those areas inside the polygon regions in the image figures are shown at 100% transparency, and the background areas are shown at 50% transparency, to give contrast.

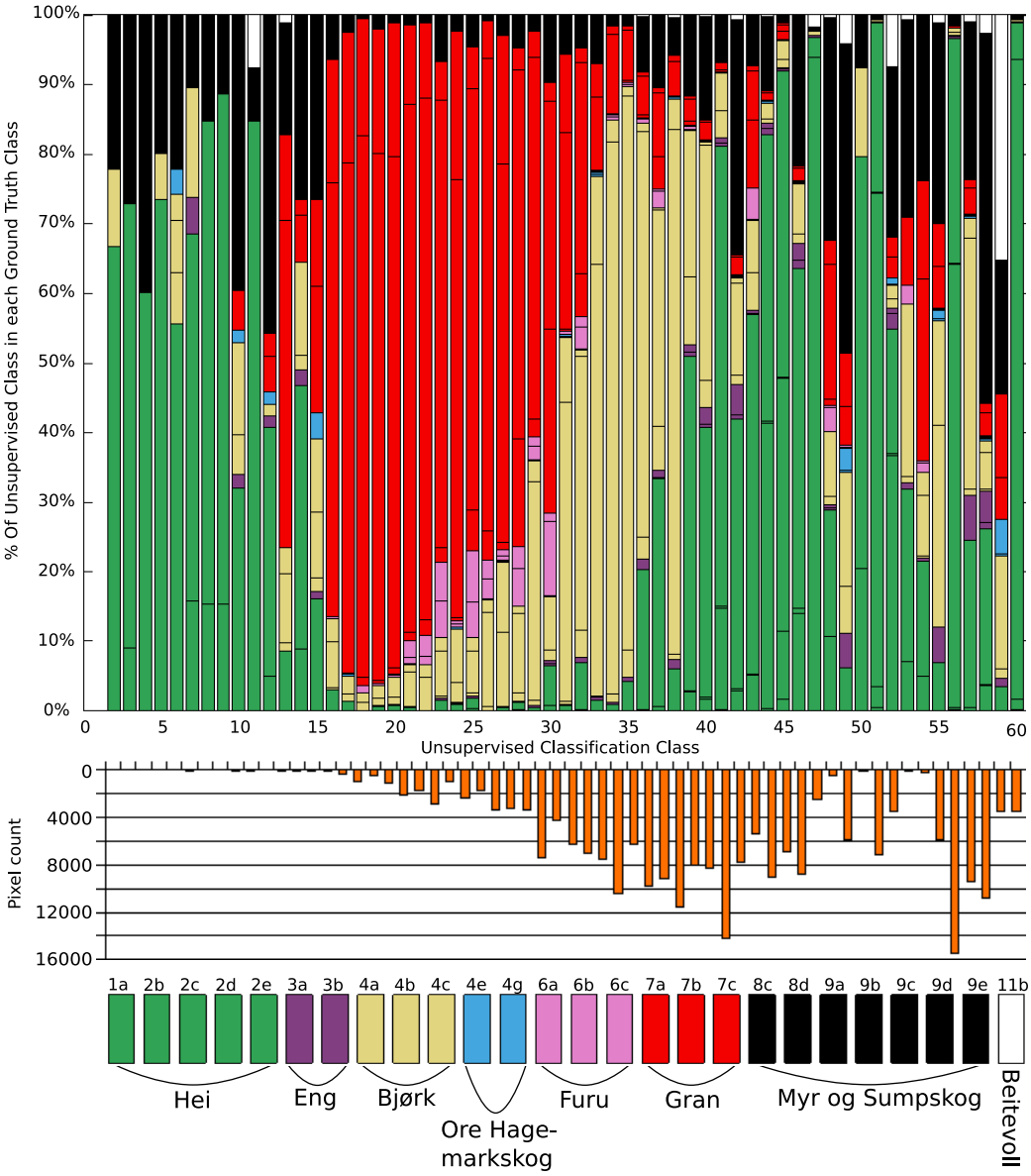

Figure 5.31: Unsupervised Classification with 60 clusters. This plot contains the same information as that shown in figure 5.30. It has however been coloured in a different way to make the appearance of the umbrella vegetation classes better. This plot gives a clear indication that the spectral groupings in the image represent the vegetation types of Birch, Spruce and Alpine grasses / heath. This unsupervised classification does not indicate the spectral independence of any of the individual vegetation types however.

Homogeneous and Non Homogeneous Polygons

Figure 5.32 shows a section of an aerial photo over Venabygd. The polygons drawn over the aerial photo are as similar to those outlined in the NIJOS vector

vegetation layer as possible. They have been drawn (by hand) to illustrate how areas are defined in the different vegetation classes. As described in the dataset chapter (3), the vegetation maps were created through extensive field work. Air photos were used in this process to define the borders between vegetation groups and outline polygons for the individual vegetation classes. The polygons drawn here (fig 5.32) represent vegetation classes that belong to all 3 grazing quality classes.

The purple polygon has vegetation type 9c (*grasmyr*). The turquoise polygon also being 9c (*grasmyr*). They are shown here to illustrate how polygons are not necessarily homogeneous. The purple polygon shows a wide range of spectral values. There are colours ranging from very dark grey through to light grey, pink, and even red in the image. When extracting spectral information from polygons like this, one receives a range of values that also fit in to many of the other grazing quality and vegetation classes. The polygon variation plots in figure 5.12 give an idea of the range of values a polygon can have, and this image is an illustration of how this is possible. This polygon as a whole could not be used as training data for vegetation class 9c for example. A more defined and narrowed set of spectral values would have to be found.

The green polygon has 9a-*Rismyr* vegetation type. It is a fairly homogeneous polygon. Like the purple and turquoise polygon this green polygon lies also under the *myr* types. The colours in the polygon are quite different to those in the purple polygon as it has no greys or blues and is a paler red / pink colour. 9a and 9c have the potential grazing quality of LG. In terms of grouping these polygons together for an indication of LG grazing type, this also results in a significant range of spectral values.

The pink polygons are of type 4b-*Blåbærbjørkeskog* which covers much of the area in this image. They are distinctly different from the 3 just discussed. They have a bright red colour and a distinctly different texture. The texture in the image is a produced by the birch trees in this polygon. The yellow polygon is of type 4cg / 3bs meaning that it has the main vegetation type of 4c-*engbjørkeskog* with more than 50% grass. It has a secondary vegetation type of 3b-*Høgstaudeeng*, with 50% coverage of *vier*. This polygon looks very similar to the two pink polygons.

As described in the dataset chapter various generalisation methods have to be taken in order to produce an effective and readable vegetation map. The polygons in the NIJOS map have been defined in terms of the vegetation class which covers the majority of the polygon area. These generalisations have a large effect in terms of classification accuracy and the comparison of results to these ground truth classes.

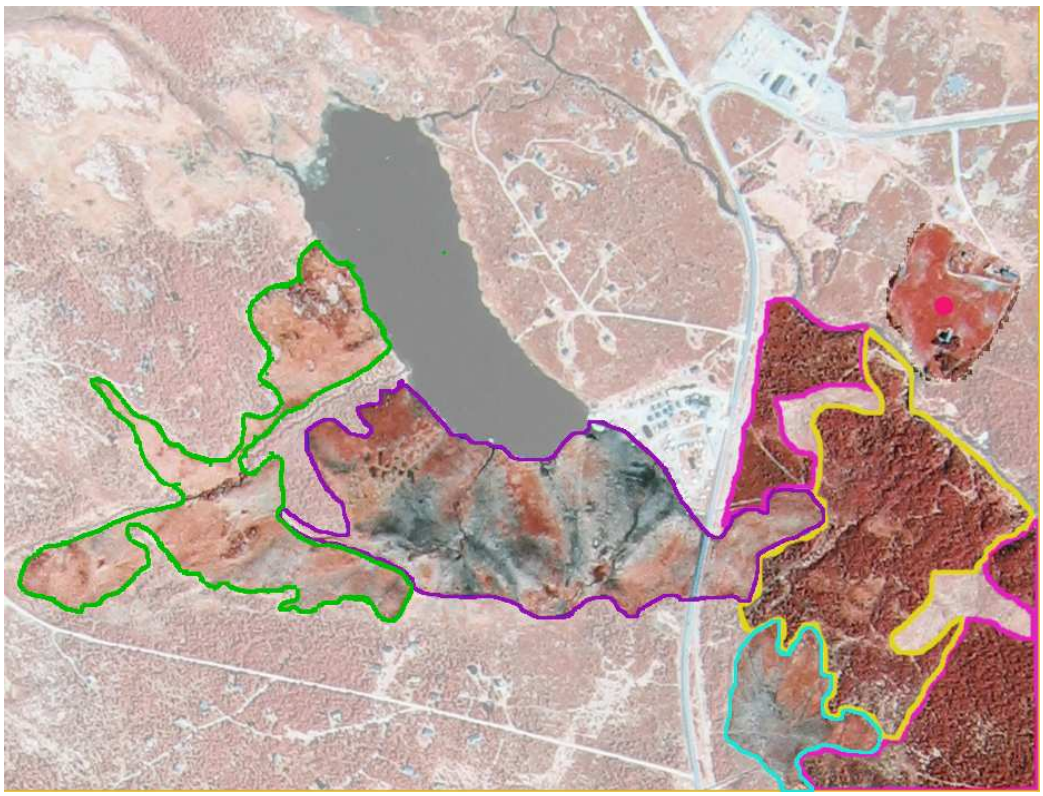

Figure 5.32: Clipped section of an aerial photo with polygon regions drawn on as like to those defined by NIJOS as possible. The green polygon shows a fairly homogeneous region. The purple polygon however shows a wide range of spectral values. There are colours ranging from very dark grey through to light grey, pink, and even red in the image. When extracting spectral information from polygons like this, one receives a range of values that also fit in to many of the other grazing quality and vegetation classes. This polygon as a whole could not be used as training data for vegetation class 9c for example. A more defined and narrowed set of spectral values would have to be found. In terms of grouping all these polygons together for an indication of LG grazing type, this also results in a large range of spectral values. The red and yellow polygons are examples of vegetation types that do not have clear borders. This leads to increased uncertainties.

Polygon Borders

Those polygons that border with birch forest have borders that are easier to define because birch has a distinctive colour. The forest areas are not only a different colour but also a different texture which shows up clearly in the high resolution airphotos.

The built up areas seen in figure 5.32 (to the right of the lake) are also areas that are fairly easy to define as they have sharp borders. Man made areas, even if

they are vegetated, are often sectioned off, bordered with fences and are created in clearly defined shapes. Another example of this is the agricultural fields in the image, one in particular to the right and in the middle of the image, with a red dot in the middle, is very easily distinguished from it's neighbours. It has been classified as pasture. Borders between some vegetation classes however are not so easy to define, and lead to further uncertainties.

The pink and yellow polygons are examples of vegetation types that do not have clear borders. The pink polygons represent birch trees with blueberry undergrowth (4b-*Blåbærbjørkeskog*) and the yellow polygon represents the main vegetation class of *4c-Engbjørkeskog*. There are no clear borders between these two, and the map makers have had to make subjective decisions. Even though these two types are both birch tree types they do not represent the same potential grazing quality. Vegetation type 4c has the potential grazing quality of VG, whereas 4b has the potential grazing quality class of G.

One of the problems with grazing quality classes that involve tree stands is that they are not classified in terms of the grazing quality of the tree type, but the grazing quality of the undergrowth. The reflectance information appearing in air-photos and satellite images are mostly reflections from the canopy (i.e. tree tops). There is less reflectance from the undergrowth (depends on tree type and density). This makes distinguishing grazing classes, based on undergrowth quality, using satellite or airphoto images very difficult. The higher the image resolution, the greater possibility for reflectance of the undergrowth to be recorded. The satellite images used in this thesis have a 25m resolution. This type of resolution does not give detailed information about the understorey. This was clearly seen in the unsupervised classification results, compared to both the grazing quality and vegetation classes, where there was not enough spectral information to have independent clusters representing a single vegetation type, and especially 2 vegetation types of the same umbrella type e.g. Birch.

Demoted or Promoted Polygons

The turquoise polygon drawn in figure 5.32 shows a polygon defined as the vegetation type 9cgs (*grasmyr*). In general this vegetation class (9c) is classified as having a LG grazing quality however when additional attributes play in, then they can be moved up or down a grazing quality class. This particular polygon has been promoted to a G Grazing quality class. It has the additional attribute, g, meaning that the area has been affected by grazing and hence has more than 50% grass coverage. It also has a second attribute, s, which indicates that the area has 50%

coverage of *vier*. The purple polygon has no additional attributes or secondary vegetation classes. In terms of spectral differences, the two 9c polygons (purple & turquoise) look very similar and it is doubtful whether a classifier would be able to separate between the two even with aerial photo resolution. These two polygons look more similar than the turquoise and pink polygons which have the same grazing quality (G).

Colour Spread within a Grazing Quality Class

Figure 5.33 shows a similar area of the aerial photo as figure 5.32. The polygons that are drawn represent those from the VG grazing quality class. The red polygons belong to *3b-Høgstaudeng* vegetation class and the green to *4c-Engbjørkeskog*. The image is shown here to give a visual illustration of the range of colours and hence spectral values within one grazing class. Colours range from almost white, through to very dark red and some of the polygons even include small streams which appear as black. Because some of the waterways are too small to be drawn separately on the map, they are classified by the vegetation surrounding them, this drastically changes the spectral information for the polygon as a whole. There are large colour spreads within each grazing class. The colours within one grazing class are also recognisable in the other grazing classes, illustrating the spectral similarity between classes.

Information Content in a Satellite Image

There is a large difference in the information content of a satellite image compared to an airphoto. A clip taken from the satellite image is shown to give a comparison. Figure 5.34 shows a small area of the satellite image similar to the area shown in figure 5.32. The satellite image is the c-corrected reflectance image shown in an infrared colour composite (RGB-4,3,2). This band combination is the most similar band combination to the airphotos, which were photographed on infrared colour film.

A comparison shows what the different land cover types look like. The 9c polygon area for example (purple polygon) looks fairly dark and purple in the satellite image, which is similar to what is appearing in the aerial photo. Some of the other areas, however, look very different. The pixel size is drastically different and a lot of the detail seen in the airphoto is not apparent in the satellite image.

The purple and turquoise polygons shown in figure 5.32 looked fairly similar in the airphoto but very different in the satellite image. The purple polygon in figure

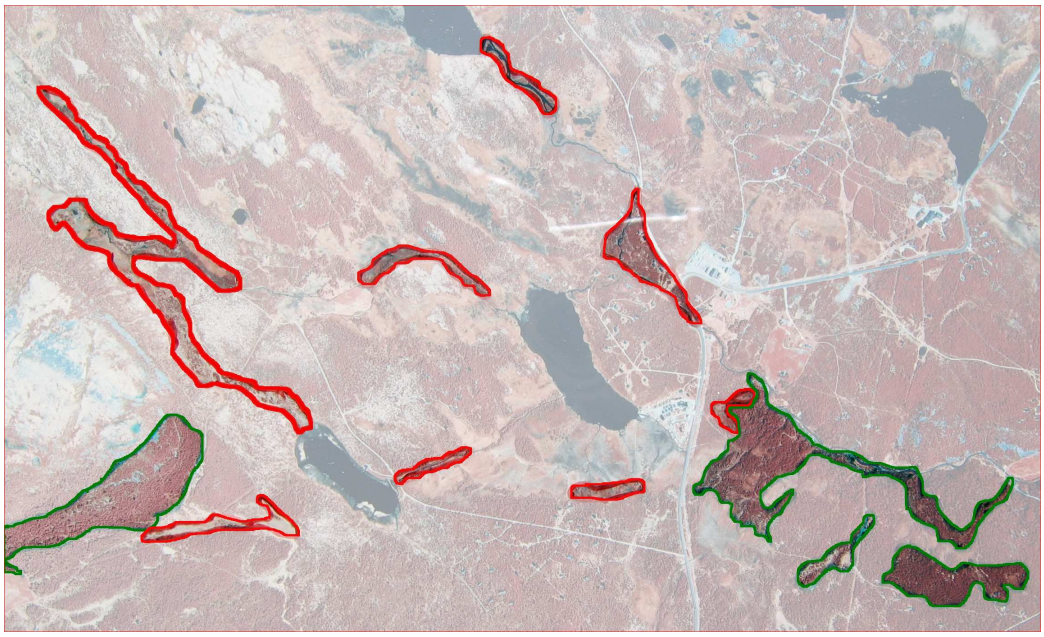

Figure 5.33: Aerial photo clip, overlaid with polygons from the Very Good grazing quality class. The red polygons belong to *3b-Høgstaudeng* vegetation class and the green to *4c-Engbjørkeskog*. The image is shown here to give a visual illustration of the range of colours and hence spectral values within one grazing class. This class shows quite a variation. Colours range from almost white to very dark red, and some of the polygons even include small streams which appear as black. Because some of the waterways are too small to be drawn separately on the map they are classified by the vegetation surrounding them, this drastically changes the spectral information for the polygon as a whole. The colours within one grazing class are also recognisable in the other grazing classes, illustrating the spectral similarity between classes.

5.32 looks blue and grey in the satellite image, whereas the turquoise polygon is a pink colour with a small patch of blue. These are swamp vegetation types meaning that the water content of these areas is likely to be quite variable. The satellite and airphoto are not taken on the same day, they are taken in different years so this could also give reason to the difference in appearance. The satellite image is taken on the 24.07.1994 and the airphoto on 25.06.1995. In the satellite image the impervious surfaces and lakes have been masked out so they appear completely black. When comparing the image to the aerial photo it is easy to see which areas corresponds to lakes and which are developed areas.

Figure 5.35 shows the vegetation classes as defined by NIJOS. The area covers a similar one to that of the satellite and aerial photo area. It is difficult to describe all the variation between the polygon outlines, and the information content in both the satellite image and aerial photo, so this figure is shown here to give the reader

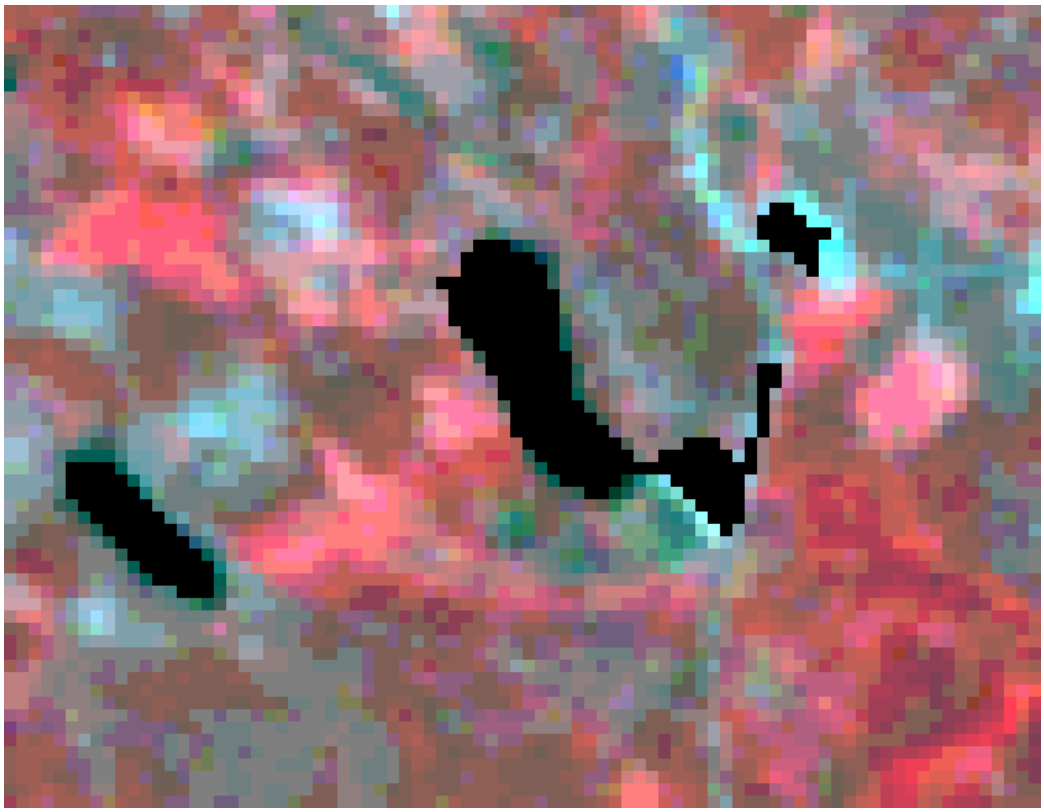

Figure 5.34: Clipped area of the c-corrected satellite image (reflectance). Shown in an infrared false colour composite, bands 4,3,2. The satellite image has a very different pixel size to the airphoto and much of the detail seen in the airphotos is not apparent. The purple and turquoise polygons shown in figure 5.32 looked fairly similar in the airphoto but very different in the satellite image.

a chance to assess some of the differences visually.

5.6 Supervised Classification

The maximum likelihood supervised classification results are shown as an image in figure 5.36. As mentioned in the methods all roads, rivers, houses, lakes and fields were masked out of the c-corrected satellite image before classification was run, this can be seen in image B. Visually the classification performed fairly well especially in the top part of the image. The border areas along the bottom and along the left hand side had some differences however. Many of the white (G) areas in the original image were classified as LG and VG. The classified image is also much more pixelated than the original, as the original image shows the

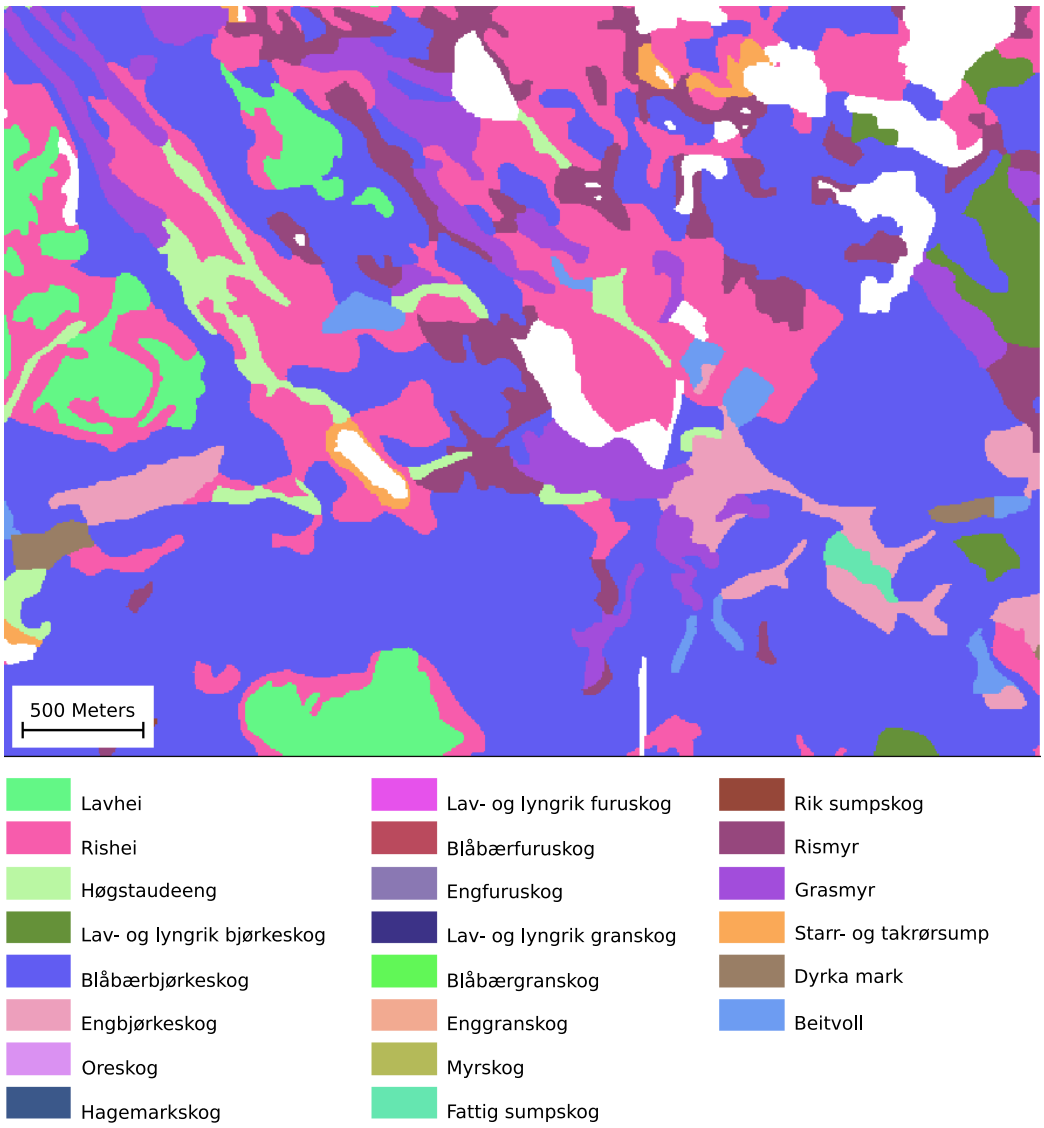

Figure 5.35: NIJOS Vegetation class map

smooth polygon regions. A considerable amount of the differences between the original and classified image is due to the generalisation of areas by polygons. This has to be taken into account when reviewing the error assessments.

A confusion matrix was calculated to assess the accuracy of the classification. The confusion matrix expresses the number of sample units (i.e. pixels) assigned to a particular class relative to ground truth. The columns represent the ground truth data and the rows represent the classification generated from the remotely sensed data. The table indicates the accuracies of each category as well as the errors

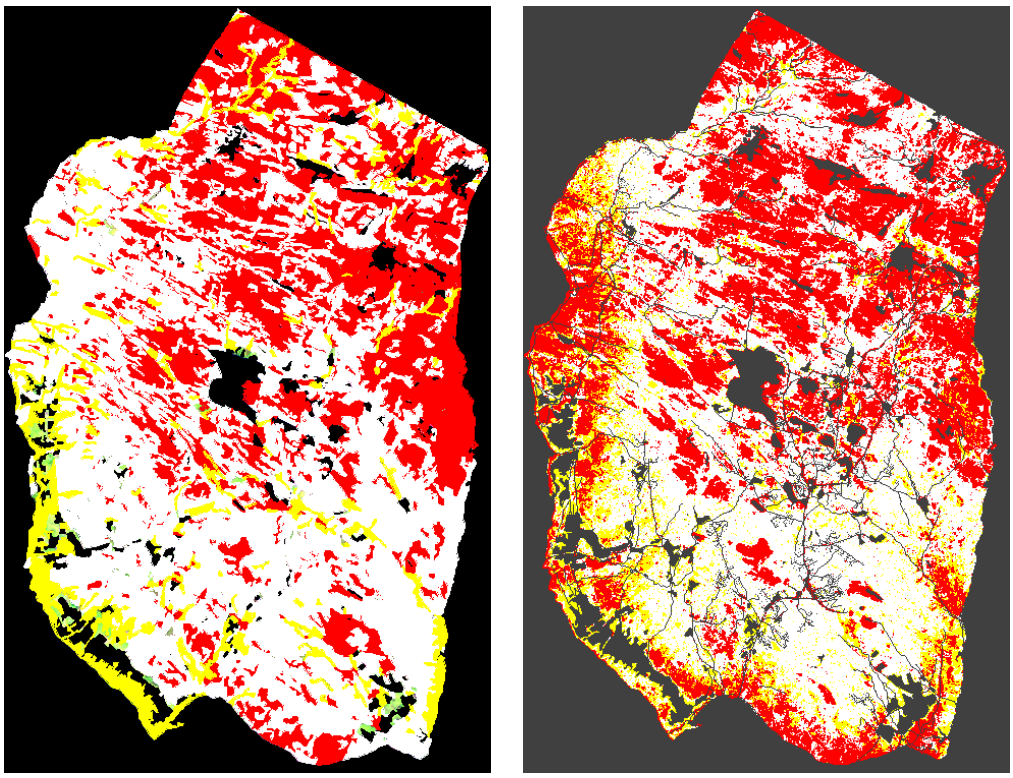

A: NIJOS Grazing classes
Yellow = Very Good
White = Good
Red = Less Good
Black = masked pixels

B: Supervised Classification

Figure 5.36: The supervised classification was run using a MLC on the c-corrected image (24.07.1994). All roads, rivers, houses, lakes and fields were masked out of the c-corrected satellite image before classification was run.

of inclusion (commission errors) and errors of exclusion (omission errors). The producer's and user's accuracy were also calculated. (Congalton, 1991).

The commission errors shown in table 5.17 show the percentage of extra pixels classified in that class. The omission errors indicate the percentage of pixels that were left out of a particular class. The results show that, for example, 68% of the VG pixels were left out of the VG class (i.e. they ended up being classified as something else). 79% of the pixels were extra pixels (i.e. from other classes) that had been classified in the VG class. The LG and G classes had less commission and omission errors. This is reflected in table 5.18, where the LG and G classes had much better user's and producer's accuracy than the VG.

The LG grazing class showed equal user's and producer's accuracy. This class had a 62% chance of being classified correctly, and a 62% chance that those pixels classified as LG were actually LG when compared to the ground truth. The G grazing class had similar results to the LG with a Producer's accuracy of 65% and a user's accuracy of 70%. The VG grazing class had very poor accuracies with a 32% probability of a VG grazing pixel being classified in the right class. There was only a 20% probability that those pixels classified as VG actually were of the VG class. These results are also reflected in many of the other analyses where it has been shown that the VG class was the hardest to separate from the rest.

The overall accuracy of the classification was 61.38% (146543 / 238730). This is computed by dividing the total number of correctly classified pixels in the matrix by the total number of pixels. This classification result is not good enough for mapping grazing classes and gives reason for performing the classification differently, as well as re-evaluating what is possible to map with a 25m resolution satellite image.

Grazing Class	Commission %	Omission %	Commission (Pixels)	Omission (Pixels)
Less Good	37.37	38.42	32534 / 87051	34016 / 88533
Good	30.28	34.80	37456 / 123699	46039 / 132282
Very Good	79.33	67.72	22197 / 27980	12132 / 17915

Table 5.17: Commission and Omission Errors for supervised classification.

Class	Prod. Acc. %	User Acc. %	Prod. Acc. (Pixels)	User Acc. (Pixels)
Less Good	61.58	62.63	54517 / 88533	54517 / 87051
Good	65.20	69.72	86243 / 132282	86243 / 123699
Very Good	32.28	20.67	5783 / 17915	5783 / 27980

Table 5.18: Producer's and User's accuracy for supervised classification.

5.7 Comparison: Aerial Photo, Satellite & Classifications

The following three tables (5.19, 5.20 & 5.21) contain examples of the NIJOS polygons shown on aerial photographs, the satellite image, the unsupervised classification and supervised classification. The polygons chosen are a representation of the spread of colours and information within polygons, within one grazing class, and between grazing classes. Approximately 10-12 polygons from each

grazing class were chosen to display covering as wide a spectrum of vegetation types as possible. The idea with this analysis was to visualise the complex nature of polygons and classes. This has been previously demonstrated in a more numerical and quantitative way. 2 examples for each grazing class are displayed in the next three tables, the remaining images are shown in tables C, C, & C in appendix C.

The photos used were taken on the 25.06.1995. They were taken with infrared film and had a scale of approximately 1:22,000. The satellite image used for comparisons was the topographically c-corrected image from the 24th July 1994. All examples are shown in a 5,4,3 band combination (MIR (Red), NIR (Green), Red (Blue)). The colours of the supervised classification images shown in these tables indicate the following: Yellow = Very Good, White = Good, Red = Less Good, and dark Grey = masked pixels.

The unsupervised classification results used here are the same as those computed for 60 clusters. The unsupervised classification results compared to the vegetation and grazing classes are shown in barplots from figure 5.25 to figure 5.30. The clusters shown are represented in different colours, the numbers of those clusters included in each polygon are written in the corresponding table for each image. A comparison can be made between the clusters found in each polygon with the results shown in the barplots. The unsupervised clusters numbers are given in terms of the majority and minority in the polygon. The minority usually meant 3 pixels or less depending on the size of the polygon. The assignment of clusters as majority or minority was done subjectively and is meant as a rough indication, although every cluster included in the polygon was noted. Comments for each of the images were written in the tables.

The LG grazing quality class contains 1009 polygons with 147 unique combinations of vegetation types and attributes. The vegetation types defined as LG grazing quality exhibit a wide variety of visual colours. Row 3 for example is *Lavhei* with more than 50% *lavdekning* and appears very white in the aerial photo and satellite image. Row 8,9, and 10 are not only very dark green in contrast but also look very similar to each other despite the fact that some are Spruce types and some birch. As mentioned before, it is mainly the undergrowth that has been given the classification LG quality by NIJOS and not the canopy tree type, which is what a satellite sensor and camera registers.

The G grazing class comprises of 767 polygons which contain 112 unique combinations of vegetation types and additional attributes. The comparisons showed again a great mix of colours and many mixed classification results. Example 5 showed a very good supervised classification with nearly the whole polygon ob-

taining the correct classification.

The VG grazing quality class contains 244 polygons over the Venabygd area with 71 combinations of vegetation types and additional attributes. Example 7 showed the best results from the supervised classification.

	Aerial Photo	Satellite Image	Unsupervised	Supervised
1	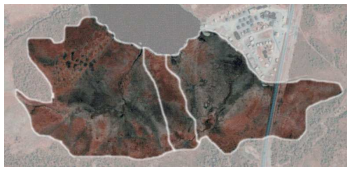 Left: *Grasmyr* (9c). Middle: *Grasmyr* (9cs) $>$ 50% *vier*. Right: *Grasmyr* (9c)	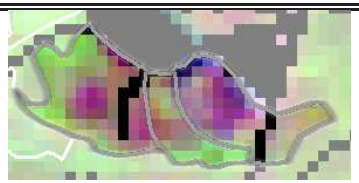 Detailed aerial photo with more wet swamp and less wet vegetation regions. Makes for a complex spectral signature of the area. Inhomogeneous. The light green represents chlorophyll content and the pink-minerals, soil and water.	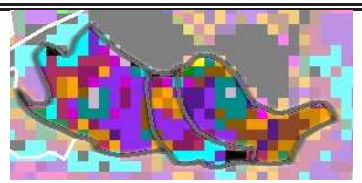 Classes: 17, 20, 22, 23, 24, 25, 27, 29, 31, 33 36, 40, 41, 43, 49, 53 56, 57	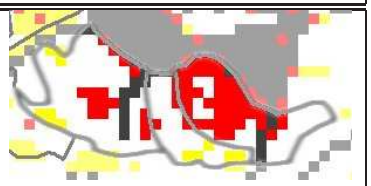 Not a good classification, all 3 classes are represented.
3	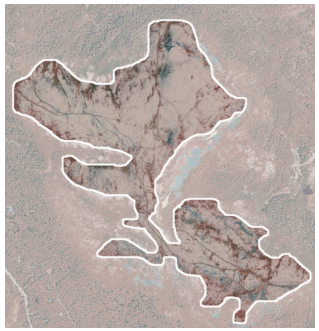 *Lavhei* (2cx) $>$ 50% *lavdekning*	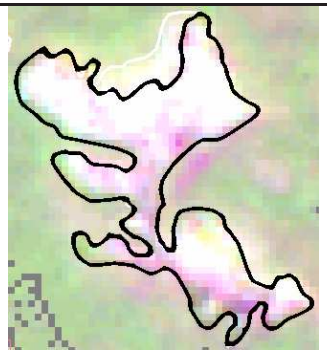 Pale satellite image. Reflects the colour spread in the aerial photo.	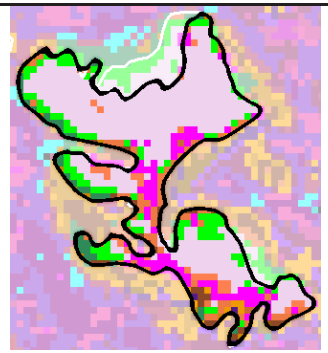 Majority: 47, 52, 56, 60, 40 Minority: 46, 45, 41	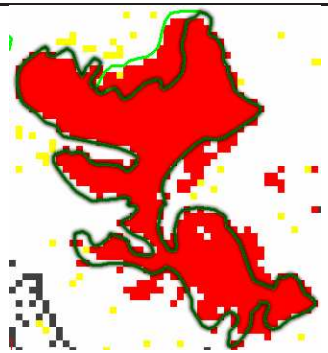 V. good classification. Same vegetation type as example 2, polygon content and results are very similar.

Table 5.19: Selected polygons - Less Good grazing quality class

	Aerial Photo	Satellite Image	Unsupervised	Supervised
4	 Bottom: *Blåbærfuruskog/lav og lyngrik furuskog* (6b/6a) Top: *Blåbærgranskog/Enggranskog* (7b/7c)	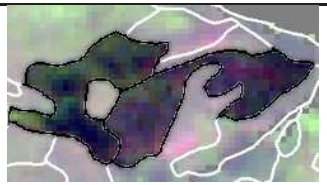 The top polygon is dominated by spruce and the bottom by pine. They both look fairly similar	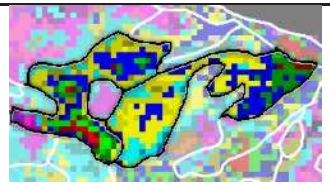 Majority: 25, 26, 28, 22, 21 Minority: 27, 23, 30, 29 Majority: 23, 16, 24 Minority: 25, 25, 27, 21, 20, 19, 18, 17, 22	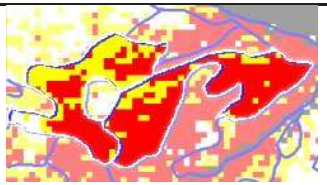 Almost none of the pixels in either polygon were classified as good. A dominance of Very good (yellow) and Less Good (red), two extremes.
9	 Right side: *Blåbærgranskog* (7b&) Left side: *Blåbærgranskog* (7b)	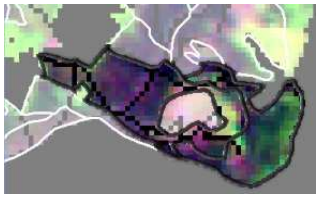 Example 7 is the same vegetation type, the polygons look fairly similar in some parts. Follows the colour change in the aerial photo well.	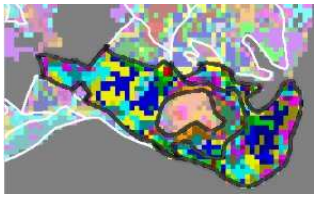 Majority: 24, 22, 21, 20, 25, 26, 27, 28, 29, 30, 31. Minority: 55, 32, 33, 34, 36, 37, 54, 19, 18, 17, 43 Majority: 25, 26, 23, 28, 29, 22, 30, 21, 20, 58, 43. Minority: 19, 57, 32, 41, 42, 40, 36, 55, 37, 33, 24, 46, 54, 18, 17, 16	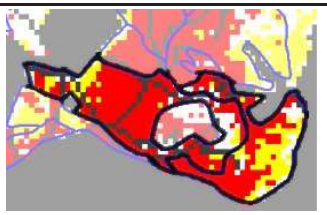 Many classes involved in the unsupervised classification Supervised classification showed mostly Less Good, with a bit of Very Good, but very little Good (white) as it should have been.

Table 5.20: Selected polygons - Good grazing quality class

	Aerial Photo	Satellite Image	Unsupervised	Supervised
2	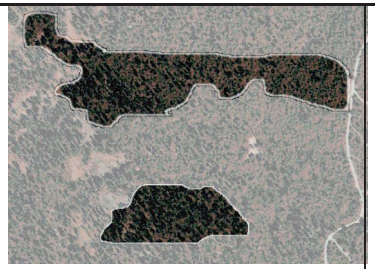 Top: *Engbjørkeskog* / and *Blåbærbjørkeskog* with at least 25% *Gran* coverage (4c/4b*) Bottom: *Engbjørkeskog* (4c)	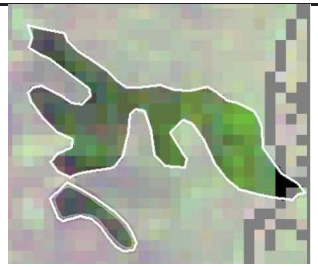 The top polygon is darker on the lefthand side and lighter on the right. This shows up in the way the polygon was classified (see supervised).	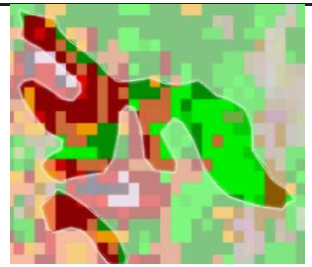 Majority: 17, 18, 19, 20, 21, 33, 41, 43, 45; Minority: 15, 16, 44	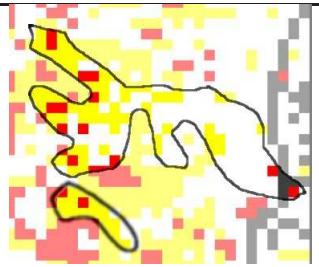 The darker areas seem to have been classified as Very Good and Less Good, and the lighter areas as Good.
4	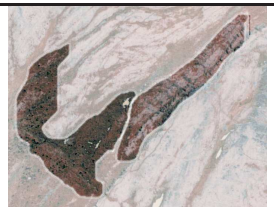 Top: *Høgstaudeng* with $> 50\%$ *vier* coverage and 25% *Gran* (3bs*) Bottom: *Lågurteng* with *kalkkrevende myrvegetasjon* (3ak)	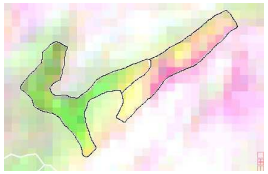 Polygons look quite different on both areal photo and satellite image even though they are both of Very Good type.	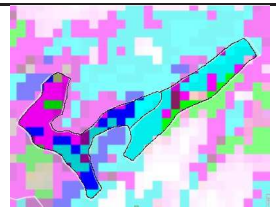 Majority: 28, 29, 31, 33, 36, 52, 53, 55, 56 Minority: 20, 32, 36	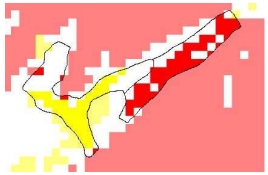 Can see the different colours in the satellite image are being classified in different grazing classes. The top polygon was classified as mostly Very Good, but the bottom polygon was the opposite and was classified as Less Good.

Table 5.21: Selected polygons - Very Good grazing quality class

Chapter 6

Discussion

This thesis used the grazing quality classes defined by the Norwegian Institute for Land Inventory (NIJOS), as a basis for testing how well grazing quality could be mapped using Landsat satellite imagery. The objective for this thesis was to investigate the possibility of discriminating between the predefined grazing classes, identifying how much information could be obtained from the Landsat images and how well a grazing quality map could be produced from these. The aim of this thesis was to use the brightness values in the Landsat images to find a pattern that connected these, with the predefined grazing quality classes of NIJOS. The following chapter gives a summary and discussion of the main results.

Initial Class Separation

Different plants dominate at different times of the year because of variations in the growing seasons of individual species. Having images from different parts of the growing season are therefore an asset when assessing vegetation spectral separability and can improve classification (de Colstoun et al., 2003; Pax-Lenny and Woodcock, 1997; Wolter et al., 1995). The initial separation analysis started with a set of multitemporal images.

Histograms were made to illustrate the spectral distributions of the NIJOS grazing quality classes, for each band of 5 images ranging across different growing seasons. They showed a clear pattern of change in radiance values from May through to October. This was related to the change in foliage density and vegetation maturity. The radiance values in the near infrared (NIR) band increased from May to June to July and then decreased again from July to August to October. Ra-

diance values in the red band were similar in the spring and summer images and decreased in the autumn images. The greatest difference between the distributions in the red and NIR bands was seen in the mid summer image (24. July). This steep change between low reflectance in the red band and high reflectance in the NIR, is a typical characteristic of vegetation at peak maturity.

The results showed that the blue band, had the highest radiance values in the visible spectrum. This is atypical of vegetation, which usually has the highest values in the green band. The increased reflection in the blue band could be explained by Rayleigh scattering. Rayleigh scatter occurs when radiation interacts with atmospheric molecules (e.g. N_2, CO_2, & O_2) and other tiny particles that have smaller diameters than the radiation wavelength. The affect of Rayleigh scatter is inversely proportional to the fourth power of the wavelength (Lillesand et al., 2004). Hence, there is a much stronger tendency for shorter wavelengths to be scattered by this mechanism than longer wavelengths (i.e. the blue band is more affected).

Data in the green band, for all three images, had higher radiance values than in the red band. This is to be expected as the vegetation absorbs more in the red and blue bands, than in the green band (i.e. chlorophyll absorption).

Histogram distribution is a very common and useful way of looking at remote sensing data, it gives an understanding of the spectral signatures of the different land cover types present in an image. Cingolani et al. (2004) used this procedure for looking at the spectral signatures (i.e. histogram distribution) for all Landsat bands in their dataset. They also incorporated the use of the normalised difference vegetation index (NDVI) values, for the vegetation types in their mountain rangeland study areas.

The spectral distributions of the 3 grazing classes had very similar distributions in all bands, overlapping almost entirely. The greatest difference in distribution in a single band, between the grazing classes, was seen in the blue band of the 29.07.1999 image. The histogram plots did not give any indication of where it was possible to separate between the classes for classification.

A follow up analysis involving statistical separation statistics, showed that separation was very poor between grazing classes in single date images. The greatest distance between two region of interest (ROI) class pairs, occurred between the Less Good (LG) and Very Good (VG) classes. The result was 1.2 using the Jeffries-Matusita (JM) separation method and was achieved using the mid summer image from the 24.07.1994. Good (G) and VG were the hardest classes to separate between. Of the 5 image dates ranging from May - October, the mid summer image (July) showed the best separation for all grazing classes.

After these initial grazing quality class separation analyses, it was not possible to see any straight forward separation between the three grazing classes. The next phase then broke the grazing classes into smaller units to try and improve separation. These units corresponded to the individual vegetation types defined by NIJOS.

The histograms for the vegetation classes showed how the individual vegetation classes affected the overall distribution of each grazing class. Class 2c (*lavhei*) in the LG grazing class, for example, had a distribution that reached quite outside the range of the majourity of vegetation classes in that grazing class in bands 1, 2, and 3. This can cause problems for the separation of grazing classes and their average spectral properties, which are used for classification.

In the VG grazing quality class, vegetation classes 4c (*Engbjørkeskog*) and 7c (*Enggranskog*) together, showed a slightly different distribution to the other vegetation classes in bands 1, 2 and 3. The distributions of 4c and 7c were then dissimilar in band 4, with 7c extending from the majourity of vegetation distributions. 2c, 4c, and 7c cover 11.5%, 2.4%, and 3.1% of the Venabygd area respectively (Bryn and Rekdal, 2002). All 3 of these classes are some of the main types of vegetation in the area so they could not be removed to improve classification.

The vegetation classes that had distributions extending beyond the distribution of the majourity of vegetation classes in each grazing class, were affecting the spectral signature of the grazing class and perhaps aiding to the difficulty of separating grazing classes. No vegetation type singled its self out completely from the rest in any of the grazing quality classes. Separation between any single vegetation classes was not made apparent from these plots.

The initial grazing and vegetation class separation analyses did not indicate sufficient separation between classes when using a single date multispectral Landsat image.

Composite Images

Not being possible to separate between grazing classes with a single image, a multitemporal approach was tested. A stack of three images from different parts of several growing seasons was created.

The composite image visualised the dominant features in each of the NIR bands of the images from May, July and October. Lillesand et al. (2004) notes that merging various combinations of bands from the different dates to create colour composites, can aid the interpreter in discriminating the various vegetation types

present.

The composite image showed the dominant radiance values in the July image belonged to vegetated areas. This can indicate that a mid summer image is a good choice for the classification of vegetation using a single date image. The dominating pixels in the October image related to areas with snow and ice coverage. The dominating areas in the May image corresponded to reflections from bare rock and soil. Several small areas showed a dominance from all three dates.

The results from the separation statistics run on the 18 band stack, showed a significant improvement in separation between all grazing class pairs from the single date results. The LG & VG ROI class pairs could be fairly well separated. G & LG, and G & VG could not be separated, but their separation distance had increased considerably from the single date images.

In agricultural crop surveys, for example, distinct spectral changes during growing seasons can permit discrimination on multi-date imagery, that would not have been possible given any single date. A field of winter wheat, might be indistinguishable from bare soil when freshly seeded in the autumn and spectrally similar to an alfalfa field in the spring. An interpretation of imagery from either date alone would be unsuccessful, regardless of the number of spectral bands. If data were analysed from both dates however, the winter wheat fields could be clearly identified, since no other field cover would be bare in late autumn and green in late spring (Lillesand et al., 2004). The complex nature of natural vegetation makes the situation much more complicated however.

Extensive literature and research examples exist on the use of multi-temporal image analysis for the classification of vegetation. de Colstoun et al. (2003), Pax-Lenny and Woodcock (1997) and Wolter et al. (1995) agree that images from different parts of the growing season are an asset when assessing vegetation spectral separability. Classification results are improved with the use of multi-temporal imagery.

Millington and Alexander (2000) state that the approach for vegetation mapping with the most promise is that based on multi-temporal analysis of satellite imagery. Their work looked at remote sensing phenology with seasonal changes in vegetation at the species, community, ecosystem or biome level.

The results from the multi-temporal analysis showed promise and should be explored further, as a possibility for grazing quality mapping using Landsat images. Further improvements could be made by adding additional dates or trying other date / image combinations from various parts of the growing season. Despite the promising results, proceeding analyses in this thesis focused on one mid summer

image. This was to reduce the complexity of the situation. An image from the middle of the summer was chosen. The image chosen was the 24th July 1994 image as it had the best separation results between grazing quality classes. More importantly, a summer image would ensure that all vegetation types are present and are a part of the signal recorded in the image.

Teillet (1986) had a dataset of 7 Landsat Thematic Mapper (TM) images and found that the autumn, winter, and spring images were not suited for forest classification in a mountainous area in Switzerland. This was because of the lower sun angles in the spring and summer, which cast shadows and the fact that the foliage of the various forest types were not fully developed. Cingolani et al. (2004) also used just one image from the middle of the growing season to classify mountainous vegetation in Argentina with Landsat data.

NDVI

The distribution of NDVI values for each grazing class showed that although all three classes overlapped. The LG class covered the lower values, with the G class in the middle and the VG grazing class covering the highest values which ranged up to 0.7. The peaks in the LG and G distributions were clearly separate, where as the G and VG peaks were much closer together. This is reflected in many of the other analyses where the two classes VG and G are much harder to separate between than the LG and G. The NDVI analysis emphasised the importance of the information content in the red and NIR bands. These are critical data in the analysis and detection of different vegetation types.

NDVI has been used in many studies of vegetation based on remote sensing (Kawamura et al., 2005; de Colstoun et al., 2003; Edwards et al., 1999; Cingolani et al., 2004; Pax-Lenny and Woodcock, 1997; Giannetti et al., 2001; Bock, 2003).

Image variation

The image variation set of analysis followed on from the initial separation results, which illustrated that the defined grazing and vegetation classes did not have spectral properties that made it easy to separate between. The second group of analyses therefore, started to look closer at the dataset, to try and understand what was varying in the image and why. It looked at what lay behind the variation within individual vegetation and grazing classes. It covered analysis on the spectral variation, terrain variation, and illumination variation of the image.

Spectral Variation

The plots of polygon mean, min, max and standard deviation, showed that the vegetation classes had a large within class variation. This variation occurred because of the mixture of elements in each polygon consisting of various vegetation species and the addition of reflectance from soil and other objects. Additional variance can occur because of the generalisation of polygons created through the mapping process. For example, the border definitions of polygons can be subjective, especially between similar vegetation types. This can lead to extra variation and "noise", to a polygon assumed to contain mostly "rishei", for example.

To reduce the affect of neighbouring vegetation on the spread of reflectance values within a class. All polygons in the grazing and vegetation classes were buffered inwardly by 50m. The buffered data showed a great improvement in clarity. The within and between polygon variation was greatly reduced leaving a clearer spectral representation for each class.

After buffering, the classes LG & G were separable using both separation algorithms. When using the transformed divergence separation method the LG & VG could also be separated.

The large improvement in separation after buffering proved that the neighbouring vegetation types had a great affect on within polygon variation. Millington and Alexander (2000) discuss the nature of vegetation boundaries, and agree that boundaries between most vegetation communities are zones of gradual transition. This poses a problem when hard line borders are drawn. This means that the border zone around vegetation polygons are likely to be a mixed with neighbouring vegetation types.

Many of the vegetation class pairs belonging to different grazing classes could be separated after buffering and the selection of pure main class vegetation polygons. Some of the problem vegetation ROI class pairs were; 7b (*Blåbærgranskog*) & 7c (*Enggranskog*), 2e (*Rishei*) & 9a (*Rismyr*), 2e (*Rishei*) & 9c (*Grasmyr*), 4b (*Blåbærbjørkeskog*) & 9c (*Grasmyr*), and 4b (*Blåbærbjørkeskog*) & 9a (*Rismyr*).

Scatter plots for a selected group of vegetation classes in band combinations of 2, were drawn up to visualise the spectral measurement space. This gave no visual separation between any of the vegetation classes studied.

Cingolani et al. (2004) wrote about the high within-pixel heterogeneity in their study area in the Argentinian mountains. It was described as the result of the interaction of disturbance factors (such as fire and grazing) with complex topographical and geomorphological patterns. These produce different vegetation commu-

nities and mosaic types. They observed that, of their reference sites, only 12% of them, contained 95% or greater cover of a single structural type. The influence of free ranging grazers combined with natural environmental gradients often creates complex and heterogeneous vegetation patterns (Cingolani et al., 2004).

Terrain Variation

The physical environment is often regarded as one of the most important factors controlling the spatial heterogeneity of the landscape in mountain areas (Hoersch et al., 2002). The topography (i.e. variation in elevation), especially in an alpine environment, controls the variation in energy (i.e. temperature), water, nutrients, geomorphological processes and disturbance factors, and hence the variation and distribution of vegetation. As spatial information on site factors (e.g. rainfall and temperature) is commonly lacking in mountain areas, the use of a digital elevation model (DEM) is a potential substitute for use in vegetation analyses (Hoersch et al., 2002; Walsh and Davis, 1994; Bridge and Johnson, 2000; Barrio et al., 1997).

Since the geographic space of a vegetation type in a high mountain environment is closely related to topographic relief, it is likely that landform parameters such as elevation, slope and aspect are important input parameters for spatial analysis and modeling of vegetation distribution in mountain landscapes. In a complex system of site factors, topography is the major (indirect) factor for vegetation distribution (Barrio et al., 1997). Thus topography creates a patchwork-like pattern of small scale vegetation habitats (Hoersch et al., 2002).

Elevation

With elevation having such a great impact on where vegetation types are found in a region (especially alpine) then elevation could be brought into an algorithm to classify the vegetation groups. Elevation was tested as a feature for separating vegetation classes that had overlapping spectral distributions in one band. Pairs of vegetation classes from unlike grazing classes were plotted against elevation. Of the vegetation classes plotted, 9c (*Grasmyr*) and 7c (*Enggranskog*) could be separated.

Elevation is a good attribute to add for separating vegetation types occurring in the valley with those higher up on the slopes, but that both cover similar reflectance values. All the Pine and Spruce vegetation types in Venabygd were only found below 1000m a.s.l. These types could be separated from those with similar spec-

tral values that occurred above 1000m in the Venabygd area. Although *Grasmyr* does occur in small areas below 1000m a.s.l. in the Venabygd area, it is mainly found above this. This vegetation type, can therefore be separated with those of 6a (*Lav- og Lyngrik furuskog*), 6b (*Blåbærfuruskog*), 6c (*Engfuruskog*), 7a (*Lav- og lyngrik granskog*), 7b (*Blåbærgranskog*) and 7c (*Enggranskog*) purely on the basis of elevation.

The results showed that some pairs were separable using the elevation information and others were not. This test was only looked at between vegetation class pairs within single image bands. It does however give some positive results to the use of elevation in a classification algorithm.

Slope & Aspect

Some vegetation species in mountainous environments prefer growing on steep slopes, as they have become well adapted (e.g. with special roots) and thrive from a less competitive environment. Some species congregate on slopes that face in a certain slope direction (aspect) e.g. towards the sun (i.e. a slope facing south or north, depending on the hemisphere). Because slope is the reason why gravity induces the flow of water above and below the surface, slope (e.g. concave and convect slopes) can give an indication of how wet the soil usually is, whether water drains through and to that area or away from it (e.g. ridge) (Hoersch et al., 2002). All these terrain aspects affect the way vegetation is distributed.

The affects of slope and aspect on the main vegetation classes in Venabygd showed that some vegetation types, mostly the tree types, tended to favour slopes that lay in a certain range of compass directions. As the slope value increased this compass direction range narrowed. Grasses, shrubs and swamp vegetation however, were distributed fairly evenly on slopes facing in all directions. Most vegetation types had the majourity of their pixels below slopes of approximately $20°$. Some had a more sparse distributions that increased up to $35°$. This included 2e (*Rishei*) and 2c (*Lavhei*).

Hoersch et al. (2002) noted that only large topographic structures can be derived from a 25m resolution DEM. A DEM at this resolution did not represent the fine scale variations in curvature and thus soil moisture or exposure towards wind and weather impacts, which affect the distribution of vegetation. With the continuous availability and increased accuracy of digital elevation models (e.g. laser), better data could be available for future analyses.

Illumination Variation

Meyer et al. (1993) states that in the visible and NIR bands, the direct sun radiation is the only illuminating factor in an image, when neglecting atmospheric influence and adjacency effects. If the terrain were additionally completely flat and all objects had a Lambertian reflectance (equal reflectance in all directions) characteristics, the reflected energy measured by a sensor (radiance) would only depend on the direct irradiance and the reflectance of the ground objects. Most objects however, including forest and vegetation, have non-Lambertian reflectance characteristics. The effects of topography on scene radiance cannot be neglected in an alpine region and thus need to be taken into consideration.

The aim of correcting for illumination is that two pixels of the same land cover type, will reflect the same amount of radiation, regardless of the amount of illumination incident on the pixel. Two topographic correction methods were calculated on the July image to correct for the variation in illumination. These images were masked for all other pixels but those contained in the three grazing classes. The uncorrected image, c-corrected and cosine corrected images were compared along with comparisons in separation ability between vegetation and grazing classes after correction.

The differences in separation possibilities between the 3 images was marginal. The cosine correction method appeared was slightly better at separating between the ROI pairs of selected vegetation classes. The noticeable changes in image data were seen when looking at the regression models of the 3 images. The regression model for the original image showed that, with increased illumination, there was an increase in reflectance values. The cosine correction method showed that reflectance values were higher, when illumination was reduced. This was the result of a gross over-correction for those pixels in low illumination areas. This is because the cosine method does not take the fact that pixels also receive a considerable amount of diffuse illumination into account. This is a highly undesirable affect. The c-correction regression model showed very good regression results, indicating that regardless of illumination, reflection values were fairly equal for the same land cover type.

Even though the separation statistics did not show that any one image was significantly better than the other, the regression models backed the decision for using the c-correction image for supervised classification. Meyer et al. (1993) also agreed that the C-correction algorithm showed the best results over the cosine correction algorithm and an uncorrected image when it was tested on forest classification in the mountains of Switzerland. Meyer et al. (1993) found the results from the c-correction method to be similar to those for the statistical-empirical

and minnaert correction methods. A topographic correction is therefore highly suggested for any future studies in this area.

de Colstoun et al. (2003) used topographically corrected Landsat images to map vegetation in the Delaware Water Gap National recreation area near Milford in the US. Millington and Jehangir (2000) studied the difficulties encountered in mapping vegetation and land cover change in dissected mountain environments using a study area in the Himalayas of northern Pakistan. The data used was corrected for topographic effects using a solar radiation model for the entire study catchment of the day of image acquisition. They masked out areas of snow, ice and cloud before topographic correction. Ahmad et al. (1992) presents an alternative method for topographic corrections without using a DEM.

Unsupervised Classification

Comparisons with a 60 class unsupervised classification and the NIJOS grazing classes, showed that the G grazing class dominated in several of the unsupervised clusters. The LG class also dominated in some of the clusters but was not as clearly represented as the G class and was often mixed in with other classes. The VG class was not well represented at all, occurring mostly in a mixture with the G class and sometimes with all classes. Many of the results have indicated that the VG class is the hardest to separate from the rest.

The unsupervised classification results were also compared to the vegetation classes. These comparisons showed some very interesting results. As with the grazing classes, the different unsupervised classifications (clusters of 10-60) followed the same pattern throughout. What was noticed from this comparison was that a number of the main vegetation classes stood out as umbrella classes, containing a mixture of individual vegetation classes in each cluster, but a mixture that belonged to the same umbrella vegetation type.

There are 3 spruce (*Gran*) types in the Venabygd area and these were grouped together in the clusters, dominating some of them completely. As individual vegetation classes however, they did not dominate any of the clusters, even when classifying with 60 clusters. This was the case for almost every vegetation class. The only individual vegetation classes that showed some independence were 7b (*blåbærgranskog*), 2e (*Rishei*), 4a (*Blåbærbjørkeskog*), and 2c (*lavhei*).

The *Hei* vegetation types stayed grouped together and dominated several of the clusters. The same situation was observed for the *Bjørk* vegetation types. The *Eng* vegetation types were very spread over the clusters and covered little percentage

of any one cluster. The same went for the *Ore / Hagemarkskog* vegetation types as well, although these vegetation types covered very little of the Venabygd area. The *Furu* vegetation types together cover less than 2% of the Venabygd area and were also almost not visible in the clusters. The *Myr og sumpskog* vegetation types, which cover approximately 12% of the Venabygd area, were very spread out through the clusters. They were combined with all of the umbrella vegetation types and did not dominate any of the clusters.

The unsupervised classification showed that there was not enough spectral information in the Landsat reflectance image to distinguish between the sub-umbrella types of vegetation. It has shown that the spectral information could outline 3 clear vegetation groups: Spruce, Birch, and alpine grass. Even the pine and swamp vegetation types were not dominating in any of the unsupervised clusters. In the Venabygd area there are 27 main vegetation types. If secondary vegetation types are included along with additional attributes, there are 363 individually defined vegetation groups. 60 classes might not have been sufficient and the results could therefore have been improved by increasing the number of clusters. This should be attempted in future studies. A summary of studies in Nordic countries using satellite imagery (mostly Landsat) commented on by Kalliola and Syrjanen (1991), showed that treeless vegetation categories such as mires (*myr & sump*) and alpine heaths, tended to appear as forests in satellite classifications unless they were separated using digitized masks. the results shown here also confirmed this observation, that the mire classes were mixed in with all the tree classes (see fig 5.31). Kalliola and Syrjanen (1991) also noted that from these studies the inner composition of many vegetation complexes were beyond the resolution (20-30m) of the satellite images. That again has been shown the results presented in this thesis.

Analyses have shown that there are problems in comparing the grazing vegetation types of those areas under tree cover and those above the tree line. This suggests that separating the forest areas from the non-forest areas before classification, could have positive effects. Future attempts at classification for grazing quality, should incorporate this into part of the classification algorithm. In addition the type of information available below the tree line is different to that above the tree line and results could be improved by using alternative classification algorithms for forested areas and non-forested areas.

Wolter et al. (1995) noted that forest classifications using single data Landsat TM data have been only moderately successful in separating forest cover types in the northern Lake States region, especially down to the genus or species level. Wolter et al. (1995) developed a method that incorporated multi-temporal TM and Multispectral Scanner (MSS) images that capture the phenological changes of the dif-

ferent tree species. They were then able to classify 22 forest types with an overall accuracy of 80%. The initial results obtained from using a multitemporal dataset showed promise and the use of multitemporal images should not be underestimated in future studies.

Using an unsupervised classification is a very commonly procedure for use on remote sensing data and the classification of vegetation, see (Kalliola and Syrjanen, 1991; Vogelmann et al., 1998; Cingolani et al., 2004) for research examples. Vogelmann et al. (1998) used the data from an unsupervised classification on Landsat images to map regional land cover in US standard federal regions. This was followed by the labeling of clusters using aerial photographs.

Cingolani et al. (2004) used an unsupervised classification with 10 classes on Landsat images to stratify their field sampling according to spectral patterns. The test area was a heterogeneous mountainous area in Argentina. They decided on the number of classes after visual examination of different band combinations. The resulting structural types that were seen by the unsupervised classification were then adjusted to define meaningful ecological structural groups. Additionally for each ground truth stand in the Cingolani et al. (2004) paper they recorded the topographic position, slope, aspect and altitude.

From the preceding sets of results it has not been shown possible to separate and hence be able to classify, the grazing quality classes outlined by NIJOS. The separation of grazing quality classes did not improve by breaking the classes down into the NIJOS defined vegetation classes because it was not possible to separate between these individual vegetation classes using the 25m resolution Landsat TM image. The results illustrated that it was possible to obtain information from 3 main umbrella vegetation classes, Spruce, birch and alpine grass. These could then be connected back to the grazing classes in some way.

Trying to separate all three NIJOS grazing classes might not be possible with a Landsat image. The spectral values of the VG class are not distinct enough from the other classes. Newly defined grazing classes may have to be defined to produce a grazing quality map. These could represent a more general Good and Not Good grazing quality, which could then could then be linked back to the NIJOS classes. All the preceding results indicate that aiming for a grazing map that focuses on just 2 classes Good and Not Good grazing could be effective. These classes may also have to differ from the definition of the NIJOS G and LG grazing classes. Incorporation of elevation, slope and aspect into a classification algorithm has also been shown to have positive effects and should be considered in future studies. Topographic correction should definitely be incorporated and the use of a multitemporal dataset should be explored further.

Airphoto Inspection

An assessment of the NIJOS mapping methods and ground truth data was conducted by analysing aerial photos over the area and comparing those to the information content of the satellite image and vegetation polygons. The inspection of airphotos started with selecting certain examples. The polygon outlines were drawn onto the aerial photo allowing a comparison to the vegetation classes. A number of factors were noticed when studying these examples. The bright green areas in the satellite images appeared to represent the chlorophyll content in the land cover. The pink / dark pink areas were a representation of minerals, soil and water. An alternative grazing map to mapping the 3 NIJOS classes could be a grazing quality map indicating the level of chlorophyll content in a pixel as an indication of grazing quality. The NDVI analysis showed that the grazing qualities were clearly linked to red and NIR bands. The red band gives a direct indication of the level of chlorophyll absorption in the vegetation.

These comparisons emphasised those mapping methods that can lead to subjectivity in the results, when using this information as ground truth. Polygon border locations are defined as hard lines, whereas vegetation on the ground changes type gradually. These affects lead to zones of mixed vegetation types around the edges of polygons.

Millington and Alexander (2000) discussed the nature of vegetation boundaries and agreed that it is generally accepted that boundaries between most vegetation communities, are zones of gradual transition and not hard lines. They acknowledge the problems of mapping gradual transitions when producing hard line boundary maps. Modern mapping techniques in a geographic information system (GIS) can allow soft and fuzzy borders to be mapped, but this technique was not used in the vegetation maps used in this thesis.

NIJOSs vegetation map is an overview map meaning that polygons have to be generalised to a certain extent. This can mask some of the vegetation detail and smooth the mosaic characteristic of vegetation that is often occurs in natural vegetation. Green and Hartley (2000) note that the relatively straightforward task of mapping vegetation patch boundaries from aerial photography (a technique also used by NIJOS), can be affected by multiple sources of error e.g. georeferencing and subjective photo interpretation. Ahmad et al. (1992); Chica-Olmo and Abarca-Hernandez (2000) and Wyatt (2000) discuss further details on the use and restrictions of remotely sensed data for vegetation mapping.

These affects have to be taken into account when evaluating the statistics extracted based on the polygon regions and the comparison of results to these ground truth

data.

Supervised Classification

A supervised classification was run on the c-corrected mid summer image. Before the classification was done additional information was added to the image to remove areas that could produce errors in the classification result. Road and tractor networks, stream networks, rivers, lakes, agricultural land, and housing locations were all masked out of the image. The comparison of airphotos to the vegetation classes had revealed that many of the polygons classified as grazing quality for sheep also had small waterways running through them and contained small amounts of developed areas. Vogelmann et al. (1998) also used ancillary data including a DEM land cover and infrastructure data along with Landsat TM images, to regionally map land cover in the US.

The supervised classification was run using a Gaussian Maximum Likelihood Classifier (MLC). The MLC is a very common method used with remote sensing data. Clark et al. (2001) for example, evaluated the influence of image acquisition date and satellite imaging system, on the accuracy of plant community maps created from Landsat TM 5 and SPOT3 HRV data, using a maximum likelihood classification procedure.

A confusion matrix was calculated to give an error assessment of the classification. The overall accuracy was 61%. The G and LG grazing classes had the highest accuracy results, but the VG grazing class was only classified with a 32% producer's accuracy and a 21% user's accuracy. These results illustrated again, the trend that has been noted throughout all analyses, that the VG grazing quality does not have spectral values unique enough to be separated from the G quality class.

Congalton (1991) and Congalton and Green (1999) recognise the confusion matrix or error matrix, as the most common way to represent the classification accuracy of remotely sensed data. They note that it has been used by many researchers and should be adopted as the standard reporting convention.

The comparison of unsupervised classification, supervised classification and satellite image per polygon, to the airphotos highlighted the difficulty in classification. Many of the polygons had pixels classified in all 3 grazing quality classes. The analysis gave a visual understanding of the complex nature of vegetation even when the reflectance was averaged over a 25m pixel.

One of the main issues arising from the use of 25m resolution data is that each pixel contains a mixture of spectral signatures from several plants, perhaps of different species, in addition to reflections from the soil and adjacency affects. This leads to the suggestion for a sub pixel classification such as spectral unmixing, which focuses on identifying the combination of spectral signatures that are apparent in a satellite image pixel. The unsupervised classification using 60 clusters revealed that the spectral groupings in the images are a mixture of vegetation types. To identify each type it could be necessary to go to the sub pixel level. Spectral unmixing is likely to be a very effective form for classification in virgin areas when using Landsat images and is strongly suggested for applications in future studies.

From the inspection of aerial photos and the many analyses on the satellite images, it was clear that each pixel is affected by its neighbour and by a mixture of vegetation species. Chica-Olmo and Abarca-Hernandez (2000) note that most classical mathematical algorithms for image classification do not usually consider the spectral dependence existing between a pixel and its neighbours, i.e. spatial autocorrelation. Chica-Olmo and Abarca-Hernandez (2000) suggest adding textural information which can be analysed from the autocorrelation structure of the data and then used to improve classification. This improvement would arise from the hypothesis that a pixel is not independent of its neighbours and, furthermore, that its dependence can be quantified and incorporated into the classifier (Chica-Olmo and Abarca-Hernandez, 2000). They illustrate a method for doing this with univariate and multivariate textual measures of spatial variability. Such a method could be incorporated with the data used in this thesis to improve classification.

NIJOS grazing classes are designed from a bottom up approach. This approach starts with a detailed classification of the vegetation in an area into more than 30-40 main vegetation types. These main vegetation types can then contain secondary vegetation types plus additional attributes, which leads to the possibility for hundreds of unique combinations. Each of these combinations is then given a grazing quality class for sheep or cattle. The results shown in this thesis indicate that classifying the grazing quality classes defined by NIJOS (Less Good, Good and Very Good) is not possible with Landsat images. To achieve a better classification the following options are recommended: use higher resolution data (such as airphotos), increase the temporal resolution of the dataset, or use a more top down approach to classifying grazing quality that redefines the grazing quality classes.

Hoersch et al. (2002) compared two vegetation maps resulting from the classification of low and high spatial resolution remotely sensed data. The 25 m spatial resolution data (equivalent to the satellite data used here) was able to discriminate

20 vegetation classes (these included water, ice, infrastructure and cleared land). The 5 m spatial resolution data was able to distinguish 52 vegetation classes using a majority filtering technique.

Results have lead to the suggestion for a more hierarchical top down approach when using Landsat data. A forest / non-forest classification is a suggested first step. This could be incorporated into a decision tree classifier. The second step would then be to define an appropriate set of rules for each of the two first classes (forest and non-forest). Analyses in this thesis have shown that using elevation, slope, aspect, ancillary data such as road and river networks and topographic correction (with the c-correction method) have improved the possibility for classification through better separation and spectral definition of vegetation classes.

Decision trees have been preferred to statistical classifiers in the literature for coarse-scale applications because they do not make any implicit assumptions about normal distributions in the input data, as an MLC would (used in this thesis). These classifiers can also accept a wide variety of input data, including non-remotely sensed ancillary data, and in the form of both continuous and/or categorical variables. Decision trees have been shown to provide improved accuracies over the use of other more traditional classifiers. However, despite these proven benefits, the use of decision trees for applications with higher spatial resolution data such as Landsat TM and Enhanced Thematic Mapper (ETM) has not yet fully been explored (de Colstoun et al., 2003).

Increasingly, advances in the fields of pattern recognition and machine learning have led to the application of decision tree and neural network classifiers, particularly with regards to land cover classifications at global to continental scale. In fact, decision trees are used in the global land cover classification algorithms for the MODerate Resolution Imaging Spectroradiometer (MODIS) (de Colstoun et al., 2003).

de Colstoun et al. (2003) explored decision tree classifiers for a multi-temporal satellite data set from the ETM+ instrument, to map 11 land cover types in a National Park near Milford, US. Using land cover classes as specified by the National Vegetation Classification Standard at the Formation level, the final land cover map had an overall accuracy of 82% when tested against a validation data set acquired on the ground. This same accuracy was 99.5% when considering only forest vs. non-forest classes. de Colstoun et al. (2003) noted that the usage of ETM+ scenes acquired at multiple dates improves the accuracy over the use of a single date, particularly for the different forest types.

The use of Landsat scenes acquired at different seasons and/or years to improve land cover classification is not a new concept. Many studies have shown that clas-

sification results have improved with the use of multitemporal images rather than single time-shots. Having a reduced number of images however, can give large savings in imagery cost and processing effort. Among many other studies Pax-Lenny and Woodcock (1997) looked at agricultural lands in Egypt for calculating area estimates of non-productive and productive land. They assessed the effects of the number and timing of images on these estimates and found that the average overestimation of non-productive lands in the Nile Delta was around 5% when using a data set of 9 images, but over 300% with a data set containing only 2 images. Generally, their data sets that included more images from the peak of the growth season resulted in higher accuracies, although in some cases having a mixture of peak and low growth season gave greater accuracy.

de Colstoun et al. (2003) used 2 Landsat ETM dates for a decision tree classification of 8 vegetation types in a National Park area in the US and found that when using a second image this reduced the errors made from using either scene by nearly half and generally reduced the confusion between all cover types; Evergreen forest, deciduous forest, mixed forest, woodland, shrubland, grassland, wetland and cropland.

The image data set used in this thesis covered dates from different growing seasons ranging from 1994 to 2004. Images from different growing seasons had to be obtained because of the lack of cloud free images during a single growing season. Pax-Lenny and Woodcock (1997) noted that although there is a great deal of literature about the use of multi-temporal dataset for the classification of vegetation, there is little published research that focuses on the effects of using images that cross growing seasons. The results from this thesis indicated that it is not possible to map the grazing quality classes of NIJOS using a single date image. The composite image analysis gave positive results to the use of multitemporal data and this should be explored further in future studies.

Bock (2003) looked at detailed biotope classification using object-based methods. He used dual date Landsat TM images from spring and summer. 22 wet grass and moor land vegetation types were classified. The object-based method was successfully applied in order to identify hot spots for an update of the biotope register.

Hoersch et al. (2002) found advantages using an object-based technique in vegetation classification especially for indication of single dwarf shrub plants and agglomerations of species at their upper elevation limit. The extraction of nearly circular patches of dwarf shrubs was simplified in the object-based approach by the integration of object shape, compactness, texture and context/topology besides their raw spectral characteristics of traditional per-pixel classification.

Texture was used to inspect birch trees in airphotos in this thesis for example. The polygons outlined by NIJOS were often very large and too course to contain information from a single vegetation type in the satellite image. An object-based approach could be a way around this, allowing shapes to be defined unlike the square borders of the pixels and more attuned to the irregular shapes of vegetation groupings. An object-based approach would be an appropriate technique for the mapping of virgin areas.

Improvements could have been made to the supervised classification results obtained here, through the use of alternative classifiers. Discriminant functions for example, were assessed by Cingolani et al. (2004) and Lewis (1998). Principle component analyses could have been incorporated or a nearest neighbour classifier could have been used. A k nearest neighbour classifier was used by Haapanen et al. (2004) for example, to delineate forest / non-forest areas using Landsat TM and ETM in the US. The use of Hidden Markov models and phenology has also been assessed with multitemporal satellite data with applications to mountain vegetation classification (Aurdal et al., 2005a,b).

The majourity of literature on classifying grazing lands with satellite remotely sensed data focuses on the intensity and impact of grazing on the environment. They often use vegetation indices such as NDVI, and focus more on the changes in ”greenness” distribution and density. Very little focus has been on the quality of grazing vegetation (Kawamura et al., 2005; Edwards et al., 1999). Results from this thesis suggested that a ”greenness” scale could be a very effective way of indicating grazing quality using Landsat images. This could be incorporated into a decision tree classifier for example, as mentioned earlier.

Chapter 7

Conclusions

The aim of this thesis was to classify the grazing quality classes defined by the Norwegian Institute for Land Inventory (NIJOS) (Less Good, Good and Very Good) using Landsat data. The results from this thesis showed that it was not possible to classify these grazing quality classes with high accuracy. Difficulties lay in the insufficient amount of unique spectral information, for each grazing class, available in a single Landsat Thematic Mapper (TM) image. The separation of the Less Good class posed the most difficulties.

Results revealed that it was possible to obtain information for the classification of three main vegetation types: birch, spruce and alpine heath & grasses. A grazing map could be produced from these three classes and then linked back to the NIJOS grazing classes.

Improved results were obtained after a topographic correction (c-correction method) of the image. It is recommended that topographic correction be incorporated into any future applications for the mapping of grazing quality in the Venabygd area.

Elevation was proved to be a feature possible of separating vegetation types covering similar reflectance values. Slope and aspect were also proved to affect the way in which vegetation types were distributed. A digital elevation model (DEM) was not incorporated into the supervised classification run on the data in this thesis, but is highly recommended for inclusion in algorithms for future classifications of vegetation.

Results proved that the affects of neighbouring vegetation types around the border regions of vegetation types are highly influential and greatly affect classification possibilities. Results also showed that the 25m resolution Landsat pixels contained a considerable mix of information from more than single vegetation types.

These results lead to the suggestion for the use of higher resolution imagery. They also give support for applying spectral unmixing and object-based classification methods in future studies.

Improved separation results were obtained when using a multitemporal dataset. The supervised classification performed in this thesis was run on a single date image, but results from analyses on a multitemporal dataset showed promise. The further examination of multi-date images for the classification of grazing quality classes is recommended.

NIJOS has appointed its grazing classes from a bottom up approach. They are based on highly specific vegetation classes defined in the field, which are not visible in the Landsat data. The results from this thesis have lead to the suggestion for a more hierarchical top down approach when using Landsat data. A forest / non-forest classification is a suggested first step. This could be incorporated into a decision tree classifier. The proceeding steps should then involve the incorporation of slope, aspect, elevation, ancillary data on roads, river networks and other infrastructure data, into the classification algorithm.

Bibliography

Ahmad, W., Jupp, L. B., and Nunez, M. (1992). Land cover mapping in a rugged terrain using Landsat MSS data. *International Journal of Remote Sensing*, 13:673–683.

Armitage, R. P., Weaver, R. E., and Kent, M. (2000). Remote sensing of semi-natural upland vegetation: the relationship between species composition and spectral response. In Alexander, R. and Millington, A. C., editors, *Vegetation Mapping: From Patch to Planet*, chapter 6. John Wiley and Sons Ltd.

Aurdal, L., Huseby, R. B., Eikvil, L., Solberg, R., Vikhamar, D., and Solberg, A. (2005a). Use of hidden markov models and phenology for multitemporal satellite image classification: Applications to mountain vegetation classification. In *Proceedings MultiTemp 2005, 3 rd International Workshop on the Analysis of Multi-temporal Remote Sensing Images*. Biloxi, Mississippi, USA.

Aurdal, L., Huseby, R. B., Vikhamar, D., Eikvil, L., Solberg, A. S., and Solberg, R. (2005b). Classification of multitemporal satellite images using phenological models. EO-Tools Project (SAMBA) 830110, The Norwegian Computing Centre.

Barrio, G. D., Alvera, B., Puigdefabregas, J., and Diez, C. (1997). Response of high mountain landscape to topographic variables: Central Pyrenees. *Landscape Ecology*, 12:95–191.

Bock, M. (2003). Remote sensing and GIS-based techniques for the classification and monitoring of biotypes. case examples for a wet grass-and moor land area in northern Germany. *Journal for Nature Conservation*, 11:145–155.

Bridge, S. R. J. and Johnson, E. A. (2000). Geomorphic principles of terrain organisation and vegetation gradients. *Journal of Vegetation Science*, 11:57–70.

Bryn, A. and Rekdal, Y. (2002). Vegetasjon og beite på Venabygdsfjellet. Technical Report Document 8/02, NIJOS - Norwegian Institute for Land Inventory, Ås.

Chander, G. and Markham, B. (2003). Revised Landsat-5 TM radiometric calibration procedures and post-calibration dynamic ranges. *IEEE Transactions on Geoscience and Remote Sensing*, 41(11):2674–2677.

Chica-Olmo, M. and Abarca-Hernandez, F. (2000). Computing geostatistical image texture for remotely sensed data classification. *Computers and Geosciences*, 26:373–383.

Cingolani, A. A., Renison, D., Zak, M. R., and Cabido, M. R. (2004). Mapping vegetation in a heterogeneous mountain rangeland using Landsat data: an alternative method to define and classify land-cover units. *Remote Sensing of Environment*, 92:84–97.

Clark, P. E., Seyfried, M. S., and Harris, B. (2001). Intermountain plant community classification using Landsat TM and SPOT HRV data. *Journal of Range Management*, 54(2):152–160.

Congalton, R. G. (1991). A review of assessing the accuracy of classifications of remotely sensed data. *Remote Sensing of Environment*, 37:35–46.

Congalton, R. G. and Green, K. (1999). *Assessing the Accuracy of Remotely Sensed Data: Principles and Practices*. Mapping in Sciences Series. Lewis Publishers.

CRISP (2001). Centre for remote imaging, sensing & processing. website: `www.crisp.nus.edu.sg/\~research/tutorial/optical.htm`.

de Colstoun, E. C. B., Story, M. H., Thompson, C., Commisso, K., Smith, T. G., and Irons, J. R. (2003). National park vegetation mapping using multitemporal Landsat 7 data and a decision tree classifier. *Remote Sensing of Environment*, 85:316–327.

Edwards, M. C., Wellens, J., and Al-Eisawi, D. (1999). Monitoring the grazing resources of the Badia region, Jordan, using remote sensing. *Applied Geography*, 19:385–398.

ENVI (2003). *The Environment for Visualising Images - Software help document*. ENVI 4.2.

Fiella, I. and Penuelas, J. (1994). The red edge position and shape as indicators of plant chlorophyll content, biomass and hydric status. *International Journal of Remote Sensing*, 15(7):1459–1470.

Geoland (2005). Geoland Project. Geoland is an integrated GMES project on land cover and vegetation co-ordinated by Inforterra, Gmbh, and Medias-France. Website: `www.gmes-geoland.info`.

Giannetti, F., Montanarella, L., and Salandin, R. (2001). Integrated use of satellite images, DEMs, soil and substrate data in studying mountainous lands. *JAG*, 3(1):25–29.

Goodchild, M. F. (1994). Intergrating GIS and remote sensing for vegetation analysis and modeling: methodological issues. In Walsh, J., Davis, F. W., and Peet, R. K., editors, *Applications of remote sensing and geographic information systems in vegetation science*. OPULUS Press Uppsala, Sweden. Also printed in Journal of Vegetation Science 5: 615-626.

Green, D. R. and Hartley, S. (2000). Integrating photo-interpretation and GIS for vegetation mapping: Some issues of error. In Alexander, R. and Millington, A. C., editors, *Vegetation Mapping: From Patch to Planet*, chapter 7. John Wiley and Sons Ltd.

Haapanen, R., Ek, A. R., Bauer, M. B., and Finley, A. O. (2004). Delineation of forest nonforest land use classes using nearest neighbour methods. *Remote Sensing of Environment*, 89:265–271.

Hashimoto, T., Takagi, M., Kajiwara, K., and Fujino, C. (1993). Remote sensing note. Published concerning the National Centre for Geographic Information and Analysis (NCGIA) project in the June 1993 issue of Photogrammetric Engineering and Remote Sensing. Available online at `http://www.profc.udec.cl/\~gabriel/tutoriales/rsnote/contents.htm`. ©Japan association of Remote Sensing.

Hoersch, B., Braun, G., and Schmidt, U. (2002). Relation between landform and vegetation in alpine regions of Wallis, Switzerland. a multiscale remote sensing and GIS approach. *Computers, Environment and Urban Systems*, 26:113–139.

Houston, A. and Rycroft, M., editors (1999). *Keys to Space: An interdisciplinary approach to space studies*. McGraw-Hill Primis Custom Publishing. Written by the International Space University.

Huggett, R. and Cheesman, J. (2002). *Topography and the Environment*. Person Education Limited.

Jensen (1996). *Introductory Digital Image Processing: A remote sensing perspective*. Prince Hall series in Geographical Information Science, 2nd edition.

Kalliola, R. and Syrjanen, K. (1991). To what extent are vegetation types visible in satellite imagery? *Annales Botanici Fennici*, 28(1):45–57.

Kawamura, K., Akiyama, T., Yokota, H., Tsutsumi, M., Yasuada, T., Watanabe, O., and Wang, S. (2005). Quantifying grazing intensities using geographic information systems and satellite remote sensing in the Xilingol steppe region, inner Mongolia, China. *Agriculture Ecosystems and Environment*, 107:83–93.

Larsson, J. Y. and Rekdal, Y. (1997). Veiledning i vegetasjonskartlegging M 1:50 000. Technical Report Document 5-97, Norsk institutt for jord- og skogkarlegging. Available online at `www.nijos.no`.

Lewis, M. M. (1998). Numerical classification as an aid to spectral mapping of vegetation communities. *Plant Ecology*, 136:133–149.

Lillesand, T. M., Kiefer, R. W., and Chipman, J. W. (2004). *Remote Sensing and Image Interpretation*. John Wiley and Sons Inc.

Lunetta, R., Congalton, R., Fenstermaker, L., Jensen, J., McGwire, K., and Tinney, L. (1991). Remote sensing and geographic information system data integration: error sources and research issues. *Photogrammetric Engineering and Remote Sensing*, 57(6):677–687.

Matlab (2005). *Matlab Help Files*. The MathWorks Inc. Release 14, Service pack 2.

Meyer, P., Itten, K. I., Kellenberger, T., Sandmeier, S., and Sandmeier, R. (1993). Radiometric corrections of topographically induced effects on landsat tm data in an alpine environment. *Journal of Photogrammetry and Remote Sensing*, 48(4):17–28.

Millington, A. C. and Alexander, R. W. (2000). Vegetation mapping in the last three decades of the twentieth century. In Alexander, R. and Millington, A. C., editors, *Vegetation Mapping: From Patch to Planet*, chapter 18. John Wiley and Sons Ltd.

Millington, A. C. and Jehangir, S. (2000). Mapping vegetation in complex, mountainous terrain. In Alexander, R. and Millington, A. C., editors, *Vegetation Mapping: From Patch to Planet*, chapter 12. John Wiley and Sons Ltd.

NASA (2006). The Landsat-7 science data user's handbook. Available online at `http://landsathandbook.gsfc.nasa.gov/handbook/handbook_toc.html`. A living document prepared by the Landsat Project Science Office at NASA's Goddard Space Flight Center in Greenbelt, Maryland.

Pax-Lenny, M. and Woodcock, C. E. (1997). Monitoring agricultural lands in Egypt with multitemporal Landsat TM imagery: How many images are needed? *Remote Sensing of Environment*, 59:522–529.

Richards, J. A. (1986). *Remote Sensing Digital Image Analyses*. Springer, Berlin.

Siedlicka, A., Nystuen, J. P., Englund, J. O., and Hossack, J. (1987). Lillehammer bergrrunnskart M 1:25,000. Norges geologisk undersøkelse.

Soille, P. (2003). *Morphological Image Analysis, Principles and Applications*. Berlin, Springer Verlag, 2nd ed edition.

Song, C., Woodcock, C. E., Seto, K. C., Leney, M. P., and Macomber, S. A. (2001). Classification and change detection using Landsat TM data: When and how to correct atmospheric effects. *Remote Sensing of Environment*, 75:230–244.

Teillet, P. M. (1986). Image correction for radiometric effects in remote sensing. *International Journal of remote sensing*, 7(12):1637–1651.

USGS (2006). United states geological survey (USGS) Landsat website. `http://landsat.usgs.gov/`.

Vogelmann, J. E., Sohl, T. L., Campbell, P. V., and Shaw, D. M. (1998). Regional land cover characterisation using Landsat Thematic Mapper data and ancillary data sources. *Environmental Monitoring and Assessment*, 51:415–428.

Walsh, S. J. and Davis, F. W. (1994). Applications of remote sensing and geographic information systems in vegetation science: Introduction. In Walsh, S. J., Davis, F. W., and Peet, R. K., editors, *Special features in vegetation science 6*. IAVS and OPULUS Press AB.

Wolter, P. T., Mladenoff, D. J., Host, G. E., and Crow, T. R. (1995). Improved forest classification in the northern lake states using multi-temporal Landsat imagery. *Photogrammetric Engineering and Remote Sensing*, 61:1129–1143.

Wood, J. D. (1996). *The Geomorphological characterisation of digital elevation models*. PhD thesis, University of Leicester, UK. Available online at `http://www.soi.city.ac.uk/\~jwo/phd`.

Wyatt, B. K. (2000). Vegetation mapping from ground, air and space - competitive or complementary techniques? In Alexander, R. W. and Millington, A. C., editors, *Vegetation mapping*, pages 3–18. Wiley.

Appendices

Appendix A

General steps for classification

This list, adapted from Jensen (1996), identifies the general steps needed to process a satellite image and extract land cover information.

- Describe nature of the land-cover classification problem
  - Specify the geographic region of interest
  - Define the classes of interest,
  - Do you want to use continuous, or discrete values
  - Determine if it is to be a hard or fuzzy, or contextual classification
  - Determine it is to be a per-pixel, sub-pixel or object-orientated classification.
- Acquire remote sensing data and ground cover reference data
  - Select on the criteria: Spatial, spectral, temporal, and radiometric resolution, and the ground coverage (i.e. swath width)
  - Atmospheric, soil moisture, phonological cycle, etc.
  - Choose ground reference data based on: a priori knowledge of the study area.
- Process remote sensor data to extract thematic information
  - Radiometric correction (e.g. for sun's azimuth, elevation, atmospheric conditions)
  - Geometric correction (calibration of image co-ordinate system to geographic co-ordinate system)
- Select appropriate image classification logic:
  - Parametric (e.g. maximum likelihood, clustering)
  - Non-parametric (e.g. nearest-neighbour, neural network)

  - Non-metric (e.g. rule based decision-tree classifier)

- Select appropriate image classification algorithm:
  - Physical models
  - Statistical/empirical models
  - Supervised, e.g. Parallelepiped, minimum distance, maximum likelihood.
  - Others (hyperspectral matched filtering, spectral angle mapper)
  - Unsupervised e.g. Chain method, multiple pass ISODATA
  - Others (fuzzy c-means)
  - Hybrid (involving artificial intelligence)
  - Expert system, decision-tree, neural network
- Extract data from initial training sites (if required e.g. with supervised classification)
- Select the most appropriate bands using feature selection criteria:
  - Graphical (e.g. scatter plots)
  - Statistical (e.g. transformed divergence, JM distance)
- Extract training statistics
- Give information labels to pixels or image objects (i.e. for unsupervised classification)
- Post Processing
  - Filters (e.g. majority filter, clump, and sieve)
  - Combine classes
- Perform accuracy assessment
  - Qualitative confidence-building
  - Statistical measurement
  - Create and analyse error (confusion) matrix (e.g. Producers accuracy and user's accuracy or Univariate and multivariate statistical analysis)
- Accept or Reject previously stated hypothesis.

Appendix B

Vegetation Attributes

B.1 Vector Table

B.2 Vegetation Attribute Symbols

AREA(m^2)	PERIMETER(m)	FTEMA	VEG1	VEG2	TILLEGG1	TILLEGG2	KARTSIGN	SAU	STORFE
26214,33	1189,1	4351	2e				2e	2	2
7250,12	379,9	4351	2c		x		2cx	1	1
380450,44	5773,72	4351	2c	2e	x}	v	2cx}/ev	1	1
16212,53	874,09	4351	3b		s		3bs	3	3
84689,94	1785,13	4351	2c	2b	v}	}	2cv}/b}	1	1
42837,05	1448,21	4351	2c	1b	x		2cx/1b	1	1
11332,58	521,25	4351	1b				1b	2	2
25330,33	897,23	4351	9c	3b		s	9c/3bs	1	2
43724,45	960,27	4351	2c	2e	x	x	2cx/ex	1	1
288425,72	3756,93	4351	2c		v}		2cv}	1	1
492,06	109,09	4351	9a				9a	1	1
2648,62	241,21	4351	9c				9c	1	2
35310,98	1261,04	4351	3b	9a	s		3bs/9a	3	3
87122,13	2135,26	4351	2c	2e	x	x	2cx/ex	1	1
65379,5	1325,93	4351	2e		x		2ex	1	1
34012,02	1195,55	4351	2e	3b		s	2e/3bs	2	2
33150,78	1273,7	4351	9a	2e			9a/2e	1	1
7710,34	354,02	4351	1b				1b	2	2
70996,03	1603,04	4351	2c	2e	x	x	2cx/ex	1	1
38106,5	792,24	4351	2e	3b		s	2e/3bs	2	2
48877,43	1987,68	4351	9c	9a			9c/a	1	2
51928,6	1631,44	4351	2c		x		2cx	1	1
39747,43	1167,32	4351	2e		v		2ev	2	2

Table B.1: This is an excerpt from the attribute table of the Venabygd vegetation vector file produced by NIJOS. Each line corresponds to a polygon which has a number of attributes associated with it (identified in the columns). FTEMA is the SOSI code given for the area type. Tillegg is the additional attribute sign. These signs are described in the dataset chapter. Kartsign is the sign symbol written on the map for that particular polygon. Sau is the code given for the grazing quality of the polygon for sheep, and Strofe is the grazing quality given to the polygon for cattle.

Symbol	Tilleggsinformasjon	
⟠	**Stein og blokker** Arealer med 50-75% stein og blokk	
⩓	**Bart fjell** Arealer med 50-75% bart fjell	
v x	**Lav** Arealer med 25-50% lavdekning Arealer med mer enn 50% lavdekning	
⊃ s	**Vier** Arealer med 25-50 % dekning av vier Arealer med mer enn 50 % dekning av vier	
j	**Einer** Arealer med mer enn 50 % dekning av einer	
n	**Finnskjegg** Arealer med mer enn 75% dekning av finnskjegg	
k	**Kalkmyr** Kalkkrevende myrvegetasjon. Blir ikke kartlagt systematisk	
g	**Grasrik vegetasjon** Beitepåvirka vegetasjon med mer enn 50% grasdekning	
* + o) 0 ɔ	**Treslag** Gran Furu Lauv Gråor Selje	Tilleggssymbol for treslag blir brukt i vegetasjonsfigurer der det i tillegg til hovedtreslaget finnes minst 25% kronedekning av annet treslag. For skogtyper der treslaget ikke ligger i typenavnet, viser første tilleggssymbol hovedtreslaget. Dette gjelder hagemarkskog og fukt- og sumpskog. Åpen mark får symbol for treslag når kronedekninga er mellom 5-25% av arealet.
]	**Skogtetthet** Skogareal med 25-50% kronedekning	

Figure B.1: This table describes all the additional attributes that a vegetation type can have. A vegetation type can have up to 2 additional attributes. Copied from Bryn and Rekdal (2002).

Appendix C

Comparison Tables: Airphotos, unsupervised & supervised classification, satellite image

Table C.1: Selected polygons - Less Good grazing quality class

	Aerial Photo	Satellite Image	Unsupervised	Supervised
2	*Lavhei* (2cx) $> 50\%$ *lavdekning*	Very pale area with touches of light red	Majority: 47, 51, 56, 60, 52, 46, 45, 44, 41 Minority: 40, 57	Almost classified uniformly as Less Good
4	*Rishei* (2ex) $> 50\%$ *lavdekning*	The *lav* shows up as white in this band combination	Majority: 52, 58, 46, 44, 42, 40 Minority: 57, 38	Mottled coloured polygon giving a divided classification.

Table C.1 Less Good Grazing – continued from previous page

	Aerial Photo	Satellite Image	Unsupervised	Supervised
5	*Rishei* (2ex) $> 50\%$ *lavdekning*	Fair amount of light blue in areal photo, and quite a pink satellite image. This is the same vegetation type as in example 4, but here the polygons look quite different	Majority: 56, 44, 39, 41, 43, 46, 51 Minority: 32, 52, 58, 30, 25, 37	Less Good / Good supervised classification, similar half/half combination as was shown in the previous example with the same vegetation type.
6	*lav og lynrik bjørkeskog* (4a]v) Forested area with $25-50\%$ tree crown coverage. Area has $25-50\%$ *lavdekning*	Combination of various shades of green and pink	Majority: 40, 41, 39, 42, 44 Minority: 43, 46, 36, 56, 57	Classified as mostly Good quality, but this polygon is of Less Good grazing quality.

Table C.1 Less Good Grazing – continued from previous page

	Aerial Photo	Satellite Image	Unsupervised	Supervised
7	*Blåbærbjørkeskog* (4b})	Almost homogenous colour in the satellite image although you can see the dark speckle from the trees in the aerial photo	Majority: 45, 43 Minority: 41, 46 Very homogenous unsupervised classification	Very homogenous for a supervised classification, this could provide good training data for Less Good.
8	*Lav og lynrik furuskog* (6a*). At least 25% *Gran* tree in this area		Majority: 25, 27, 26, 29, 31, 32, 34, 35, 36, 37 Minority: 28, 22	A very dark green polygon to be of Less Good quality. Classified as 25% Spruce (*) in with the Pine. Inhomogeneous classifications.

Table C.1 Less Good Grazing – continued from previous page

	Aerial Photo	Satellite Image	Unsupervised	Supervised
9	*lav og lynrik furuskog* (6a&)	Very mottled satellite image	Majority: 32, 34, 35, 36, 43, 28, 29, 30, 37 Minority: 40, 41, 42, 38, 39, 57, 46, 26, 44	Unclear supervised classification. Certainly not a good indication of Less Good for classification purposes.
10	Majourity *lav og lynrik granskog* and 25-50% *lavdekning*, Minority *Blåbærgranskog* (7av/7b)	Very dark purples in this polygon	Majority: 28, 22, 25, 26, 30 Minority: 29, 32	Good supervised classification, most pixels being shown as Less Good, with a few pixels classified as Very Good.

Table C.1 Less Good Grazing – continued from previous page

	Aerial Photo	Satellite Image	Unsupervised	Supervised
11	*Fattig Sumpskog* (8c&)	Very homogenous looking satellite polygon	Majority: 55, 49, 38 Minority: 33, 57	Satellite image looks very homogeous but these classification results show otherwise. No pixels were classified as Less Good Quality. Was classified as Good, and Very Good
12	*Rismyr* (9a)	Can distinctly see the road that was masked out on the satellite image on the aerial photo	Majority: 59, 49, 58, 52, 46 Minority: 40, 41, 42, 55, 57, 33	Very complex polygon. This is verified by the areal photo, satellite image and unsupervised classification results.

Table C.2: Selected Polygons - Good Grazing Quality

	Aerial Photo	Satellite Image	Unsupervised	Supervised
1	 Right side: *Rishei* / *Lavhei* with $>$ 50% *lavdekning* (2e/2cx) Left side: *Rishei* (2e)	 Both polygons look fairly similar in the aerial photo and satellite image	 Majority: 6, 41, 43, 46 Minority: 42, 38, 44, 45, 44 Majority: 56, 51, 41, 45, 43 Minority: 44, 60, 46, 39, 30	 Classified as a mixture of Less Good and Good Both polygons show a similar classification pattern

Table C.2 Good Grazing – continued from previous page

	Aerial Photo	Satellite Image	Unsupervised	Supervised
2	*Rishei* (2e)	Same type as example 1, but here the satellite image shows varying reflectances and more green (i.e. near infrared (NIR))	Majority: 41, 58, 44, 57, 42, 46, 56 Minority: 43, 39, 45, 52	Poor classification, mixture of all three classes.

Table C.2 Good Grazing – continued from previous page

	Aerial Photo	Satellite Image	Unsupervised	Supervised
3	*Blåbærbjørkeskog* (4b)		Majority: 38, 36, 40, 44, 57, 55, 42, 34, 37 Minority: 35, 41, 39, 43, 46, 33, 32, 58	This showed fairly good results, with most pixels receiving the correct Good quality class name.
5	Majority *Rik sumpskog* and Minority *Grasmyr* which is *kalkkrevende myrvegetasjon* (8d&/9ck)	Nice homogenous polygon	Majority: 31, 34, 33, 55, 38, 49, 57 Minority: 32, 39	Quite homogeous, and obviously a good example of NIJOS style Good grazing quality area.

Table C.2 Good Grazing – continued from previous page

	Aerial Photo	Satellite Image	Unsupervised	Supervised
6	*Blåbærbjøkeskog* (4b)	Same vegetation type as example 3, although this polygon is darker in both aerial photo and satellite image	Majority: 29, 26, 27, 22, 24, 31, 34, 28 Minority: 32, 33, 25, 54, 48, 38, 21	Mixed classification
7	*Blåbærgranskog* (7b&)	Can see a large man made cleared area that has been included in the polygon.	Majority: 31, 42, 28, 29, 26, 32, 34, 58, 30, 37, 38, 57, 27, 24 Minority: 33, 35, 36, 55, 49, 22, 21, 20, 19, 18, 17	Mixed classification

Table C.2 Good Grazing – continued from previous page

	Aerial Photo	Satellite Image	Unsupervised	Supervised
8	*Grasmyr* which has $>$ 50% grass coverage and $>$ 50% coverage of *Vier* (9cgs)		Majority: 40, 42, 58, 57, 55 Minority: 49, 63, 38, 39, 33	Complex polygon. Supervised classification results don't show a a good representation of Good grazing.

Table C.3: Selected Polygons - Very Good Grazing Quality

	Aerial Photo	Satellite Image	Unsupervised	Supervised
1	Top: *Hgstaudeeng* with $> 50\%$ *vier* coverage and *grasmyr* (Veg3bs/9c!) Middle: *Hgstaudeeng* with $> 50\%$ *vier* coverage (3bs) Bottom: *Hgstaudeeng* with $> 50\%$ *vier* coverage and *Rishei* (3bs/2e)	The area that had a stream running through has been masked out for classification. Can be seen on the aerial photo.	Majority: 23, 24, 27, 31, 32, 53, 55; Minority: 20, 22, 55, 43	Classification was fairly uniformly Good grazing, however this polygon is defined as Very Good grazing, so that is incorrect.

Table C.3 Very Good Grazing – continued from previous page

	Aerial Photo	Satellite Image	Unsupervised	Supervised
3	*Rishei* with $>$ 50% grass coverage (2eg)	Polygon contains stream, roads and houses so most was actually masked out for classification. The surrounding areas of these are often affected however and can affect classification	Majority: 23, 24, 27, 31, 32, 33, 53, 57; Minority: 20, 43, 47	Mixed classification, mostly which is Good.
5	*Blåbærbjørkeskog* with $>$ 50% grass coverage (4bg)		Majority: 19, 20, 21, 23, 33, 31 Minority: 21, 53	Classified almost uniformly as Good, but this polygon is of Very Good grazing quality.

Table C.3 Very Good Grazing – continued from previous page

	Aerial Photo	Satellite Image	Unsupervised	Supervised
6	*Oreskog* (4e)	A large polygon with many different colours.	Majority: 14, 15, 16, 17, 19, 29, 33, 45, 46, 53 Minority: 33, 14, 29	A Large polygon to be classified as one vegetation type, and shows a large range of values. Classification showed pixels from all grazing quality classes.
7	*Engfuruskog* (6c)		Majority: 53, 31, 29 Minority: 20, 23, 33	Classified as mostly Good with only a few spots of Very Good.

Appendix D

Acronyms & Abbreviations

asr 'at satellite radiance'

DEM digital elevation model

DN digital number

EC European Commission

EM electromagnetic

ESA European Space Agency

ETM Enhanced Thematic Mapper

G Good

GIS geographic information system

GMES Global Monitoring for Environment and Security

JM Jeffries-Matusita

LAI leaf area index

LG Less Good

masl Meters above sea level

MIR Mid Infrared

MLC Maximum Likelihood Classifier

MODIS MODerate Resolution Imaging Spectroradiometer

MSS Multispectral Scanner

NDVI normalised difference vegetation index

NIJOS Norwegian Institute for Land Inventory

NIR near infrared

NPS National Parks Service

NR the Norwegian computing centre

ONP Nature Protection Observatory

RGB red, green, blue

ROI region of interest

SWIR short wave infrared

TIN triangular irregular network

TM Thematic Mapper

USGS United States Geological Survey

VG Very Good

VMP Vegetation Mapping Program